

Aus dem Bereich Physiologie  
Theoretische Medizin und Biowissenschaften  
der Medizinischen Fakultät  
der Universität des Saarlandes, Homburg/Saar

# **The role of Flower splice variants in regulating endocytosis in primary cytotoxic T lymphocytes**

**Dissertation**

**zur Erlangung des Grades eines Doktors der Naturwissenschaften der  
Medizinischen Fakultät**

**der UNIVERSITÄT DES SAARLANDES**

**2021**

vorgelegt von: **Keerthana Ravichandran**

geb. am: 22.12.1987 in Salem, Tamil Nadu, India.

Tag des Promotionskolloquiums: 08-12-2021

Dekan: Prof. Dr. M. D. Menger

Vorsitzender: -----

Berichterstatter: PD Dr. Elmar Krause  
Prof. Dr. Frank Schmitz

*Dedicated to my beloved parents  
And Guru*

## **Table of Contents**

<b>Acknowledgements .....</b>	<b>7</b>
<b>List of Figures.....</b>	<b>9</b>
<b>List of Tables .....</b>	<b>11</b>
<b>Abbreviations .....</b>	<b>12</b>
<b>Abstract.....</b>	<b>13</b>
<b>Zusammenfassung.....</b>	<b>14</b>
<b>1. Introduction: .....</b>	<b>16</b>
<b>1.1 Immune response – The cellular defense mechanism .....</b>	<b>16</b>
<b>1.2 Immunity: Innate vs adaptive reaction .....</b>	<b>17</b>
<b>1.3 T Lymphocytes: Maturation and activation .....</b>	<b>19</b>
<b>1.4 Cytotoxic T Lymphocytes: The Immunological synapse .....</b>	<b>20</b>
<b>1.5 The effector and memory subsets of CD8<sup>+</sup> T lymphocytes.....</b>	<b>22</b>
<b>1.6 Lytic granule exo- and endocytosis .....</b>	<b>24</b>
<b>1.7 Proteins involved in the exo-endocytic machinery .....</b>	<b>25</b>
<b>1.8 Flower protein: Regulator of calcium mediated endocytosis .....</b>	<b>27</b>
<b>1.9 Flower in health and disease.....</b>	<b>29</b>
<b>2. Aim of the study .....</b>	<b>32</b>
<b>3. MATERIALS AND METHODS .....</b>	<b>34</b>
<b>3.1 Materials .....</b>	<b>34</b>
<b>3.1.1 Chemicals .....</b>	<b>34</b>
<b>3.1.2 Mounting medium .....</b>	<b>40</b>
<b>3.1.3 Yeast strains: .....</b>	<b>40</b>
<b>3.1.4 Bacteria and Cell Lines .....</b>	<b>40</b>
<b>3.1.5 Mouse Strains.....</b>	<b>40</b>
<b>3.2 Methods.....</b>	<b>41</b>
<b>3.2.1 Positive isolation of Primary murine CD8<sup>+</sup> T lymphocytes.....</b>	<b>41</b>
<b>3.2.2 Long term culturing of Primary murine CD8<sup>+</sup> T lymphocytes.....</b>	<b>41</b>
<b>3.2.3 Subset analysis of CD8<sup>+</sup> T lymphocytes using Flow cytometry.....</b>	<b>41</b>
<b>3.2.4 Cell Proliferation assay .....</b>	<b>42</b>

3.2.5 Degranulation assay .....	43
3.2.6 Calcein-AM based Real-time killing assay .....	43
3.2.7 Electroporation of CTLs .....	44
3.2.8 Target cell culture.....	44
3.2.9 Coating coverslips.....	44
3.2.10 Organs and CTL lysate preparation.....	45
3.2.11 Western blotting .....	45
3.2.12 Plasmids .....	46
3.2.13 anti-RFP antibody labelling.....	51
3.2.14 Flower topology using Halo tag constructs: .....	52
3.2.15 Localization studies .....	52
3.2.16 High pressure freezing and freeze substitution for electron microscopy .....	53
3.2.17 Yeast two hybrid assay (Y2H) .....	53
β-galactosidase assay: .....	55
3.2.18 Cloning of bait and prey proteins in yeast-two hybrid vectors .....	55
3.2.19 Semi-quantitative PCR.....	57
3.2.20 Structured Illumination Microscopy (SIM) .....	58
3.2.21 Endocytosis of CG and Flower Rescue experiment.....	59
3.2.22 Confocal microscopy .....	59
3.2.23 Total Internal Reflection Fluorescence Microscopy (TIRF-M) .....	60
3.2.24 Transferrin Receptor 1 (TfR1) flow cytometric internalization assay ...	60
3.2.25 Immunocytochemistry.....	61
3.2.26 Software used .....	61
<b>4. Results .....</b>	<b>62</b>
4.1 Flower is expressed in the mouse spleen and primary cultures of CD8 <sup>+</sup> .....	62
T cells .....	62
4.2 Flower KO CTLs show similar proliferation rates and CTL subset profile to Wild type CTLs.....	63
4.3 Loss of Flower reduces the killing efficacy of CTLs but does not affect exocytosis of CGs directly .....	65

4.4 Flower KO blocks endocytosis of Synaptobrevin2 but does not affect Transferrin receptor (TfR1) uptake .....	67
4.5 Mouse CTLs express 5 splice variants of murine Flower protein.....	70
4.6 FweA tagged at either the N- or C-terminus was able to rescue endocytosis of Syb2 in Flower KO CTLs .....	73
4.7 Not all mouse Flower isoforms are able to rescue endocytosis of cytotoxic granule material.....	74
4.8 Flower topology in the plasma membrane determined by Halo tag fusion constructs.....	76
4.9 FweA is localized to plasma membrane upon bead activation .....	78
4.10 The Flower rescuers of endocytosis show vesicular localization while the non-rescuers localize to the ER .....	81
4.11 The N- and C-terminal YXX $\phi$ motifs are important for Syb2 endocytosis .....	83
4.12 The YXX $\phi$ motif does not interact with AP2mu subunit in yeast .....	85
4.13 The Exon 3 of Human Flower is important in Syb2 endocytosis .....	87
4.14 Exon 3 is an important part of murine Flower for Syb2 endocytosis .....	89
4.15 The conserved tyrosine residue in exon3 of mouse Flower is mainly responsible for aiding Syb2 endocytosis .....	90
4.16 The C-terminus of drosophila Flower is important in Syb2 endocytosis ..	93
5. Discussion.....	96
5.1 Validation of the Flower KO model.....	96
5.2 Comparing the Flower splice variants among different species.....	97
5.3 Importance of YXX $\phi$ motif in aiding endocytosis.....	100
5.4 Exon3 as the common factor that imparts specific function in Flower isoforms.....	101
5.5 Localization and topology of Flower.....	103
5.6 Proposed model of mouse Flower isoforms in aiding Syb2 endocytosis ....	104
6. Outlook.....	106
7. References.....	107
8. Publications .....	115
9. Disclosure.....	116

## **Acknowledgements**

I would like to first thank my supervisor, Professor Dr. Jens Rettig, whose expertise in formulating the research questions and methodology brought great interest and enthusiasm in my work. The insightful feedback during every conversation pushed me to sharpen my thinking and has brought my work to a higher level. His friendly nature, positive attitude and timely jokes have always calmed the stressful days and made me work hard towards my goal.

I would like to extend my sincere thanks to Dr. Elmar Krause for his valuable and straightforward suggestions in structuring my thesis study beautifully and for his guidance throughout.

My heartfelt thanks to Dr. Claudia Schirra for all the enthusiastic and wonderful discussions that made my thesis work very fruitful. She has always supported me and acknowledged my work and been a dear mentor, leading me throughout. Working with her has always made me learn new things.

I would like to thank Dr. Ute Becherer for her valuable guidance throughout my study. Her ideas and motivation have always helped me. Her scientific input was of great help throughout my entire work.

In addition, I would like to thank Dr. David Stevens, Dr. Olaf Pongs, Dr. Hsin-Fang Chang, Dr. Ulrike Hahn and Dr. Varsha Pattu for their scientific discussions and support in my project.

I would like to thank Dr. Veit Flockerzi, Dr. Dieter Bruns and all IRTG1830 members for the great and lively scientific discussions. I thank IRTG1830 for the funding and Dr. Gabrielle Amoroso for her marvellous support during my PhD.

Many thanks to the best and lovely technicians Anja Bergsträßer, Margarete Klose, Katrin Sandmeier, Nicole Rothgerber, Anne Weinland, Jacqueline Vogel, Tamara Paul, and Silke Bruns-Engers. My sincere thanks to the secretaries Bernadette Schwarz, Andrea Berger, and Josephine Kretschmer for all the help in administrative work.

I thank all my friends and former colleagues Olga Ratai, Hawraa Bzeih, Hsin-Fang Chang, Angelina Staudt, Praneeth Chitirala and Marwa Sleiman for their nice company and fun moments. I especially thank Mayur Dembla, Ekta Dembla, Archana Yanamandra and Mazen Makke for always being there for any help and for being very good friends. My extended thanks to Nadia Alawar and Szumin Tu for their timely help and nice conversations. I would like to thank the new Ph. D students for their nice gifts and chats during lunch break.

----Acknowledgements----

And my biggest thanks to my family for all the belief they had in me and the support they have shown from the beginning. Thank you, Dad and Mom, without your prayers, love and care, I could not have reached this goal. My special thanks to my father and mother-in law for their full support and accepting me as I am.

Last but the best, my heartfelt thanks to my hubby and my best-half, Praneeth Chitirala for his support and helping me balance home and work without any stress. My love to Vishnu for understanding me and being such a good son. Last but not the least, thanks to my Guru and the Almighty for giving me such wonderful people in life and helping me understand success and failure equally.

Thank you.



## List of Figures

<i>Figure 1: The three lines of defense against infection.....</i>	<i>16</i>
<i>Figure 2: Cells involved in innate and adaptive immune response.....</i>	<i>17</i>
<i>Figure 3: The branches of humoral and cellular immune response.....</i>	<i>18</i>
<i>Figure 4: Positive and negative T cell selection in the thymus .....</i>	<i>20</i>
<i>Figure 5: Cytotoxic T cell immunological synapse architecture.....</i>	<i>21</i>
<i>Figure 6: Cell surface markers and cytolytic effector molecules of CTL subsets .....</i>	<i>23</i>
<i>Figure 7: Endocytic recycling of proteins is necessary for serial killing ability of cytotoxic cells.....</i>	<i>25</i>
<i>Figure 8: Proteins involved during synapse assembly and disassembly in cytotoxic T cells.....</i>	<i>26</i>
<i>Figure 9: Flower phenotype and exo-endocytosis coupling at the presynaptic terminal .....</i>	<i>28</i>
<i>Figure 10: Determination of cell fitness by the Flower code .....</i>	<i>30</i>
<i>Figure 11: Survival of the fittest selection during tissue homeostasis and Cancer.....</i>	<i>31</i>
<i>Figure 12: Overview of Flower splice variants from drosophila (A), mouse (B) and human (C) .....</i>	<i>32</i>
<i>Figure 13: Principle of CFSE based cell proliferation assay .....</i>	<i>42</i>
<i>Figure 14: Overview of CTL transfection procedure .....</i>	<i>44</i>
<i>Figure 15: Representation of Halo tag-Atto staining procedure.....</i>	<i>52</i>
<i>Figure 16: Representation of staining procedure for localization study.....</i>	<i>52</i>
<i>Figure 17: Principle of Yeast two hybrid study.....</i>	<i>54</i>
<i>Figure 18: Quality check of isolated RNA on an agarose gel. ....</i>	<i>56</i>
<i>Figure 19: Schematic diagram showing a brief procedure of TfR1 internalization assay .....</i>	<i>61</i>
<i>Figure 20: Flower protein is expressed in mouse primary cytotoxic T lymphocytes (CTLs) and is upregulated after activation.....</i>	<i>62</i>
<i>Figure 21: Fwe KO CTLs show similar proliferation stages compared to WT cells ..</i>	<i>64</i>
<i>Figure 22: Fwe KO CTLs show similar CTL subsets compared to WT cells .....</i>	<i>65</i>
<i>Figure 23: Exocytosis of CG granules is unaffected, but the killing efficiency is decreased in Fwe KO CTLs .....</i>	<i>66</i>
<i>Figure 24: Fwe KO CTLs show a block in Syb2 endocytosis.....</i>	<i>68</i>
<i>Figure 25: Fwe KO CTLs do not show defect in TfR1 internalization.....</i>	<i>69</i>
<i>Figure 26: Murine Flower transcript variants .....</i>	<i>70</i>
<i>Figure 27: Except for FweA2, mRNA for all murine splice variants is present in primary cytotoxic T lymphocytes .....</i>	<i>71</i>
<i>Figure 28: Expression of Flower isoforms-mTFP fusion constructs in mouse CTLs..</i>	<i>72</i>

Figure 29: *FweA* tagged with *mTFP* at either *N*- or *C*-terminus can rescue block in *Syb2* endocytosis ..... 74

Figure 30: The *Flower* splice-variants differ in their ability to rescue *Syb2* endocytosis in *Flower KO CTL* ..... 75

Figure 31: Both *N*- and *C*-termini of *Flower* splice variants are facing the cytoplasm of a *CTL* ..... 77

Figure 32: *FweA* is localized to the plasma membrane after *CD3/CD28* bead stimulation..... 79

Figure 33: *FweA* is present at the plasma membrane of *CTLs* ..... 80

Figure 34: Vesicular localization versus *ER* localization between *Flower* rescuers and non-rescuers of endocytosis..... 82

Figure 35: Mutation of the *C*- and *N*-terminal amino acid motifs *YRWL* (26-29 aa) and *YARI* (147-150 aa) mutant of *FweA* cannot rescue the block of *Syb2* endocytosis ..... 84

Figure 36: *YRWL>AAAA* (26-29 aa) mutation of *FweB* prevents partial *FweB*-rescue of *Syb2* endocytosis..... 85

Figure 37: Yeast two hybrid assay shows no interaction of *YXX $\phi$*  based motifs in *FweA* with *AP2mu*..... 86

Figure 38: Isoforms lacking *Exon3* in human *FWE* could not rescue the block of *Syb2* endocytosis..... 88

Figure 39: Deletion of *Exon3* in *mFweB* isoform could not rescue the block of *Syb2* endocytosis..... 89

Figure 40: Conserved Glutamate(*E*), Proline(*P*) and Tyrosine(*Y*) amino acids among *Cg6151-P* containing proteins..... 91

Figure 41: Mutation of Tyrosine residue (*Y104A*) in *FweA* isoform has severe block of *Syb2* endocytosis ..... 92

Figure 42: *dFwe<sup>ubi</sup>* and not *dFwe<sup>LoseA</sup>* or *dFwe<sup>LoseB</sup>* could rescue *Syb2* endocytosis... 94

Figure 43: Mutation of *Y109A* in *dFwe<sup>ubi</sup>* isoform cannot rescue the block of *Syb2* endocytosis..... 95

Figure 44: Protein sequence of mouse *Flower* isoforms ..... 98

Figure 45: Comparison of mouse *FweA* protein sequence with the *drosophila Fwe* isoforms..... 100

Figure 46: Localization and possible function of mouse *Flower* isoforms in endocytosis ..... 105

## List of Tables

<i>Table 1: Common Reagents and Chemicals .....</i>	<i>34</i>
<i>Table 2: Reagents and Chemicals for western blot .....</i>	<i>35</i>
<i>Table 3: Commercial Kits.....</i>	<i>36</i>
<i>Table 4: Antibodies.....</i>	<i>37</i>
<i>Table 5: Media and solutions .....</i>	<i>38</i>
<i>Table 6: Sequences of mouse Flower isoforms.....</i>	<i>46</i>
<i>Table 7: Sequences of human FLOWER isoforms.....</i>	<i>47</i>
<i>Table 8: Sequences of drosophila Flower isoforms.....</i>	<i>48</i>
<i>Table 9: Sequences of mouse Flower mutants.....</i>	<i>49</i>
<i>Table 10: Flower isoform constructs generated and used in this study .....</i>	<i>50</i>
<i>Table 11: Primers used for cloning Flower peptides into yeast vectors .....</i>	<i>57</i>
<i>Table 12: Primers used for RT-PCR.....</i>	<i>58</i>
<i>Table 13: Table summarizing Flower isoforms into rescuers and non-rescuers of CG endocytosis category based on the experimental results obtained from Fwe KO CTLs .....</i>	<i>104</i>

## Abbreviations

APC	Antigen presenting cell
a. u.	Arbitrary units
BSA	Bovine serum albumin
CTL	Cytotoxic T lymphocyte
°C	Degree Celsius
CGs	Cytotoxic granules
Ca <sup>2+</sup>	Calcium
CFSE	Carboxyfluorescein succinimidyl ester
CME	Clathrin mediated endocytosis
cSMAC	Central supra-molecular activation cluster
dSMAC	Distal supra-molecular activation cluster
ER	Endoplasmic Reticulum
d/mFwe /hFWE	drosophila / mouse Flower /human Flower
EGFP	Enhanced Green fluorescent protein
h	Hour
HEPES	4-(2-Hydroxyethyl)-1-piperazineethanesulfonic acid
IS	Immunological synapse
KO	Knock-out
KI	Knock-In
LAMP1	Lysosomal-Associated Membrane Protein 1
min	Minute
MTOC	Microtubule organizing center
NK	Natural Killer
PBS	Phosphate buffer saline
pH	Potential hydrogen
pSMAC	Peripheral supra-molecular activation cluster
PCR	Polymerase chain reaction
RE	Recycling endosomes
SEM	Standard error of the mean
SIM	Structured illumination microscopy
SNARE	Soluble N-ethyl-maleimide-sensitive attachment protein receptor
SV	Synaptic vesicle
Syb2	Synaptobrevin2
TCR	T-cell receptor
TGN	Trans Golgi network
TfR1	Transferrin Receptor1
t-SNARE	Target-SNARE
mTFP	monomeric-teal fluorescent protein
TIRFM	Total internal reflection microscope
v-SNARE	Vesicular-SNARE
VAMP	Vesicle associated membrane protein

## Abstract

Cytotoxic T lymphocytes (CTLs) are important immune defense fighters, attacking intracellular pathogens such as viruses and bacteria, and are major players in tumour surveillance. The immunological synapse (IS) between T cells and antigen presenting cells is the focal point for exocytosis of cytotoxic granule contents leading to target cell apoptosis and/or lysis. Exo- and endocytosis are among the most fundamental pathways in cells. Both of these pathways are highly interdependent, as several proteins contribute to the dynamic function. The transmembrane protein Flower (Fwe) is associated with synaptic vesicle endocytosis in neurons and is also known for its important role in regulating cytotoxic granule (CG) endocytosis in primary cytotoxic T lymphocytes (CTLs). The major aim of this study is to characterize the function of Flower splice variants in the endocytosis of CG material and to subsequently decipher the mechanism of Flower's role in endocytosis.

Flower is expressed in primary mouse CD8<sup>+</sup> T cells and is upregulated during differentiation from naïve to effector cells. RT-PCR shows the expression of four mouse Flower isoforms (FweA, B, D and E) in brain and activated CTLs. Real-time killing assays with different effector: target cell ratios showed a clear defect in killing efficacy of Flower deficient CTLs in comparison to wild-type cells. Fwe deficient CTLs showed accumulation of the CG marker protein Synaptobrevin2 (Syb2) in the plasma membrane at the IS indicating that it is not endocytosed. Since Transferrin receptor1 (TfR1) internalization into the cells was not affected, it appears that endocytosis of a CG-independent protein was not completely blocked. Only reintroduction of FweA, the longest isoform, was able to fully rescue Syb2 endocytosis while introduction of FweB and E showed partial rescue. Expression of FweD did not rescue Syb2 endocytosis and resulted in behavior similar to Fwe KO cells. The incomplete rescue by FweB and E was likely caused by differences in the C-terminus region. Comparison of the rescue phenotype induced by drosophila and human Flower isoforms gave indications that the C-terminus (140-171 aa) and conserved exon3 (81-99 aa) regions are the major regions involved in aiding Syb2 endocytosis. Various mutated constructs involving the YXX $\phi$  motif region YRWL and YARI at the N- and C-termini and mutation of the highly conserved tyrosine residue (Y104A) in the exon3 region showed no rescue of endocytosis which might indicate the importance of the Flower isoforms in various functional and downstream pathways of endocytosis. Flower topology studies using Halo tag-Atto488 staining show that the N- and C-termini of Flower are cytosolic. CD3/CD28 bead activation triggers the movement of Flower to the plasma membrane where it is mainly localized at the IS. A vesicular localization of the Flower constructs which rescue endocytosis was seen specifically at the IS whereas the Flower constructs which did not rescue endocytosis were localized to the endoplasmic reticulum (ER). Inability to traffic to the plasma membrane likely explains the inability of some isoforms to support endocytosis. Thus, the results of this study have allowed us to characterize the role of the naturally truncated splice variants in regulating CG endocytosis in primary murine CTLs.

## Zusammenfassung

Zytotoxische T-Lymphozyten (CTLs) sind wichtige zelluläre Komponenten der Abwehr von intrazellulären Krankheitserregern wie Viren und Bakterien und spielen eine wichtige Rolle bei der Tumorüberwachung. Die immunologische Synapse (IS) zwischen T-Zellen und Antigen-präsentierenden Zellen ist der Ort der Exozytose von zytotoxischen Granulainhalten, die zur Apoptose und/oder Lyse der Zielzellen führt. Exo- und Endozytose sind einer der grundlegendsten Prozesse in allen Zellen. Beide Prozesse sind stark voneinander abhängig, da mehrere Proteine zusammenspielen und zur dynamischen Funktion in verschiedenen Zelltypen beitragen. Es wurde gezeigt, dass das Transmembranprotein Flower (Fwe) mit der synaptischen Vesikelendozytose in Neuronen assoziiert ist und ebenfalls eine wichtige Rolle bei der Regulierung der zytotoxischen Granula (CG)-Endozytose in primären zytotoxischen T-Lymphozyten (CTLs) hat. Das Hauptziel der vorliegenden Arbeit ist es, die Funktion von Flower-Spleißvarianten zu charakterisieren und anschließend einen möglichen Mechanismus zu entschlüsseln, wie Flower die Endozytose zytotoxischer Granulabestandteile unterstützt.

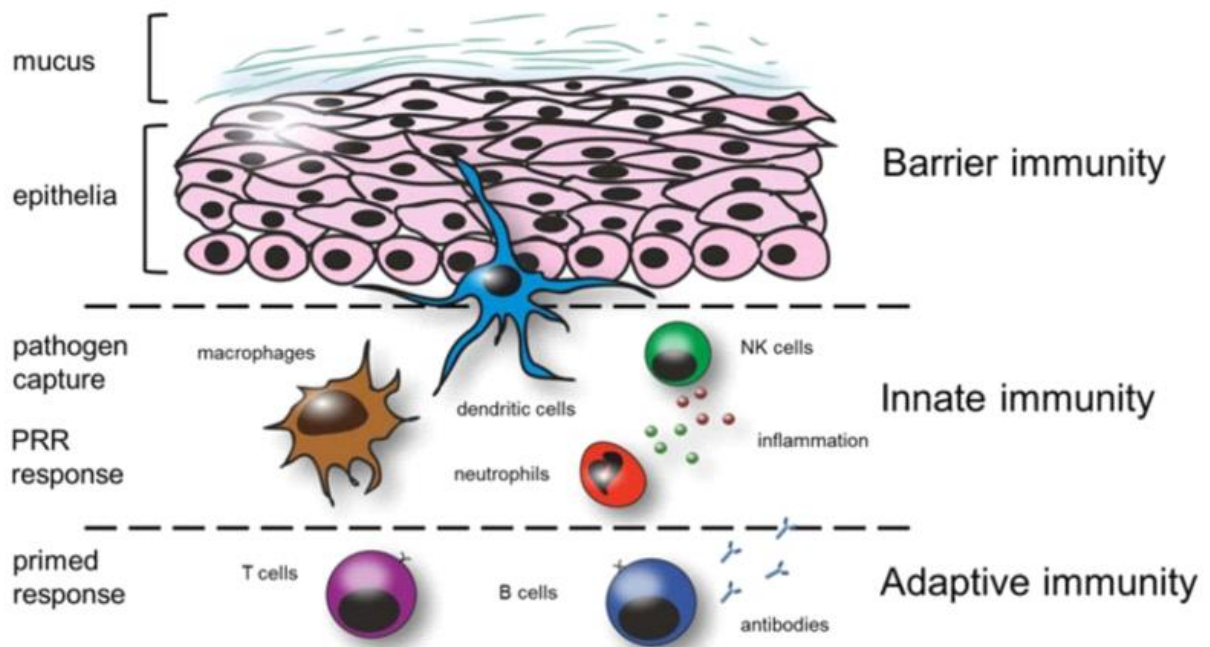
Flower wird in primären Maus-CD8<sup>+</sup>-T-Zellen exprimiert und wird während der Reifung zu Effektorzellen hochreguliert. RT-PCR zeigt die Expression von vier Maus-Flower-Isoformen (FweA, B, D und E) im Gehirn und aktivierten CTLs. Killing Assays mit unterschiedlichem Effektor:Zielzellen Verhältnis zeigten einen klaren Defekt in der Abtötungseffizienz von Flower-defizienten CTLs im Vergleich zu Wildtypzellen. Außerdem zeigten Fwe-defiziente CTLs eine Akkumulation des CG-Markers Synaptobrevin2 (Syb2) an der IS, was für einen Endozytosedefekt spricht. Die Internalisierung des Transferrin-Rezeptors1 (TfR1) war jedoch nicht beeinträchtigt. Die Wiedereinführung von Fwe-Isoformen zeigte, dass nur die längste Isoform FweA den Syb2-Block überwinden konnte, während FweB und E einen teilweisen Effekt zeigten. FweD konnte die Syb2-Akkumulation nicht verhindern. Überexprimierende Zellen verhielten sich ähnlich wie Fwe KO-Zellen. Die nur teilweise Wiederherstellung der Endozytose in Fwe-KO-CTLs durch die Maus-FweB- und -E-Isoformen im Vergleich zur A-Variante ist wahrscheinlich auf Unterschiede in der C-Terminus-Region zurückzuführen. Der Vergleich des Rescue-Phänotyps von Drosophila und humanen Fwe Isoformen gab uns den Hinweis, dass der C-Terminus (140-171 aa) und die konservierten Exon3-Regionen (81-99 aa) die Hauptregionen sind, die an der Unterstützung der Syb2-Endocytose beteiligt sind. Verschiedene Mutationen der YXX $\phi$ -Motivregionen YRWL und YARI an den N- und C-Termini und Mutationen des hochkonservierten Tyrosinrests (Y104A) in der Exon3-Region zeigten keine Wiederherstellung der Endozytose, was auf verschiedene Funktionen der Flower-Isoformen für verschiedene Schritte der Endozytose hinweisen könnte. Studien zur Flower-Topologie mit Halo-Tag-Atto488-Färbung zeigen, dass die N- und C-Termini von Flower zytosolisch sind. CD3/CD28-Bead-Aktivierung löst die Translokation von Flower an die Plasmamembran und hier hauptsächlich zur IS aus. Eine vesikuläre Lokalisation der Endozytose-wiederherstellenden Flower-Konstrukte wurde speziell an der IS beobachtet, während die erfolglosen Flower-Konstrukte eine Lokalisation am endoplasmatischen Retikulum (ER)

zeigten, was die unterschiedlichen funktionellen Aspekte der verschiedenen Isoformen betont. Die Ergebnisse dieser Studie können helfen, die Rolle der Spleißvarianten bei der Regulierung der CG-Endocytose in primären murinen CTLs zu verstehen.

# 1. Introduction:

## 1.1 Immune response – The cellular defense mechanism

The environment we live in contains various pathogens and harmful substances that cause various diseases. The host immune system has thus evolved, making use of a diverse array of specialized cells and soluble substances, that harmonize a flexible and rapid defense system capable of protecting our body from most of these pathogens. Upon re-exposure, immune memory can recognize and fight these pathogens in a more effective manner, even when the subsequent exposure occurs decades later. To cause an infection, the pathogens have to cross the three lines of defense levels of our immune system namely 1) physical and chemical barriers – the skin, mucous membrane, tears, stomach acid, etc., 2) non-specific immune responses provided by the macrophages, neutrophils, interferons, basophils, complement system, etc., and 3) specific immune responses by the T cells and B cells (Chaplin, 2010) (Figure 1).






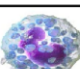
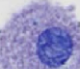


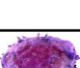
**Figure 1: The three lines of defense against infection**

Schematic diagram showing the three major defense barriers of the immune system are illustrated. When a foreign material attacks our body, the first line of protection is provided by the non-specific physical and chemical barriers followed by the second line of cover namely the innate immune response. The third line of support are the antigen-specific adaptive immune cells that maintain long lasting protection against any infection. PRR – pattern recognition receptors (Richman et al., 2017).



## 1.2 Immunity: Innate vs adaptive reaction

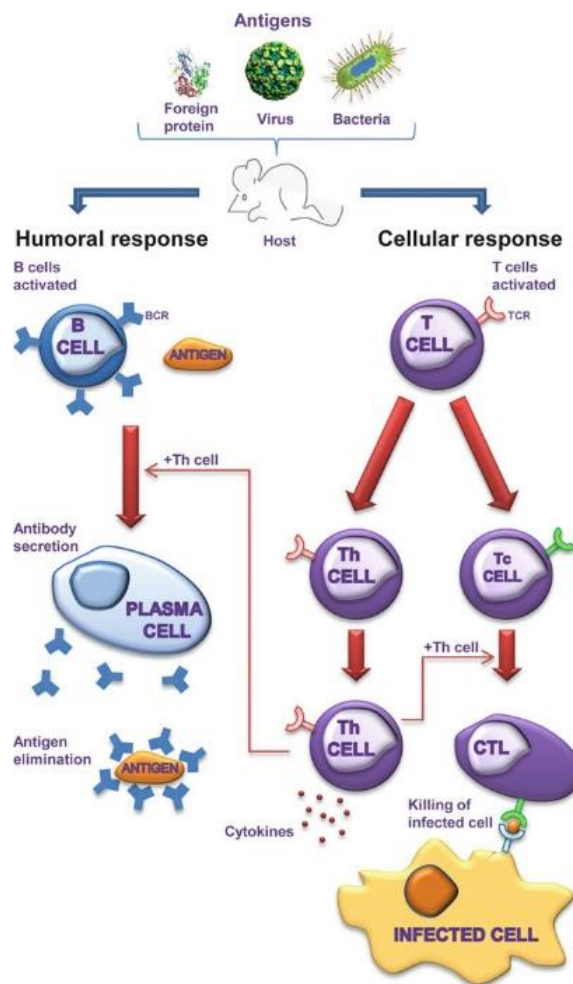
The innate or non-specific immune reaction is the primary defense against invading foreign organisms that acts in an antigen-independent manner and has no immunological memory. The response is rapid, short-lived, and does not offer maximal protection. For instance, neutrophils with a lifetime of a few hours to days do not result in a long-lasting “memory” which could produce a more effective response upon re-exposure. In contrast, the adaptive or specific immune reaction is long-lived, and antigen-specific, and can provide a fast and robust response upon subsequent encounters with the pathogen. Innate and adaptive immunity are complementary mechanisms and defects in either of these can cause severe immune suppression and host sensitivity to various diseases. Figure 2 shows the different cell types involved in innate and adaptive immunity with their approximate lifespan in a normal adult body (Marshall et al., 2018; Murphy and Weaver., 2017).

Cell	Image	% in adults	Nucleus	Functions	Lifetime	Main targets
Macrophage*		Varies	Varies	<ul style="list-style-type: none"> <li>Phagocytosis</li> <li>Antigen presentation to T cells</li> </ul>	Months – years	<ul style="list-style-type: none"> <li>Various</li> </ul>
Neutrophil		40-75%	Multi-lobed	<ul style="list-style-type: none"> <li>Phagocytosis</li> <li>Degranulation (discharge of contents of a cell)</li> </ul>	6 hours – few days	<ul style="list-style-type: none"> <li>Bacteria</li> <li>Fungi</li> </ul>
Eosinophil		1-6%	Bi-lobed	<ul style="list-style-type: none"> <li>Degranulation</li> <li>Release of enzymes, growth factors, cytokines</li> </ul>	8-12 days (circulate for 4-5 hours)	<ul style="list-style-type: none"> <li>Parasites</li> <li>Various allergic tissues</li> </ul>
Basophil		< 1%	Bi- or tri-lobed	<ul style="list-style-type: none"> <li>Degranulation</li> <li>Release of histamine, enzymes, cytokines</li> </ul>	Lifetime uncertain; likely a few hours – few days	<ul style="list-style-type: none"> <li>Various allergic tissues</li> </ul>
Mast cell		Common in tissues	Central, single-lobed	<ul style="list-style-type: none"> <li>Degranulation</li> <li>Release of histamine, enzymes, cytokines</li> </ul>	Months to years	<ul style="list-style-type: none"> <li>Parasites</li> <li>Various allergic tissues</li> </ul>
Lymphocytes (T cells)		20-40%	Deeply staining, eccentric	<ul style="list-style-type: none"> <li>T helper (Th) cells (CD4+): immune response mediators</li> <li>Cytotoxic T cells (CD8+): cell destruction</li> </ul>	Weeks to years	<ul style="list-style-type: none"> <li>Th cells: intracellular bacteria</li> <li>Cytotoxic T cells: virus infected and tumour cells</li> <li>Natural killer cells: virus-infected and tumour cells</li> </ul>
Monocyte		2-6%	Kidney shaped	Differentiate into macrophages and dendritic cells to elicit an immune response	Hours – days	<ul style="list-style-type: none"> <li>Various</li> </ul>
Natural killer (NK) cell		15% (varies) of circulating lymphocytes and tissues	Single-lobed	<ul style="list-style-type: none"> <li>Tumour rejection</li> <li>Destruction of infected cells</li> <li>Release of perforin and granzymes which induce apoptosis</li> </ul>	7-10 days	<ul style="list-style-type: none"> <li>Viruses</li> <li>Tumour cells</li> </ul>

**Figure 2: Cells involved in innate and adaptive immune response**

The different cells that take part in the immune reaction are represented in the above chart. The major players of the innate immune response are the phagocytes (macrophages and neutrophils), basophiles, dendritic cells, mast cells and Natural killer (NK) cells. In the adaptive community, T lymphocytes play a major part in protecting the body from infections. The images and the other sub-categories represent the structure and some important properties that describe the role of innate and adaptive immune cells. \* represents that Macrophage possess alternative names in different organs like kuffer cells (liver), microglial cells (neural tissue), histiocytes (connective tissue), epithelioid cells (granulomas), mesangial cells (kidney), osteoclasts (bone) and dust cells (within pulmonary alveolus) (Marshall et al., 2018).

The adaptive immune response is sub-divided into humoral and T-cell mediated or cellular immunity. In humoral immunity, the B-cell antigenic receptor encounters an antigen, gets activated, and differentiates into plasma cells that secrete specific antibodies. These antibodies neutralize the toxic nature of pathogens and thereby inhibit their effect. The antibodies can also activate the complement proteins that can directly kill bacterial cells (Figure 3) (Janeway et al., 2001). T lymphocytes or T cells are the major players of cellular immunity. These cells were named after the organ they first produced, namely the thymus. T cells eliminate infections using their antigenic receptors which recognize antigens presented as peptides on antigen-presenting cells (APC) namely dendritic cells, macrophages, and B cells (Murphy, 1996).

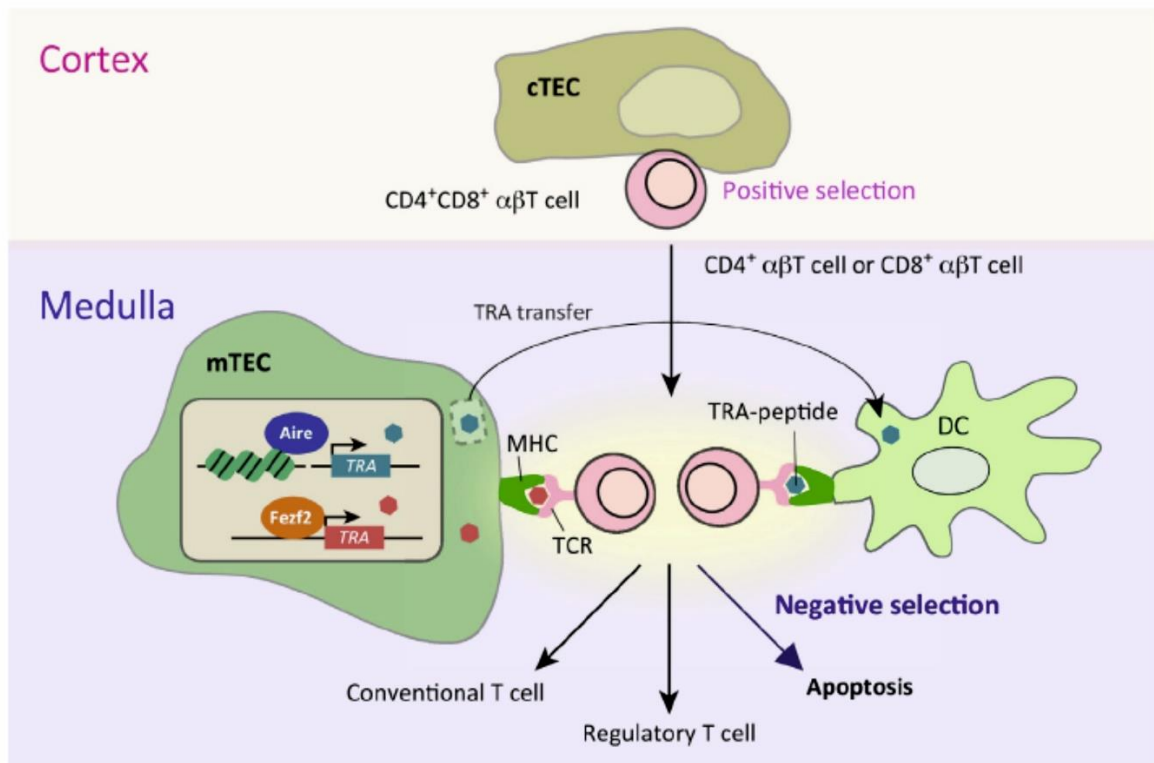


**Figure 3: The branches of humoral and cellular immune response**

Infections caused by viruses, bacteria and any foreign bodies leads to activation of humoral and cell-mediated immune reactions. The B-cell lineage of lymphocytes belongs to the humoral branch which initiates the process. When a B-cell receptor (BCR) encounters an antigen, the B-cell differentiates to plasma cells that produce antibodies that act as effector molecules neutralizing the antigenic effect. The key effectors of the cellular response are the T-cell lineage consisting of T-helper (Th) cells and cytotoxic T cells (CTL). The T lymphocytes recognize antigens presented on the respective MHC class of molecules on the surface of antigen presenting cells (APC) and secrete toxic substances like cytokines and granzymes that kill pathogen-infected cells (Barcena and Blanco, 2013).

### 1.3 T Lymphocytes: Maturation and activation

T lymphocytes are formed from haematopoietic stem cells that reside in the bone marrow. These precursor cells migrate and localize in the thymus and therefore are called thymocytes or T lymphocytes. In order to become mature lymphocytes, these precursor cells that express different cell surface markers have to undergo a series of maturation steps (Nandi et al., 2020). The thymus is divided into different lobes namely an outer cortical region and an inner medulla. The functional maturation of the thymocytes is characterized by the expression of the T-cell receptor ( $\alpha$  and  $\beta$  chains) and cell-surface proteins like the CD3 complex and co-receptors namely CD4 and CD8. Expression of these receptors in different combinations acts as markers for further differentiation and selection of these thymocytes. At the earlier stage, the thymocytes are termed double negative (DN) cells, as they lack the expression of both CD4 and CD8 co-receptors. The DN cells further differentiate and develop forming mainly the  $\alpha:\beta$  T-cell lineage and are called 'double-positive' (DP) thymocytes ( $CD4^+ CD8^+$ ). These DP cells move deep into the thymic cortex and are challenged with self-antigens presented by the MHC-I and MHCII complex expressed on the surface of cortical thymic epithelial cells (cTEC). The thymocytes that can positively interact with these MHC complex survive the selection process and the others that cannot interact undergo apoptosis. This process is termed positive selection. During this stage, The DP cells are divided into  $CD4^+$  helper T cells ( $CD4^+CD8^-$  and interact with MHC-II complex) and  $CD8^+$  cytotoxic T cells ( $CD4^-CD8^+$  and interact with MHC-I complex) (Takahama, 2006). The thymocytes that survive positive selection migrate to the thymic medulla where they are again presented with self-antigen by MHC complex molecules on medullary thymic epithelial cells (mTEC). In order to have a checkpoint on auto-immunity, negative selection of the thymocytes is performed where cells that interact strongly with self-antigens are eliminated by apoptosis. The cells that survive this process now are free to exit the thymus and enter the secondary lymphoid organs as mature naïve T cells and thus contribute to further immune surveillance (Weinreich and Hogquist, 2008) (Figure 4).



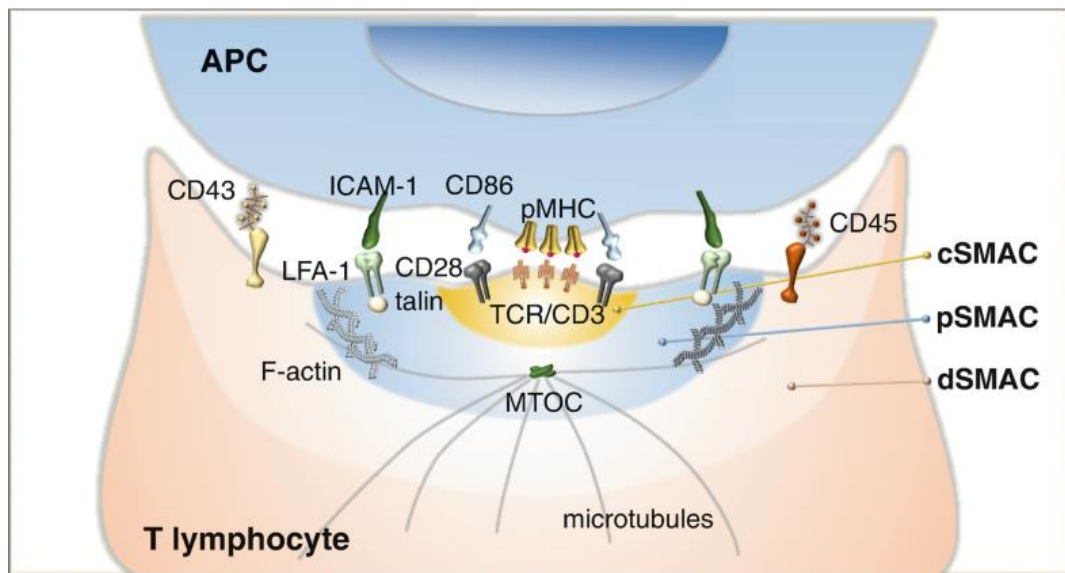
**Figure 4: Positive and negative T cell selection in the thymus**

Bone marrow derived thymocyte precursors migrate to the thymic cortex and interact with cortical thymic epithelial cells (cTECs). Based on the CD4 and CD8 T cell receptor (TCR) expression, the thymocytes interact with self-peptide MHC complexes. Thus, the cells that survive the positive selection process differentiate to either CD4 or CD8 single positive T cells that migrate to thymic medulla where they interact with medullary TECs (mTECs) that present the peptide of tissue-restricted antigen (TRA). Most of the self-reactive T cells are eliminated by negative selection and undergo apoptosis while some differentiate to conventional and regulatory T cells (Takaba and Takayanagi, 2017).

### 1.4 Cytotoxic T Lymphocytes: The Immunological synapse

The migrating cytotoxic T Lymphocytes (CTL) encounter virus-infected, allograft cells and cancerous targets for programmed cell death thereby maintaining proper immune response. They are incapable of detecting free antigens and thus need the help of antigen-presenting cells (APC) to exhibit infectious target peptides on their MHC-II complex to the TCR complex present on the surface of CTLs. Once the MHC peptide (MHCp)-TCR binding occurs, an immunological synapse (IS) is formed between the CTL and target cell, leading to a series of signalling processes for the lysis of the target cells (Groscurth and Filgueira, 1998). The CTLs are termed killer cells as they contain specialized lysosome-related organelles (LRO) called cytotoxic or lytic granules that contain toxic luminal proteins namely perforin and granzymes. These proteases are released from the CTL into the IS where they are taken up by the target cells thereby activating the caspase-mediated apoptotic pathway (Luzio et al., 2014). A minor killer pathway used by these killer cells includes the Fas ligand (FasL)-mediated apoptosis of target cells (Hassin et al., 2011).

The immunological synapse (IS) formed between CTL and APC is the main step in the activation of the killer cell. The IS formation is a well-organized bull's eye structure and the contact area is segregated laterally to form different patterns of activation complexes called supramolecular activation clusters or SMACs that determine the strength of downstream processes (Mongs et al., 1998). The central SMAC (cSMAC) is concentrated with TCR complex and is surrounded by peripheral SMAC (pSMAC) which contains the integrin protein LFA-1 (Lymphocyte function-associated antigen 1) which interacts with ICAM-1 (Intercellular Adhesion Molecule 1) present on target cells. The distal SMAC (dSMAC) is important for the active membrane movement that is concentrated with dynamic actin network and enriched with transmembrane tyrosine phosphatase CD45. This segregation is important for the priming response received by the T cell and the effector function that follows in sending important signalling for target cells death. The cSMAC acts as a site for receptor internalization and initiation of signalling processes and the pSMAC functions as a sealing ring that prevents the leakage of secreted molecules into the surrounding medium (Dustin et al., 2010; Onnis et al., 2019). Thus, IS formation plays a key role in the process of CTL activation (Figure 5).



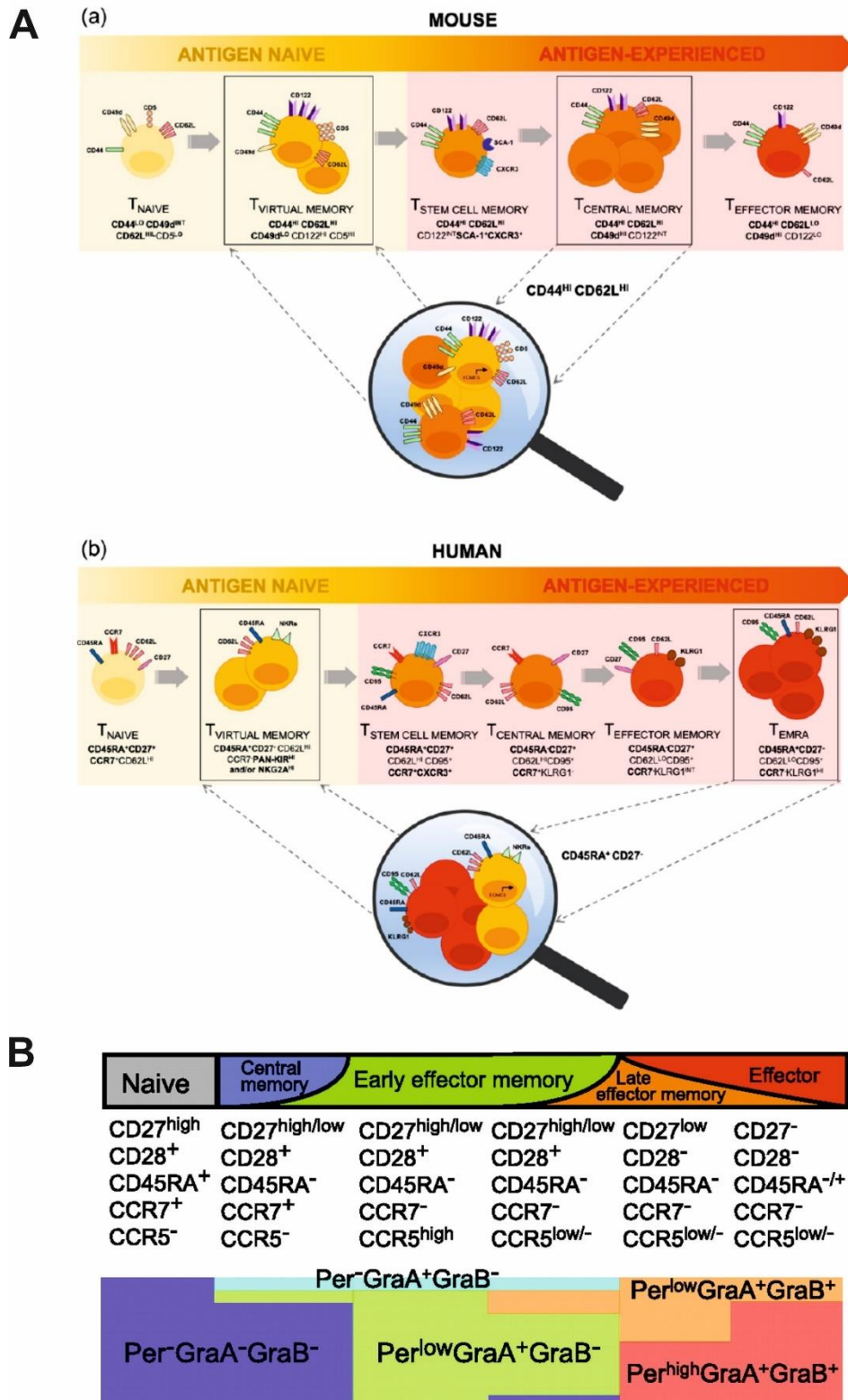
**Figure 5: Cytotoxic T cell immunological synapse architecture**

The image represents the different patterns of SMAC formation at the IS. The receptor-ligand pairs and signalling proteins involved in the immunological synapse (IS) formation between T cell and antigen presenting cell (APC) is shown here. The TCR/CD3 complex along with CD28 are enriched and aggregated to the central SMAC (cSMAC). The activation of various signalling proteins leads to drastic changes in the cell, like the rearrangement of adhesion molecules which are segregated to the peripheral supra molecular activation cluster (pSMAC) and enrichment of F-actin in the distal SMAC (dSMAC). The microtubule-organizing center (MTOC) then reorients toward the T lymphocyte-APC contact zone, thus activating the movement of cytotoxic granules to the secretory domain (Capitani et al., 2021).

## 1.5 The effector and memory subsets of CD8<sup>+</sup> T lymphocytes

Upon recognition of its cognate antigen the naive resting CD8<sup>+</sup> T lymphocyte (T<sub>N</sub>) is activated and differentiates to an effector T cell population (T<sub>eff</sub>). When an effector cell re-encounters an APC and performs antigen clearance a conventional memory T cell population (T<sub>MEM</sub>) remains. T<sub>MEM</sub> cells consist largely of the effector memory T cells (T<sub>EM</sub>) which mostly reside in tissues and are important for rapid effector function. The other population of memory cells found in the lymph nodes is the central memory cells (T<sub>CM</sub>) which are normally dormant but possesses a high antigen-specific response when they encounter the same antigen again, and are the hallmark of adaptive immunity.

In mouse, the characteristic feature of the memory T cell subsets is marked mainly by the presence of surface activation and homing receptor markers (CD44 and CD62L) that determine the different population of CD8<sup>+</sup> cells. First, the naïve CD8<sup>+</sup> T cells express high lymph node homing CD62L receptors on the surface (CD62L<sup>high</sup> CD44<sup>low</sup>). During initial activation, the naïve cells differentiate into effector cells losing the expression of both CD44 and CD62L (CD62L<sup>low</sup> CD44<sup>low</sup>) and on further differentiation, regain the receptors to form memory possess T cells. The T<sub>EM</sub> possess CD62L<sup>low</sup>CD44<sup>high</sup> markers and the T<sub>CM</sub> possess CD62L<sup>high</sup> and CD44<sup>low</sup> surface markers. In humans the T<sub>MEM</sub> population is characterized by the presence of markers, namely CD45RA and CD27 (Thiele, 2020) (Figure 6A). The major cytotoxic effector molecules stored in the lytic granules, namely Granzyme A, B and perforin, also differ in their expression level in the different T cell subsets. Studies from several healthy donors show that all three effector molecules are absent in naïve CD8<sup>+</sup> T cells (Per<sup>-</sup>GzmA<sup>-</sup>GzmB<sup>-</sup>) and after differentiation, the different T cell subsets undergo the following pathway of expression that is Per<sup>-</sup>GzmA<sup>+</sup>GzmB<sup>-</sup>, Per<sup>low</sup>GzmA<sup>+</sup>GzmB<sup>-</sup>, Per<sup>low</sup>GzmA<sup>+</sup>GzmB<sup>+</sup>, Per<sup>high</sup>GzmA<sup>+</sup>GzmB<sup>+</sup> (Takata and Takiguchi, 2006; Chattopadhyay et al., 2009) (Figure 6B).



**Figure 6: Cell surface markers and cytolytic effector molecules of CTL subsets**

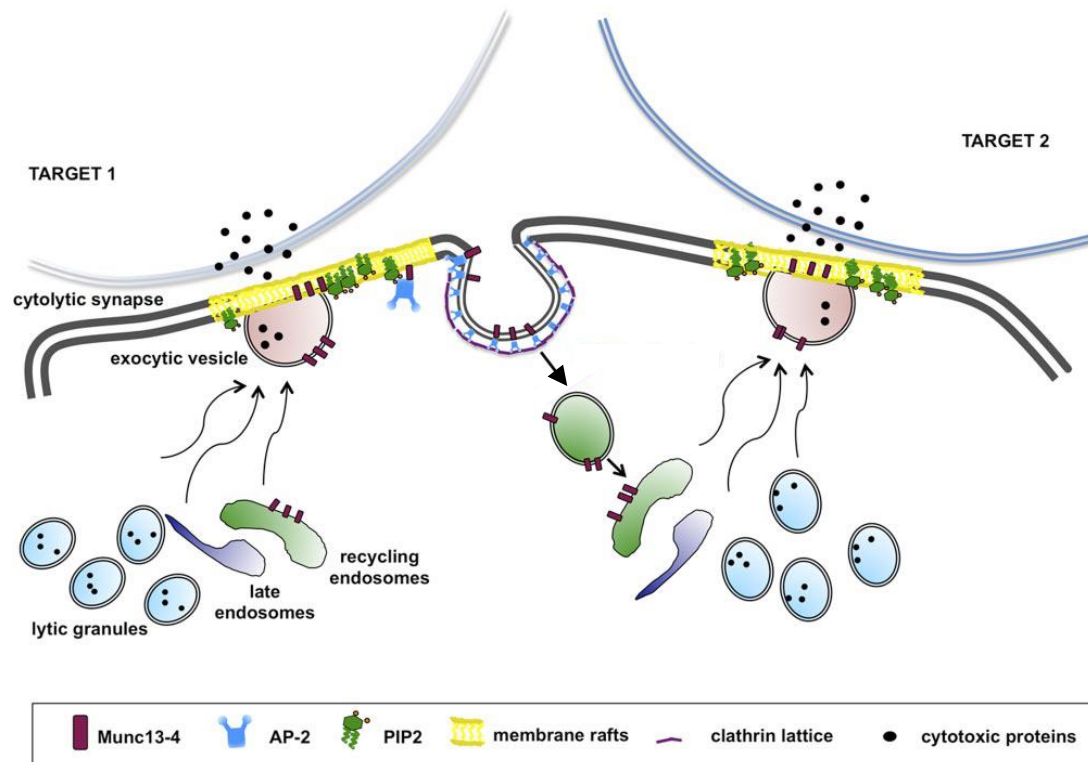
(A) Naive CD8<sup>+</sup> T cells undergo activation and differentiation into effector and memory subsets that are marked by the expression of the major homing receptors on the surface like in (a) mouse by the presence of CD44 and CD62L and (b) humans by presence of CD45RA and CD27 (Thiele D, 2020) (B) The important differentiating feature of different CD8<sup>+</sup> T cell population is the expression of cytolytic effector molecules of the CGs namely Perforin (Per), Granzyme A and B (GraA and GraB) that determine the killing efficacy of the subsets. The table represents different human CD8<sup>+</sup> T cell subsets in various colour codes that contains different combination of effector molecules (Takata and Takiguchi, 2006)

## 1.6 Lytic granule exo- and endocytosis

Granule-mediated cytotoxic release by T lymphocytes and Natural killer (NK) cells is an important effector pathway in host defense and immune regulation. Cytotoxic granules are specialized secretory lysosomes that store toxic molecules including the pore-forming perforin and serine proteases (granzymes) that are exocytosed upon TCR activation into the IS formed between the target cells. These toxins have pro-apoptotic properties that trigger caspase-dependent and -independent apoptosis of targets (Trapani, 2012).

The lytic granule fusion pathway involves several maturation steps for the exocytotic transport of vesicular structures and soluble N-ethyl-maleimide-sensitive attachment protein receptor (SNARE) - mediated vesicle membrane fusion at the IS. During synaptic cleft formation, rapid re-orientation of MTOC (microtubule-organizing centre), cytotoxic granule movement towards the IS and granule docking, priming and fusion at specialized secretory domains are pre-requisites for proper polarization and release of vesicular content to the target cells (de Saint Basile et al., 2010). Following exocytosis, the plasma membrane recovers and the membrane proteins that were added during lytic granule exocytosis are recycled back by a process called endocytosis (Saheki et al., 2012). The entire process of CG exo- and endocytosis was shown to be calcium ( $\text{Ca}^{2+}$ ) dependent and is a rapid process with a requirement of just one to two granules fused at the synaptic zone occurring within 15 minutes (Chang et al., 2016). CTLs and NK cells were not only known as killer cells but were proudly termed serial killers since they successively lyse several target cells in a short time. The two factors that are important for the advanced killing is that 1) during target recognition, only a fraction of the vesicle pool is released and 2) endocytosis of the membrane leads to newly synthesized cytotoxic proteins and refilling of the toxic content for multiple target cell lysis (Capuano et al., 2012) (Figure 7).





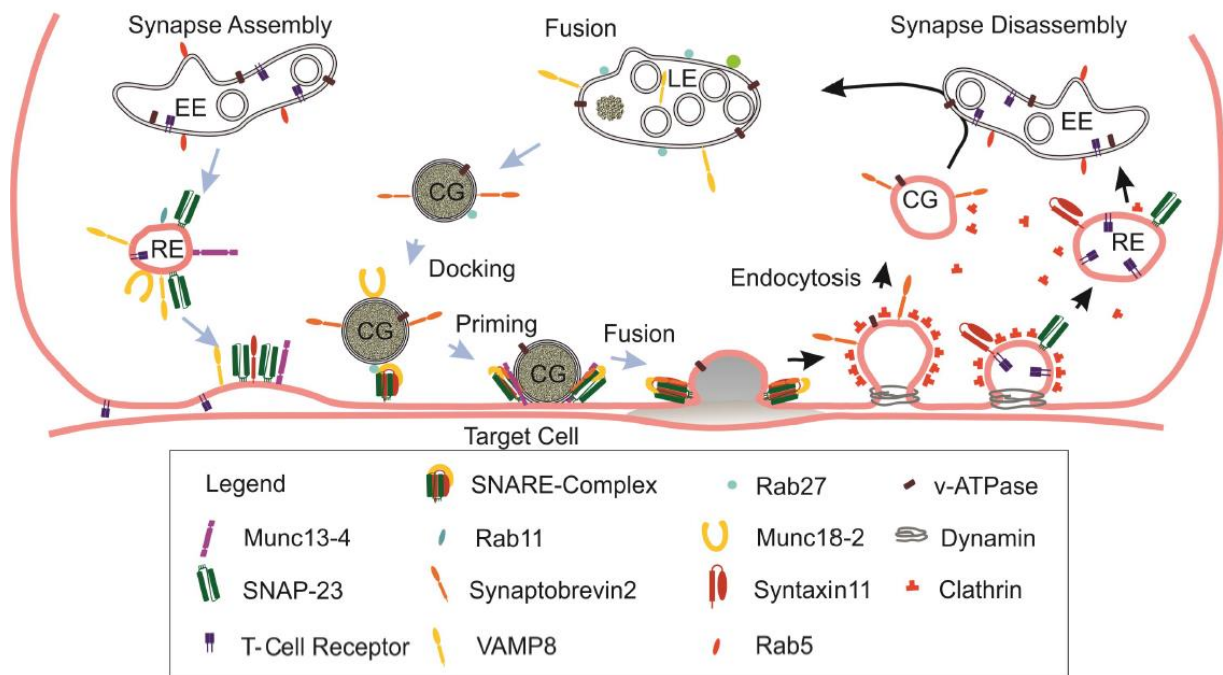
**Figure 7: Endocytic recycling of proteins is necessary for serial killing ability of cytotoxic cells**

Schematic representation of one cytotoxic cell that can subsequently kill multiple targets is shown. Cytotoxic synapse formation with target cells leads to CG exocytosis and release of granular contents that aim in killing the first target cell. One of the proteins involved in the exocytotic machinery is the Munc13-4 that gets transiently integrated to the membrane rafts during granular exocytosis followed by subsequent clathrin/AP2 mediated endocytosis and refilling of the granular content for the next round of killing with the second target cell (Figure modified from Capuano et al., 2012).

## 1.7 Proteins involved in the exo-endocytic machinery

Exocytosis and endocytosis are strongly inter-related membrane trafficking pathways that retain the surface area and composition of the plasma membrane. The two processes maintain the flow of material to and from the cell surface (Gundelfinger et al., 2003). Several studies in neuronal, cytotoxic T and NK cells have shown the presence of different classes of secretory lysosomes that might represent the different maturation stages of these granules. The secretory lysosomes are known to be precursor organelles that contain specific membrane proteins and effector molecules from the trans-Golgi network (TGN) and endosomal compartments (Benado et al., 2008). Initially, recycling endosomes containing the membrane proteins Rab11 and Munc13-4 merge with the late endosomes which contain Rab7 and Rab27a to form an exocytotic endosome or recycling endosomes (RE) (van der Sluijs et al., 2013). These REs containing the Syntaxin11 and vesicular SNARE (v-SNARE) protein VAMP8 are the first to arrive at the IS and undergo VAMP8-

mediated fusion in complex with the target SNAREs (t-SNARE) Syntaxin 4 and SNAP23. The fusion of REs is necessary for the transport of cargo proteins namely syntaxin11 into the plasma membrane which is later needed for the docking, priming and fusion of lytic granules (Marshall et al., 2015). The mature secretory lysosomes or cytotoxic granules are marked by the presence of surface LAMP1 protein and luminal proteins namely perforin, granzymes and serglycins. These granules also contain the v-SNARE synaptobrevin-2 which forms a complex with syntaxin11 and SNAP-23 necessary for the fusion and exocytosis of vesicular contents with the plasma membrane (Matti et al., 2013) (Figure 8). Loss of perforin or the SNARE proteins Munc13-4 and syntaxin11 causes severe immune disease, familial hemophagocytic lymphohistiocytosis (FHL) type1, 3 and 4 which are characterized by uncontrolled T cell proliferation, macrophage activation and hypercytokinemia (Gholam et al., 2011).



**Figure 8: Proteins involved during synapse assembly and disassembly in cytotoxic T cells**

IS assembly begins with the fusion of recycling endosomes (RE) carrying the SNARE protein VAMP8 that mediates fusion with the cytotoxic cell membrane. RE aids in delivering SNARE proteins needed for CG docking, priming and fusion. Following CG exocytosis, endocytosis of CG membrane proteins occurs via dynamin and clathrin/AP2 pathway and subsequent movement and refilling of the granular contents occurs in the cytosol (Figure modified from Rettig and Stevens, 2017)

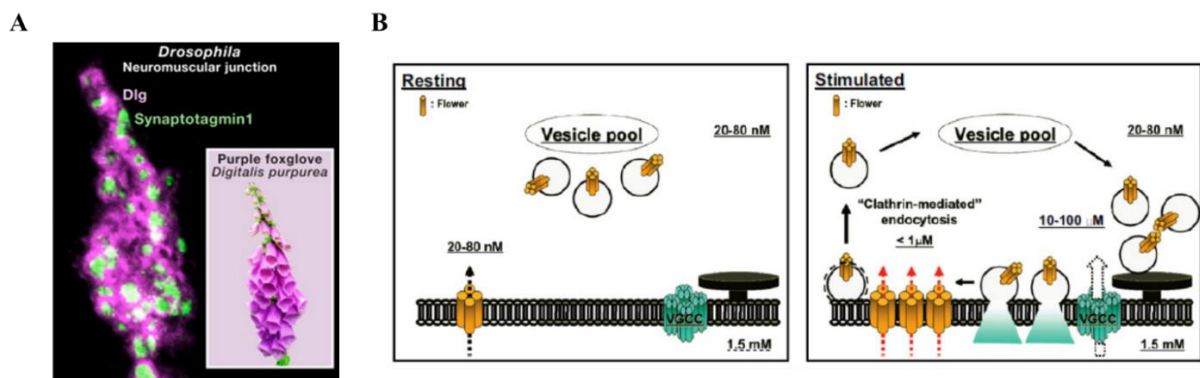
Following exocytosis, the internalization of SNARE protein synaptobrevin2 (Chang et al., 2016) and other CG membrane component like the H<sup>+</sup> V-ATPase via clathrin /AP2 (adaptor protein2) dependent pathway was shown to be important for the second round of the killing process. The CG components endocytosed at the synaptic zone were also shown to be dependent on dynamin and synaptobrevin-2 specific adaptor protein, CALM (Clathrin assembly lymphoid myeloid leukemia) (Koo et al., 2011). The endocytosed CGs are then re-acidified and merges with the late endosomes via the early endosomal pathway, where the lumen of the CGs are refilled with Granzyme B. Thus, the endocytosis of CG components is independent from the recycling endosomal protein pathway, like the TCR and other SNARE proteins. The entire process of CG membrane protein endocytosis is rapid and the cytotoxic cells thereby acquire full killing capacity for new IS formation and APC recognition (Chang et al., 2016) (Figure 8).

### **1.8 Flower protein: Regulator of calcium mediated endocytosis**

Coupled exo-endocytosis of synaptic vesicles is a well-studied mechanism to understand the neurotransmitter release at the presynaptic nerve terminals. The entire process was shown to be Ca<sup>2+</sup> dependent. The intracellular Ca<sup>2+</sup> concentration was shown to be much lower for the initiation of synaptic vesicle (SV) endocytosis than that which triggers SV exocytosis (Cousin and Robinson, 2000; Marks and McMahon, 1998). During nerve stimulus, voltage-gated Ca<sup>2+</sup> channels (VGCC) are activated by membrane depolarization that increased the local intracellular Ca<sup>2+</sup> concentrations to initiate and trigger SV exocytosis (Catterall and Few, 2008; Adler et al., 1991; Heidelberger et al., 1994). However, the role of Ca<sup>2+</sup> in triggering endocytosis remained ambiguous (Leitz and Kavalali, 2016; Maritzen and Haucke, 2018). During the time course of endocytosis, extracellular Ca<sup>2+</sup> modulates the process in VGCC independent manner (Sankaranarayanan and Ryan, 2001) and Calmodulin might function as a high affinity sensor for endocytosis (Cousin, 2000). Some data also showed the importance of high calcium for the Ca<sup>2+</sup>/calmodulin-dependent phosphatase, Calcineurin, to form a complex with Dynamin to promote endocytosis (Lai et al., 1999). These above studies suggest the role of an unknown Ca<sup>2+</sup> channel that might specifically regulate the coupled exo-endocytosis at the synapse.

In 2009, Chi-Kuang Yao and his group reported the identification of a previously uncharacterized protein that when absent affects endocytosis. The study was done in the model organism fruit fly, *Drosophila melanogaster*, where a genetic screen was performed to identify novel proteins that might affect synaptic transmission. Mutants of one lethal complementation group (3L5) consisting of two alleles, DB25 and DB56, were identified to be lethal. They identified 3L5 as a gene encoding a protein about 190 amino acids long with three or four transmembrane domains, CG6151-P, with three potential alternatively spliced isoforms, CG6151-RA, -RB, and -RC (Tweedie et al., 2009) and the three splice variants showed major difference at the C-termini. CG6151-P was seen to be evolutionarily conserved from fungi to human with an unknown

function exhibiting 39% and 61% similarity between amino acids 25 and 150 of the fly, mouse and human homologues. Some conserved protein members were annotated as putative clathrin-coated vesicle proteins but this could not be defined (Lu et al., 2020). The group later showed that the protein encoded by CG6151 localizes to synaptic vesicles and pre-active zones. DB25/25 and DB25/56 mutations displayed numerous extra boutons at the neuromuscular junctions of fruit fly which were often small, clustered, and flowery in nature. The group therefore named the gene *Flower*. Loss of *Flower* was shown to display features of endocytic mutants that include enlarged SVs, a decrease in FM1-43 dye uptake, a decrease in neurotransmitter release upon repetitive stimulation, and a pile-up of endocytic intermediates. Clustal analysis of the protein displayed a 9 amino acid motif in the second transmembrane region that showed homology to VGCCs and selectivity filters of Transient Receptor Potential channels (TRPV5 and 6) (Yao et al., 2009) (Figure 9).



**Figure 9: Flower phenotype and exo-endocytosis coupling at the presynaptic terminal**

(A) Staining of the *Drosophila* neuromuscular junction in CG6151 loss-of-function mutants shows the localization of Synaptotagmin1 (green), a presynaptic marker, in an unusual flower-like appearance with the post-synaptic marker Discs large (Dlg, magenta). The pattern resembles the classical purple foxglove (*Digitalis purpurea*, inset) and so the gene was named Flower (Yao et al., 2009; Brose et al., 2009) (B) Schematic model depicts the integration of Flower protein upon SV exocytosis and its accumulation at the pre-active zone, the site for endocytosis. The homomultimeric Flower complex thus triggers  $\text{Ca}^{2+}$  influx regulating resting intracellular  $\text{Ca}^{2+}$  levels and SV-associated protein endocytosis and is thereby removed from the cell membrane (Yao et al., 2009)

The group of Chi-Kuang Yao later in 2017, reported the function of Flower in clathrin-mediated (CME) and activity-dependent bulk (ADBE) endocytosis. Upon SV fusion, Flower is incorporated into the active zone membrane, where during mild stimulus, Flower stimulates CME and on strong stimulus promotes ADBE. Thus, the strength of stimulus decides the two different modes of the endocytic pathway that is triggered by Flower protein. The study also showed that Flower controls CME independent of  $\text{Ca}^{2+}$  channel activity while ADBE was triggered mainly upon  $\text{Ca}^{2+}$  influx (Yao et al., 2017).

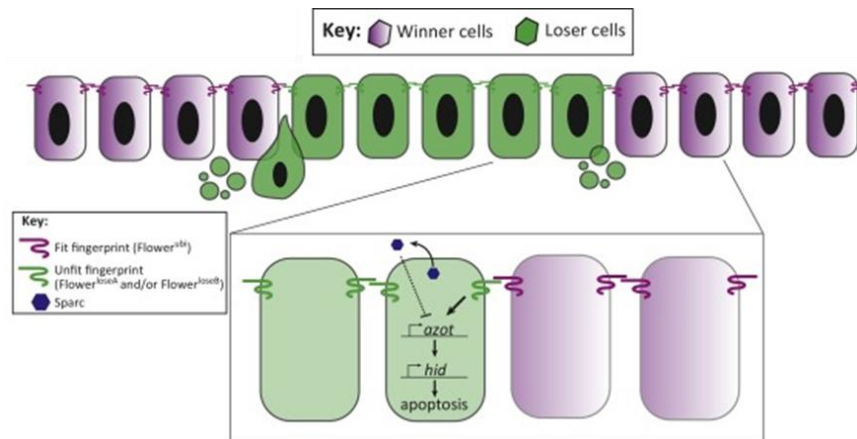
An independent study (Chang et al.,2018), showed that the mouse homologue of Flower (the longer isoform of 171aa) was expressed in mouse CTLs and localized to intracellular vesicles. To understand the function of Flower protein, real-time imaging was done on Flower knock-out (Fwe KO) CTLs that showed a block in CG endocytosis at an early stage. However, no defect in IS formation and CG exocytosis was seen. Upon re-introduction of Flower construct or increase in extracellular  $Ca^{2+}$ , endocytosis was rescued. A Flower mutant (WWYXX $\phi$ ) lacking binding sites for the endocytic adaptor AP-2 protein failed to rescue endocytosis, elucidating the importance of Flower protein in CG endocytosis of mouse CTLs (Chang et al., 2018).

## 1.9 Flower in health and disease

All organisms are prone to external insults and stress factors in their development and adult life that can affect cell survival leading to various diseases. Throughout the developmental process, a balance between survival and death of cells in every tissue marks the health status of an organism. The term 'survival of the fittest' not only fits at the individual level but also applies for heterogeneous cell population, where cells with reduced fitness are eliminated from the tissue by cells with stronger fitness level. This mechanism of cell-cell interaction and survival process is called cell competition. The concept of cell competition was first studied in late 1970s, where Morata and their group created clones to understand the different growth rates in the surrounding tissues of drosophila imaginal wing disc. The study was done using genetic mosaics for a class of mutations in the Minute genes (Morata, 1975). Later it was shown that the Minute genes encode for ribosomal proteins, and mutations of this gene is lethal and the viable heterozygous animals displayed a developmental delay due to slower rate of cell proliferation (Moreno et al., 2002). The same phenomenon was later studied by the group of Eduardo Moreno in 2010, where they describe that the cells of the multicellular organ are tagged and marked by an extracellularly exposed 'Flower code' (Figure 10). The cells of drosophila imaginal wing discs were shown to express three Flower isoforms termed dFwe<sup>Ubi</sup>, dFwe<sup>LoseA</sup> and dFwe<sup>LoseB</sup> (the earlier described CG6151 isoforms).

dFwe<sup>Ubi</sup> expressing cells were translated as cells with intact cellular fitness whereas LoseA and LoseB coded cells were weak and eliminated. The difference in Ubi and Lose isoforms was the variable C-termini that made the Lose cells real losers and formed an eat me signal when present in an environment among Ubi expressing cells. The study thus showed that the Flower code was critical and was used as a mechanism by drosophila imaginal disc epithelial cells to recognize and eliminate slow dividing cells by programmed cell death. It is also to be noted that LoseA and LoseB expressing cells in an environment among other Lose expressing cells survive and do not undergo cell death. Thus, the fit cells were termed winners that eliminated the losers by activating caspase mediated cell death and final engulfment. The homeostasis of the tissue is well maintained as the winner cells undergo proliferation and maintain the normal environment of the organ (Rhiner et al., 2010). In drosophila neurons, the cell win/lose phenotype were shown to be

maintained in a similar manner by the Flower code but competitive cells with Ubi and LoseA survived and the LoseB cells were culled and destroyed (Merino et al., 2013). Recent reports showed the function of Flower in neurodegenerative disorder, Alzheimer's disease, where Flower code helps in identifying least fit neurons in amyloid- $\beta$ -transgenic flies through cell competition (Coelho et al., 2018). All the above studies thus indicate that the Flower protein acts as a fitness fingerprint during cell competition (Rhiner et al., 2010).

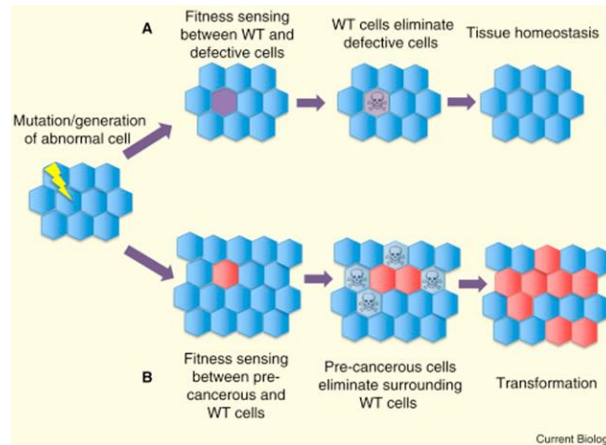


**Figure 10: Determination of cell fitness by the Flower code**

The fitness fingerprint encoded by the Flower protein on the cell surface marks a cell as winner (Flower Ubi) or loser (Flower LoseA/LoseB). In a tissue, when the winner and loser cells are in close contact, the signalling from the winner cell causes the transcription of *azot* protein and pre-apoptotic marker *hid*, leading to triggering of apoptosis. Thus, the loser cell is eliminated and the winner cell proliferates to claim its place in the surrounding environment (Moreno et al., 2016).

Imbalance in the cell fitness mechanism is normally caused during aging, cancer, and metastasis. In this context, the mammalian homologue of drosophila Flower was studied in depth to understand the function of Flower in cancer development. The mouse Flower gene encodes six splice variants which are then translated into four protein isoforms. The function and the characterization of these isoforms was studied by Petrova et al., where they showed that the four isoforms were expressed in low levels in adult tissues. The group generated a constitutive Flower knock-out mouse to study the function of Flower in skin papilloma. Results from their work showed that the expression of mouse Flower isoforms increased in cells surrounding the skin tumour environment and the Flower knock-out mice developed normally and were resistant to chemically induced skin cancer. This study suggests that Flower might be used as an early biomarker for skin cancer detection as mouse Flower promotes the expansion and proliferation of pre-cancerous cells (Petrova et al., 2012).

A role for Flower to function in cell competition in humans has recently been proposed. The human Flower isoforms 1 and 3 were designated as Lose forms and isoforms 2 and 4 as Win forms. Human cancer cells were shown to express Win forms that proliferate and expand in the presence of lose expressing stromal tissue, providing a competitive advantage to the cancer cells (Figure 11). Loss of Flower was shown to reduce the tumour growth and metastasis and induced higher sensitivity to chemotherapy (Madan et al., 2019).



**Figure 11: Survival of the fittest selection during tissue homeostasis and Cancer**

(A) Model depicting the maintenance of tissue homeostasis by identification, selection and elimination of less fit, defective cells by wild-type cells (B) Pre-cancerous cells in a tissue transform, progress and survive by detecting and signalling the apoptosis of less- fit WT surrounding cells and thereby eliminating them. Higher proliferation of the cancerous cells leads to tumour progression and metastasis (Gil et al., 2016).

Though the above experiments and studies indicate a role of Flower in the endocytic pathway and as a fitness marker, mechanistically it is still unknown how Flower splice variants signal for survival and death, or how or if the cell competition function is linked to the Flower function in endocytosis. These questions brought us to the aim of my present study to investigate the role of different Flower isoforms in endocytosis of CG material Synaptobrevin-2, in mouse CTLs and whether this process is linked to cell competition.

## 2. Aim of the study

Exo- and endocytosis are fundamental events in all cells. Both these events are highly dependent on each other as several proteins interplay and contribute to the dynamic function in different cell types. A transmembrane protein, Flower (Fwe), was shown to be associated with synaptic vesicle endocytosis in neurons (Yao et al., 2009) and its importance in activity-dependent and bulk endocytosis was shown previously (Yao et al., 2017). The immunological synapse (IS) between T cells and antigen-presenting cells is the focal point for exocytosis of cytotoxic granule contents leading to target cell lysis. Following exocytosis, endocytosis of cytotoxic granule membrane proteins, and subsequent refilling of the granular contents is a requirement for serial killing of target cells (Chang et al., 2016).

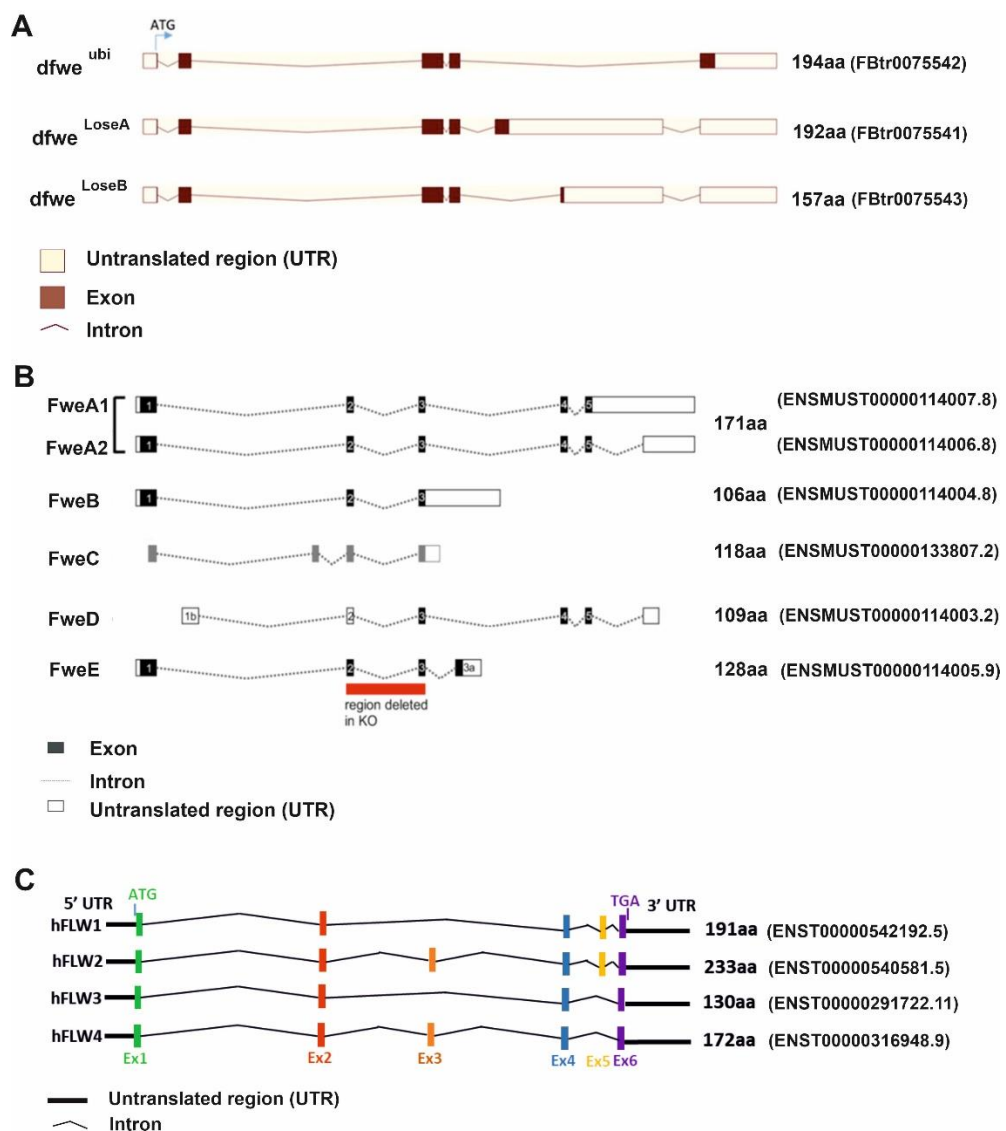


Figure 12: Overview of Flower splice variants from drosophila (A), mouse (B) and human (C)



In this study, the aim was to investigate the function of Flower splice variants during endocytosis in several species (*Mus musculus*, *Homo sapiens*, *Drosophila melanogaster*) (Figure 12). The main approach was by using CTLs from a Flower KO mouse strain and by overexpressing Flower isoforms and mutants of Flower in order to rescue the KO phenotype. Moreover, by a combination of mutation studies and state-of-the-art microscopy, questions about topology and localization of Flower could be addressed.

### 3. MATERIALS AND METHODS

#### 3.1 Materials

##### 3.1.1 Chemicals

**Table 1: Common Reagents and Chemicals**

<b>Product</b>	<b>Supplier (Catalogue Number)</b>
Agarose	Roth (5210.3)
Ammonium persulphate	Bio-Rad (1610700)
Bromophenol blue	Roth (A512.1)
BSA	Sigma-Aldrich (A4503)
Chloroform	Sigma-Aldrich (288306)
D-Biotin	Sigma-Aldrich (B4501)
Dimethyl sulfoxide (DMSO)	Sigma-Aldrich (D8418)
dNTP-Mix	Fermentas (R0192)
Ethidium bromide (EtBr)	Roth (2218.2)
Ethylenediamine tetra acetic acid disodium salt (EDTA)	Sigma-Aldrich (E6635)
Glucose	Merck (1.08342.1000)
Glutamax	Thermo Fisher Scientific (35050061)
Heat inactivated Bovine Serum (FBS)	Gibco (10500)
HEPES	Thermo Fisher Scientific (15630080)
HPLC water	Thermo Fisher Scientific (11307090)
Hydrochloric acid	Merck (9057.1000)
Isopropanol	Roth (AE73.1)
Kanamycin	Sigma-Aldrich (K-1377)
KCl	Merck (1049360500)

L-Glutamine 200 mM (100X)	Gibco (25030-024)
NaCl	Merck (1064040500)
Paraformaldehyde	Merck (1040051000)
Penicillin/Streptomycin (Pen/Strep)	Gibco (15140122)
pfu-Polymerase	Fermentas (EP0501)
Phusion High-Fidelity DNA polymerase	Thermo Fisher Scientific (F530L)
Poly-L-ornithine	Sigma-Aldrich (P4957)
Sterile Water	Sigma-Aldrich (W4502)
Tris-hydrochloride	Roth (9090.3)
Triton X-100	Sigma-Aldrich (T8787)
Trypan blue solution	Sigma-Aldrich (93595)
Tryptone/Peptone	Roth (8952.3)
Tween 20	Roth (2727.1)

**Table 2: Reagents and Chemicals for western blot**

Product	Supplier (Catalogue Number)
cOmplete mini, EDTA-free Protease Inhibitor Cocktail tablets	Roche (11836170001)
$\beta$ -Mercaptoethanol	Roth (4227.3)
Dithiothreitol	Sigma-Aldrich (10197777001)
Dodecylsulphate Na-salt in pellets (SDS)	Roth (2326.2)
Glycerol	Sigma-Aldrich (G5516)
Hybond N <sup>+</sup> nylon membrane	GE Healthcare (RPN119B)
Methanol (100%)	Roth (HN41.1)
NuPAGE LDS sample buffer 4X	Thermo Fisher Scientific (NP0007)
NuPAGE MES SDS Running Buffer 20X	Thermo Fisher Scientific (NP0002)
NuPAGE Transfer Buffer 20X	Thermo Fisher Scientific (NP00061)

Ponceau S solution 0,1%	Sigma-Aldrich (P7170)
PAGE ruler Prestained Protein Ladder	Thermo Fisher Scientific (26616)
Restore Western Blot Stripping Reagent	Thermo Fisher Scientific (21059)
Roti Nanoquant 5X	Roth (K880)
Spectra Multicolour Broad Range Ladder	Thermo Fisher Scientific (26634)
SuperSignal West Dura Extended	Thermo Fisher Scientific (34075)
SuperSignal West Pico Chemiluminescent Substrate	Thermo Fisher Scientific (34076)

**Table 3: Commercial Kits**

<b>Kits for molecular cloning</b>	<b>Company (Catalogue number)</b>
QIAquick PCR Purification Kit	Qiagen (28106)
QIAquick Gel Extraction Kit	Qiagen (28706)
Plasmid Midi Kit	Qiagen (10023)
Plasmid Mini Kit	Qiagen (27106)
EndoFree Plasmid Maxi Kit	Qiagen (12362)
<b>Kits for CD8<sup>+</sup> T cell isolation</b>	<b>Company (Catalogue number)</b>
Nucleofector kit for mouse T cells	Lonza (VVPA-1006)
Dynabeads <sup>TM</sup> FlowComp <sup>TM</sup> Mouse CD8 Kit	Thermo Fisher Scientific (11462D)
Dynabeads <sup>TM</sup> Mouse T-Activator CD3/CD28	Thermo Fisher Scientific (11453D)
CellTrace <sup>TM</sup> cell proliferation Kit	Invitrogen (C34554)
<b>Kits for transfection</b>	<b>Company (Catalogue number)</b>
Nucleofector kit for mouse T cells	Lonza (VVPA-1006)
Lipofectamine 3000	Thermo Fisher Scientific (L3000001)
<b>Kits for western blot</b>	<b>Company (catalogue number)</b>
NuPAGE <sup>TM</sup> 10% Bis-Tris Protein Gels, 1.0 mm, 10-well	Thermo Fisher Scientific (NP0301BOX)
NuPAGE <sup>TM</sup> 10% Bis-Tris Protein Gels, 1.5 mm, 10-well	Thermo Fisher Scientific (NP0315BOX)
NuPAGE <sup>TM</sup> 12% Bis-Tris Protein Gels, 1.0 mm, 10-well	Thermo Fisher Scientific (NP0341BOX)

NuPAGE™ 4-12% Bis-Tris Protein Gels, 1.0 mm, 10-well	Thermo Fisher Scientific (NP0321BOX)
<b>Labelling Kit</b>	<b>Company (Catalogue number)</b>
Alexa Fluor 647 Antibody labelling kit	Fisher scientific (A20186)

**Table 4: Antibodies**

Antibodies	Species	Dilution	Company (Catalogue number)
<b>Primary antibodies</b>			
Anti-HA	Rat	IHC 1:100 Western 1:5000	Roche (11867423001)
PE anti-mouse CD107a (LAMP-1, clone 1D4B)	mouse	FACS 1:400	Biolegend (121611)
Mouse anti-CD3ε (clone 145-2C11) (1mg/ml)	hamster	Coverslip (30 µg/ml) Live imaging (1:100)	BD Pharmingen (553057)
CA-Atto488 (1 mM stock)		ICC (500 nM)	Provided by Alexander Horn from the laboratory of Prof. Dr. Uli Kazmaier
CA-Silicon Rhodamine (SiR) (1 mM stock)		ICC (200 nM)	Provided by Alexander Horn from the laboratory of Prof. Dr. Uli Kazmaier
Alexa Fluor 647 anti-granzyme B (GB11)	rabbit	ICC 1:200	BioLegend (515405)
anti-GAPDH (clone 14C10)	rabbit	WB 1:5000	Sigma Aldrich (2118L)
Anti-Flower (polyclonal)	rabbit	ICC 1:100 Western 1:3000	Provided from AG Flockerzi
Anti-tRFP	rabbit	WB 1:1000	Evrogen (AB233)
DAPI		ICC 1:10,000	Thermo Scientific (10116287)
CD8-Alexa647	rat	ICC 1:200	Biolegend (100724)
GAPDH	rabbit	Western 1:5000	Cell signalling (14C10)
Anti-RFP	rabbit	Western 1:5000 ICC 1:1000	Genway (GWB-3BF397)
CD62L-FITC	rat	FACS 1:400	BD (553150)
CD44-APC	rat	FACS 1:400	eBioscience (17-0441)

CD25-PE	rat	FACS 1:200	BD (553866)
Purified TfR1 (CD71) (RI7217)	mouse	FACS 1:200	Biolegend (113802)
IgG2a (Isotype control)	Rat	FACS 1:200	R&D systems (MAB006)
Secondary antibodies			
Alexa 488 conjugated anti-rabbit IgG	goat	1:2000	Thermo Fisher Scientific (A27034)
Alexa 568 conjugated anti-rabbit IgG	goat	1:2000	Thermo Fisher Scientific (A-11011)
Alexa 488 conjugated anti-mouse IgG	goat	1:2000	Thermo Fisher Scientific (A28175)
HRP-conjugated anti-mouse IgG	goat	1:1000	Thermo Fisher Scientific (31430)
HRP-conjugated anti-rabbit IgG	goat	1:10,000	Thermo Fisher Scientific (31460)
HRP-conjugated anti-Rat IgG	goat	1:5000	GE healthcare (NA935V)
Anti-rat IgG2a, FITC	goat	1:400	Novus Biologicals (NB7124)

**Table 5: Media and solutions**

Media (Company (catalogue number))	Supplements
RPMI (for P815 cells) (GIBCO) (21875-034)	10% FCS, 50 $\mu$ M 2-Mercaptoethanol, 0.5% Pen/Strep, 10 mM HEPES
AIM V (for mouse primary CD8 <sup>+</sup> T cells) (GIBCO) (12055-091)	10% FCS, 50 $\mu$ M 2-Mercaptoethanol
DMEM (for HeLa cells)	10% FCS, 1% Pen/Strep
Erythrocyte lysis buffer (pH: 7.3)	H <sub>2</sub> O, 100 ml, NH <sub>4</sub> Cl, 0.829 g, (155 mM), KHCO <sub>3</sub> , 0.1 g, (10 mM), EDTA from 50 mM stock-260 $\mu$ l, pH 7.4 (0.1 mM) (Bzeih, 2016)
Isolation Buffer	PBS, 500 ml, BSA 0.5 g, (0.1%), EDTA from 0.5 M stock solution, 2 ml, (2 mM) (Bzeih, 2016)
Extracellular buffer for TIRF measurements	Composition
0 mM calcium buffer	155 mM NaCl, 4.5 mM KCl, 5 mM HEPES, 3 mM MgCl <sub>2</sub> , (pH: 7.4 and Osmolarity: 300-310 mOsm) (Bzeih, 2016)
10 mM calcium buffer	140 mM NaCl, 4.5 mM KCl, 5 mM HEPES, 2 mM MgCl <sub>2</sub> , 10 mM CaCl <sub>2</sub> (Bzeih, 2016)
Solutions for immunocytochemistry	Composition
Fixation	4% PFA in 1X D-PBS (NaOH-20 $\mu$ l, pH 7.4)
Quenching Solution	0.1 M Glycine (Glycine-0.375 g, PBS- 50 ml)
Permeabilization	0.1% Triton X-100 in D-PBS

Blocking	0.1% Triton X-100 in D-PBS+ 2%-5% BSA
<b>Solutions for western blot</b>	<b>Composition</b>
Lysis buffer	50 mM Tris-HCl (pH 7.5), 150 mM NaCl, 250 uM PMSF, 1% Triton X-100, 1 mM Deoxycholate, 1 mM EDTA, 1 mM DTT and 1 protease inhibitor tablet (Roche), and H <sub>2</sub> O
TBS (10X)	87.7 g NaCl, 24 g Tris-Cl (pH 7.5) and H <sub>2</sub> O up to 1 L
1X TBST (0.1 %) (1 L)	10x TBS-100 ml, Tween 20- 1 ml and H <sub>2</sub> O up to 1 L
1X TBS (1 L)	10x TBS-100 ml and H <sub>2</sub> O up to 1 L
MES running buffer (1X)	20x MES buffer – 50ml and water up to 1 L
Transfer buffer (1X)	20x Transfer buffer-50 ml and water up to 1 L
<b>Solutions for bacterial culture and cloning</b>	<b>Composition</b>
LB-Medium	Peptone-8 g, Yeast extract-4 g, NaCl-4 g, H <sub>2</sub> O-800 ml
Loading Buffer	Sucrose – 4 g, Bromophenol blue, Sigma H <sub>2</sub> O - 10 ml
<b>Y2H medium and solutions</b>	<b>Composition</b>
IPTG (Isopropyl β-D-1-thiogalactopyranoside)	0.1 M in dd H <sub>2</sub> O
Dropout Nitrogen Base Medium (Minimal medium) (DOB)	Clontech biosciences 27.0 g/l
Yeast selective medium -L medium -W medium -LW medium -ALWH medium	+0.69 g -Leu +DOB +0.74 g -Trp +DOB +0.64 g -Leu-Trp +DOB +0.6 g -Ala-Leu-Trp-His +DOB All the above medium was made up to 1litre with dd H <sub>2</sub> O and adjusted to pH 5.8
X-Gal solution	20 mg/ml in N, N Dimethylformamid (DMF)
X-Gal detection solution	350 µl X-Gal solution 150 µl β-Mercaptoethanol Make up to 10 ml with Z-Puffer
YPD-Medium (Clontech)	50 g YPD dissolved in 1litre of ddH <sub>2</sub> O. Autoclave
Z-Buffer	60 mM Na <sub>2</sub> HPO <sub>4</sub> 40 mM NaH <sub>2</sub> PO <sub>4</sub> 10 mM KCl 1 mM MgSO <sub>4</sub> 50 mM β-mercaptoethanol pH 7.0 Do not autoclave

### 3.1.2 Mounting medium

Mounting medium was produced by dissolving 6 g Glycerol, 2.4 g Mowiol 4-88 in 6 ml H<sub>2</sub>O and stirred for 2 h at room temperature. 12 ml of 0.2 M Tris-HCl buffer (pH 8.5) was then added and mixed at 53 °C overnight. The solution was then centrifuged at 1700 x g for 20 min at room temperature and aliquoted the clear supernatant and stored at -20 °C.

### 3.1.3 Yeast strains:

Y187 : Clontech Laboratories  
AH109 : Clontech Laboratories  
pGBKT7 : Clontech Laboratories  
pGADT7 : Clontech Laboratories

### 3.1.4 Bacteria and Cell Lines

#### Bacteria

DH5 $\alpha$ : F<sup>-</sup> endA1 glnV44 thi-1 recA1 relA1 gyrA96 deoR nupG purB20  $\phi$ 80dlacZ $\Delta$ M15  $\Delta$   
(lacZYA-argF) U169, hsdR17 (rK<sup>-</sup>mK<sup>+</sup>),  $\lambda$ <sup>-</sup>, Invitrogen - Life Technologies

#### Cell Lines

- P815 mastocytoma cell line (Mus musculus; Mast cells) from DSMZ no. ACC 1

### 3.1.5 Mouse Strains

1. C57Bl/6N (Black 6), Stock No: 005304, The Jackson Laboratory
2. Flower KO mice (Chang et al., 2018): Mouse background C57Bl/6N



## 3.2 Methods

### 3.2.1 Positive isolation of Primary murine CD8<sup>+</sup> T lymphocytes

Spleens from 8-20 weeks old C57BL/6N wild type (WT) and Flower Knockout (Flower KO) (Chang et al., 2018) mice were removed and crushed gently through a 70 µm cell-strainer (Corning Life Sciences). The splenocytes were then resuspended in RPMI medium and were centrifuged without a break. The erythrocytes were then lysed for 30 s using erythrocyte lysis buffer and cells were immediately washed again with RPMI medium. CD8<sup>+</sup> T cells were then positively isolated using the 'Dynabeads FlowComp Mouse CD8<sup>+</sup> Kit (Thermo Fisher Scientific) according to the user manual. In brief,  $5 \times 10^7$  splenocytes were incubated with 25 µl of anti-CD8 antibody in 500 µl of isolation buffer (composition in materials section) for 10 min on ice followed by washing to remove unbound antibody at 350 x g for 8 min. The pellet was then resuspended with 75 µl of CD8 antibody-coated dynabeads (provided in the kit) in 1ml of isolation buffer and mixed gently on the rotator at 4 °C. The cells were then subjected to magnetic separation for 2 min to detach unbound cells from the beads. The supernatant was discarded and the dynabead-bound cells were resuspended in 1 ml release buffer (provided in the kit) for 10 min in rotation at room temperature. The cells were again exposed to the magnet for 2 min, to release cells from dynabeads and were concentrated by centrifugation at 350 x g for 8 min. The obtained naive CD8<sup>+</sup> T cells were activated for further experiments.

### 3.2.2 Long term culturing of Primary murine CD8<sup>+</sup> T lymphocytes

The isolated naive CD8<sup>+</sup> T lymphocytes were resuspended in AIMV medium with 10% FCS and 50 µM 2-Mercaptoethanol and plated in a 24-well plate at a concentration of  $10^6$  cells per ml. Cells were activated with mouse T Cell-Activator CD3/CD28 Dynabeads at a ratio of 1:0.8 per well (cell: bead ratio). Additionally, recombinant Interleukin2 (IL2) (Thermo Fisher Scientific) was added to the final concentration of 100 U/ml for better proliferation and health of the cells. The cells were then split every 2<sup>nd</sup> day in culture maintaining the concentration of  $10^6$  cells per ml/well supplemented with fresh 100 U/ml of IL2. The experiments were performed using cells from day 2 to day 6 in culture.

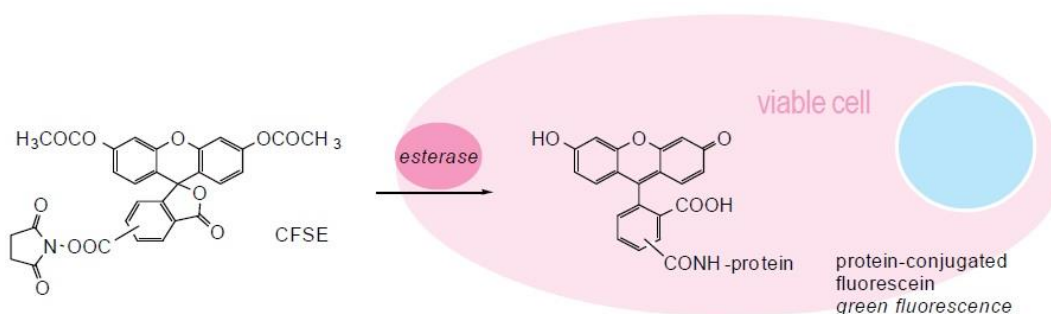
### 3.2.3 Subset analysis of CD8<sup>+</sup> T lymphocytes using Flow cytometry

$1 \times 10^6$  naive and day 5 activated WT and Flower KO CD8<sup>+</sup> T lymphocytes were taken, washed once, and suspended in 1x D-PBS. Live-cell staining of the cells was performed using FITC and APC conjugated anti-CD62L (1:800) (BD Biosciences), CD44 (1:400) (BD Biosciences) and CD25 (1:200) (BD Biosciences) antibodies in dark for 30 min on ice. The cells were then washed twice and suspended in 1 x D-PBS and analyzed by flow cytometry (BD FACS Aria III) using

FACS DIVA™ software. The data were further analyzed using the software FlowJo v10. The gating was done in comparison to the unstained CTLs.

### 3.2.4 Cell Proliferation assay

Carboxyfluorescein diacetate succinimidyl ester (CFSE) is a compound that is widely used in cell proliferation assay and *in vivo* cell tracking. The compound is cell permeable, colourless and non-fluorescent until the acetate groups are hydrolysed by intracellular cytoplasmic esterase enzyme yielding highly fluorescent carboxyfluorescein succinimidyl ester (Figure 13). The succinimidyl ester groups then covalently react with the amines on intracellular proteins to form fluorescent conjugates that are retained in the cells. This stable linkage, once incorporated into the cells, does not transfer to adjacent cells. After cells divide, each daughter cell will have approximately half the level of CFSE as the parent, and thus the fluorescence will decrease, thereby helping us to monitor cell proliferation. Live cells are covalently labelled with a very bright, stable CFSE dye. Every generation of cells appears as a different peak when analysed by a flow cytometry histogram.



**Figure 13: Principle of CFSE based cell proliferation assay**

$1.5 \times 10^6$  naive WT and Flower KO CD8<sup>+</sup> T lymphocytes were taken, washed once, and suspended in 1 ml D-PBS + 10% FCS containing CellTrace™ CFSE dye (Invitrogen C34570) at a final concentration of 5  $\mu$ M. The cells were incubated for 15 min at RT in dark by rotation to allow equal and uniform staining. The cells were then washed twice with AIMV medium for 5 min at 1100 rpm and  $0.5 \times 10^6$  cells were analysed by flow cytometry (BD FACS Aria III) using FACS DIVA™ software. Once uniform staining of cells was confirmed by flow cytometry, the remaining  $1 \times 10^6$  stained naive cells were cultured using standard conditions and stimulated with mouse T Cell-Activator CD3/CD28 Dynabeads and 100 U/ml IL2 for 5 days. Analysis of cells was performed on day 3, 4 and 5 to determine the proliferation status of cells using flow cytometry. The data were further analysed using the software FlowJo v10.

### 3.2.5 Degranulation assay

Naive cells were cultured for 3 days with anti-CD3/anti-CD28 beads and 50 U/ml IL2 in the cell to bead ratio of 1:0.4 to stimulate cells. On day 3, stimulated CTLs ( $0.2 \times 10^6$ ) were subjected to rest for 2 h by removing beads from culture. Cells were then incubated on 10  $\mu\text{g}/\text{mL}$  coated anti-CD3 (for stimulated cells) or PBS (for constitutive cells) coated on 96-well plate with 0.1  $\mu\text{L}$  anti-CD107a antibody conjugated to PE (Biolegend: Cat.no 121611) along with 0.15  $\mu\text{L}$  Golgi-stop, monensin (to block intracellular protein transport) for 3 h at 37 °C. Control CTLs were incubated in PBS-coated wells without anti-CD107a antibody conjugated to PE and Golgi-stop as a read-out for background signal for FACS analysis. Cells were then washed twice with ice-cold PBS containing 0.5% BSA and analysed by Fluorescence-activated cell sorting (FACS, BD FACSAria III). Data were analysed using FlowJo software (Celeza-Switzerland). Gating was set based on unstained, non-fluorescent control cells (Chang et al., 2018). All experiments were done in triplicates.

### 3.2.6 Calcein-AM based Real-time killing assay

P815 cells were loaded with calcein-AM (500 nM; Life Technology) in Roswell Park Memorial Institute medium (RPMI) with 10 mM HEPES for 15 min at RT, washed once, and plated into 96-well black plates with clear bottoms (BD Falcon). Triton X-100 (1%) was added to the target cells to calculate maximal target cell lysis as the positive control. Activated WT and Flower KO CTLs were added at different T cell ratios with anti-CD3 $\epsilon$  antibody to settled target cells ( $2.5 \times 10^4$  cells per well). Killing was measured at 37 °C, every 10 min for 4 h. Reading was performed at 485 nm excitation wavelength and 535 nm emission wavelength in the bottom reading mode by a GENios Pro plate reader. The fluorescence for the experimental conditions was adjusted by the parameter  $\gamma$  according to the live target cell control fluorescence. The  $\gamma$  value was measured at time zero:

$$\gamma = F_{\text{live}}(0)/F_{\text{exp}}(0)$$

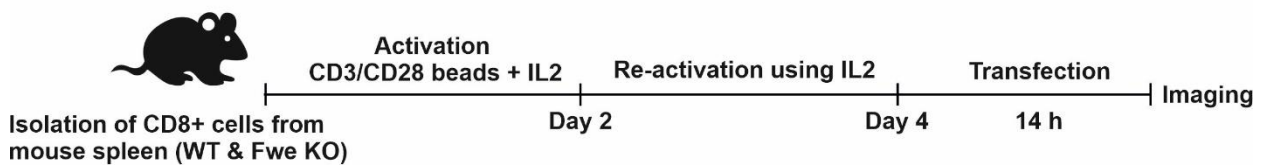
The cytotoxicity was calculated according to the loss of calcein fluorescence in target cells by using the following equation:

$$\% \text{ Target cell lysis} = (F_{\text{live}} - \gamma \times F_{\text{exp}}) / (F_{\text{live}} - F_{\text{lyse}}) \times 100$$

where  $F_{\text{live}}$  is the fluorescence of only target cell controls,  $F_{\text{exp}}$  are the CTLs with target cells, and  $F_{\text{lyse}}$  is the maximal target lysis. The details of this calcein-based killing assay were described previously (Kummerow et al., 2014; Chang et al., 2018). All experiments were performed in duplicates and averaged.

### 3.2.7 Electroporation of CTLs

The CD3/CD28 dynabeads were removed from day 4 activated CTLs and transfected overnight (12 to 14 h) with 2 to 4  $\mu\text{g}$  plasmid DNA coding for respective Flower fusion constructs (Figure 14). Electroporation was performed using Nucleofection kit (LONZA). Briefly, for one transfection, 3 to 5  $\times 10^6$  cells were washed with warm isolation buffer and resuspended in 100  $\mu\text{l}$  nucleofection solution (provided in the kit) with the corresponding plasmid DNA. Cells were then electroporated using an electroporation device (Lonza). Cells were added to the medium provided with the kit supplemented with FCS for 12 to 16 h at 37 °C and 5% CO<sub>2</sub>.



**Figure 14: Overview of CTL transfection procedure**

### 3.2.8 Target cell culture

P815 target cells (for mouse CD8<sup>+</sup> T cells) were cultured in RPMI medium (Thermo Fisher Scientific) containing 10% FCS and 0.5% Penicillin / Streptomycin antibiotics.

### 3.2.9 Coating coverslips

For live imaging of CTLs conjugated to target cells, coverslips were coated with 1 in 10 dilutions of 0.01 mg/ml poly-L-ornithine in DPBS for 30 min at RT (glass coverslips were pre-cleaned with 70% ethanol prior to coating). For fixed cell analysis, coverslips used were coated 0.01 mg/ml poly-L-ornithine for 30 min at RT.

For TIRF experiments, anti-CD3 antibody coated cover slips were used to mimic an antigen-presenting cell or a target cell. For this experiment, cover slips were first coated, as mentioned, with poly-L-ornithine, removed and then 30  $\mu\text{g}/\text{ml}$  anti-CD3 antibody (diluted from 1 mg/ml stock) in a final volume of 30  $\mu\text{l}$  per coverslip (25 mm) was added. The antibody was left on the coverslips for 2 h at 37 °C. The solution was then aspirated and the cover slips were ready to be used.

### 3.2.10 Organs and CTL lysate preparation

Different organs from P0 and adult WT and Flower KO mice (8-12 weeks old) were isolated and homogenized in protein lysis buffer enriched with protease inhibitors (see Materials and methods: Table 2) on ice using a glass homogenizer. The homogenate was then centrifuged twice at 10,000 x g for 10 min at 4 °C to remove cellular debris. The supernatant was collected, aliquoted, and snap-frozen in liquid nitrogen and stored at -80 °C. An aliquot of the lysate was used to measure the protein concentration using Quick start Bradford 1x Dye Reagent (5000205; Bio-Rad) and analyzed using a photometer (Eppendorf Biophotometer plus; DeNovix Spectrophotometer/ Fluorometer).

For CTL lysate preparation, 5-10 x 10<sup>6</sup> CTLs were lysed in protein lysis buffer with protease inhibitors (150 µl for 10<sup>7</sup> cells) in ice. Cells were incubated for 30 min at 4 °C on a rotator and centrifuged at 10,000 x g at 4 °C for 10 min. The supernatant was collected, and protein concentration was measured as described above. The lysate was snap-frozen and stored at -80 °C until use.

### 3.2.11 Western blotting

The expression of proteins was analyzed using western blotting. In brief, organs and CTL lysates were boiled at 95 °C for 7 min in 1 x LDS sample buffer (Stock 4 x; NuPAGE (NP0007)) with β-mercaptoethanol (reducing agent). The prepared samples with a final volume of 30 µl were then loaded onto 10% Bis-Tris pre-cast polyacrylamide gel (1 mm x 10 wells). Gels were run with MES buffer at 100 V for 30 min until the samples had reached the end stacking gel and then at 120 V for 2 to 2 h 30 min depending on the protein size to be detected. Spectra multicolor broad range marker was used as a running control and molecular weight marker. From 20 x stock (NuPAGE, Invitrogen), 1 x transfer buffer was prepared and methanol was also added to the buffer at a final concentration of 20%. Separated proteins were transferred to a nitrocellulose membrane soaked in 1x transfer buffer. Transfer was done for 2 h (RT, 250 mA) for smaller size proteins or 12-14 h at 4 °C for higher molecular weight. After transfer, the nitrocellulose membrane was incubated for 2 min with Ponceau S solution to check the quality of transfer. The membrane was then washed in distilled water followed by a wash with TBST (0.05% tween) 2 times, 5 min each (to wash out the Ponceau S staining) and then blocked with 5% non-fat dry milk in TBST buffer for 1 h at RT. Finally, the membrane was incubated with the primary antibody for 1 h at RT or overnight at 4 °C. The blot was washed 5 times for 5 min each. The secondary antibody coupled to HRP (horseradish peroxidase) was added (according to the species used, to generate the primary antibody; goat, mouse, rabbit) for 45 min at RT. The blot was washed 5 times (5 min each). ECL (enhanced chemiluminescent) reagent (SuperSignal West Dura Chemiluminescent Substrate; Thermo Fisher Scientific) was prepared fresh and added to the blot to visualize the bands using a

gel doc system (ProteinSimple). The pixel area and mean fluorescence intensity (MFI) were determined for densitometry analysis using ImageJ v1.46 software (<http://imagej.nih.gov/ij>, National Institute of Health).

### 3.2.12 Plasmids

A pcDNA3.1(+) expression vector with inserted cDNA of the Flower isoforms from mouse, human and drosophila and respective Flower mutants were synthesized and purchased from BioCAT. Subcloning to pMAX-FweA-mTFP (Chang et al., 2017) vector background was performed in house. Below is the detailed table of the restriction sites and Flower sequences that were ordered for synthesis in the background vector pCDNA3.1(+).

**Table 6: Sequences of mouse Flower isoforms**

Gene name	Sequence for synthesis ( <b>Kozak</b> -Gene (no stop codon))	Restriction sites
FweB	<b>GCCGCCACC</b> ATGAGCGGCTCGGGCGCCGGAGCGGCCGCGGG CCCAGCCCCGCCGGCACAGGAAGAGGGCATGACTTGGTGGTACC GCTGGCTGTGCCGCCTGGCGGGAGTGCTAGGAGCGGTGTCCTGTG CCATCTCTGGACTCTTCAACTGCGTCACTATCCACCCTCTGAACAT CGCAGCTGGCGTGTGGATGATCATGAACGCCTTCATCCTGTTGTT GTGCGAGGCTCCCTTCTGCTGCCAGTTTGTGGAGTTTGCAAACAC AGTAGCTGAGAAGGTTGACCGGCTGCGCTCCTGGCAGAAGGCTGT CTTCTACTGCGGGGCTAGCGGTGGGAGCGGCCGAAGCGGCGGT	5'EcoRI 3'XbaI
FweD	<b>GCCGCCACC</b> ATGATCATGAACGCCTTCATCCTGTTGTTGTGCGAG GCTCCCTTCTGCTGCCAGTTTGTGGAGTTTGCAAACACAGTAGCT GAGAAGGTTGACCGGCTGCGCTCCTGGCAGAAGGCTGTCTTCTAC TGCGGGATGGCCATCGTCCCCATCGTCATGAGCCTCACCTGACT ACACTGCTGGGCAATGCCATCGCCTTTGCCACGGGGGTGCTGTAT GGACTGTCTGCCCTGGGCAAAAAGGGCGATGCCATTTCTTATGCT CGGATCCAGCAGCAGAGACAGCAGGCAGATGAGGAGAAGCTGGC GGAGACTTTCGAGGGGGAAGTGGCTAGCGGTGGGAGCGGCCGAA GCGGCGGT	5'EcoRI 3'XbaI
FweE	<b>GCCGCCACC</b> ATGAGCGGCTCGGGCGCCGGAGCGGCCGCGGG CCCAGCCCCGCCGGCACAGGAAGAGGGCATGACTTGGTGGTACC GCTGGCTGTGCCGCCTGGCGGGAGTGCTAGGAGCGGTGTCCTGTG CCATCTCTGGACTCTTCAACTGCGTCACTATCCACCCTCTGAACAT CGCAGCTGGCGTGTGGATGATCATGAACGCCTTCATCCTGTTGTT GTGCGAGGCTCCCTTCTGCTGCCAGTTTGTGGAGTTTGCAAACAC AGTAGCTGAGAAGGTTGACCGGCTGCGCTCCTGGCAGAAGGCTGT CTTCTACTGCGGGCATGGTGAAGCCTTGCGAGGAGCGTGGCCAGA TGTGAGACTGCCGAACAGAAACACCATTTCCCTCGCTAGCGGTGG GAGCGGCCGAAGCGGCGGT	5'EcoRI 3'XbaI

**Table 7: Sequences of human FLOWER isoforms**

Gene name	Sequence for synthesis ( <b>Kozak</b> -Gene (no stop codon))	Restriction sites
FWE1	<p><b>GCCGCCACC</b>ATGAGCAGCTCAGGTGGGGCGCCCAGGGGCGTCCGC            CAGCTCTGCGCCGCCCGCGCAGGAAGAGGGGCATGACGTGGTGGT            ACCGCTGGCTGTGTCGCCTGTCTGGGGTGCTGGGGGCAGTCTCTT            GCGCGATCTCTGGCCTCTTCAACTGCATCACCATCCACCCTCTGA            ACATTGCGGCCCGGCGTGTGGATGATGATGGCGGTTCGTTCCCATC            GTCATCAGCCTGACCCTGACCACGCTGCTGGGCAACGCCATCGC            CTTTGCTACGGGGGTGCTGTACGGACTCTCTGCTCTGGGCAAAAA            AGCCAGACTGAGGCTGGTTCCTTCGCAGCCCAGCATCCAGGG            AGCCTGGGCCATTCTCAGAGGGGACAAGACAGGCCTTTGCCACC            CCAGCAGTTGTCTCTGGGGAAATCAGAATGCCTGCAGGGGCGAT            GCGATCTCCTATGCCAGGATCCAGCAGCAGAGGCAGCAGGCGGA            TGAGGAGAAGCTCGCGGAGACCCTGGAGGGGGAGCTGTGAAGG            GCTGGGCGCCCCTCCCTCCCTGTCCCCTCTTCTGGCTCTGTGTGG            GTCCAAGGCTAGCGGTGGGAGCGGCGGAAGCGGCGGT</p>	<p>5'EcoRI            3'XbaI</p>
FWE2	<p><b>GCCGCCACC</b>ATGAGCAGCTCAGGTGGGGCGCCCAGGGGCGTCCGC            CAGCTCTGCGCCGCCCGCGCAGGAAGAGGGGCATGACGTGGTGGT            ACCGCTGGCTGTGTCGCCTGTCTGGGGTGCTGGGGGCAGTCTCTT            GCGCGATCTCTGGCCTCTTCAACTGCATCACCATCCACCCTCTGA            ACATTGCGGCCCGGCGTGTGGATGATCATGAATGCCTTCATCTTGT            TGCTGTGTGAGGCGCCCTTCTGCTGCCAGTTCATCGAGTTTGCAA            ACACAGTGGCGGAGAAGGTGGACCGGCTGCGCTCCTGGCAGAAG            GCTGTCTTCTACTGCGGGATGGCGGTTCGTTCCCATCGTCATCAGC            CTGACCCTGACCACGCTGCTGGGCAACGCCATCGCCTTTGCTA            CGGGGGTGCTGTACGGACTCTCTGCTCTGGGCAAAAAAGCCAG            ACTGAGGCTGGTTCCTTCGCAGCCCAGCATCCAGGGAGCCTGG            GCCATTCTCAGAGGGGACAAGACAGGCCTTTGCCACCCCAGCAG            TTGTCTCTGGGGAAATCAGAATGCCTGCAGGGGCGATGCGATCT            CCTATGCCAGGATCCAGCAGCAGAGGCAGCAGGCGGATGAGGA            GAAGCTCGCGGAGACCCTGGAGGGGGAGCTGTGAAGGGCTGGG            CGCCCCTCCCTCCCTGTCCCCTCTTCTGGCTCTGTGTGGGTCCAAG            GCTAGCGGTGGGAGCGGCGGAAGCGGCGGT</p>	<p>5'EcoRI            3'XbaI</p>
FWE3	<p><b>GCCGCCACC</b>ATGAGCAGCTCAGGTGGGGCGCCCAGGGGCGTCCGC            CAGCTCTGCGCCGCCCGCGCAGGAAGAGGGGCATGACGTGGTGGT            ACCGCTGGCTGTGTCGCCTGTCTGGGGTGCTGGGGGCAGTCTCTT            GCGCGATCTCTGGCCTCTTCAACTGCATCACCATCCACCCTCTGA            ACATTGCGGCCCGGCGTGTGGATGATGATGGCGGTTCGTTCCCATC            GTCATCAGCCTGACCCTGACCACGCTGCTGGGCAACGCCATCGC            CTTTGCTACGGGGGTGCTGTACGGACTCTCTGCTCTGGGCAAAAA            GGGCGATGCGATCTCCTATGCCAGGATCCAGCAGCAGAGGCAGC            AGGCGGATGAGGAGAAGCTCGCGGAGACCCTGGAGGGGGAGCT            GGCTAGCGGTGGGAGCGGCGGAAGCGGCGGT</p>	<p>5'EcoRI            3'XbaI</p>

FWE 4	<p><b>GCCGCCACC</b>ATGAGCAGCTCAGGTGGGGCGCCCGGGGCGTCCGC  CAGCTCTGCGCCGCCCGCGCAGGAAGAGGGGCATGACGTGGTGGT  ACCGCTGGCTGTGTGCGCCTGTCTGGGGTGCTGGGGGCAGTCTCTT  GCGCGATCTCTGGCCTCTTCAACTGCATCACCATCCACCCTCTGA  ACATTGCGGCCGGCGTGTGGATGATCATGAATGCCTTCATCTTGT  TGCTGTGTGAGGCGCCCTTCTGCTGCCAGTTCATCGAGTTTGCAA  ACACAGTGGCGGAGAAGGTGGACCGGCTGCGCTCCTGGCAGAAG  GCTGTCTTCTACTGCGGGATGGCGGTCGTTCCCATCGTCATCAGC  CTGACCCTGACCACGCTGCTGGGCAACGCCATCGCCTTTGCTACG  GGGGTGCTGTACGGACTCTCTGCTCTGGGCAAAAAGGGCGATGC  GATCTCCTATGCCAGGATCCAGCAGCAGAGGCAGCAGGCGGATG  AGGAGAAGCTCGCGGAGACCCTGGAGGGGGAGCTGGCTAGCGG  TGGGAGCGGCGGAAGCGGCGGT</p>	5'EcoRI 3'XbaI
-------	---	-------------------

**Table 8: Sequences of drosophila Flower isoforms**

Gene name	Sequence for synthesis ( <b>Kozak-Gene (no stop codon)</b> )	Restriction sites
dFwe LoseA	<p><b>GCCGCCACC</b>ATGTCTTTCGCTGAAAAAATTACAGGCCTCCTGGCA  CGACCTAATCAACAAGACCCTATAGGCCCTGAGCAACCCTGGTA  CTTGAAATACGGCAGTAGACTTCTCGGCATCGTAGCTGCTTTTTT  CGCAATTCTTTTTGGCCTTTGGAACGTGTTTCAGTATTATCACTCTG  AGTGTGAGTTGCTTGGTTGCAGGCATTTTGCAGATGGTAGCAGG  GTTTGTGTAATGCTGCTGGAAGCACCTGTTGTTTTGTATGCTTC  GGGCAAGTCAATGAAATAGCAGAGAAGGTCGAATCCAAACCACT  GTACTTCCGGGCTGGGCTTTACATCGCAATGGCCATCCCTCCCAT  AATCCTGTGCTTCGGTCTCGCCAGCCTCTTTGGTTCTGGTTTGATT  TTTGGCACTGGGGTCGTTTACGGCATGATGGCCTTGGGGAAAAA  AGCAAGTCGGGAGGACATGGCCGCCGCAGCAACTAGCCCTACTC  AAATGGCTGGGTCCAGGCAGGCGGGCAGATGCAGATGGGGGG  CGATCAACATATCACTCTGATGGAAGATCCCGATGTTTGGAGAC  CAACAGCTAGCGGTGGGAGCGGCGGAAGCGGCGGT</p>	5'EcoRI 3'XbaI
dFwe LoseB	<p><b>GCCGCCACC</b>ATGTCATTTGCCGAAAAGATCACAGGTCTCCTCGCT  CGACCAAATCAACAGGACCCCATTTGGCCCCGAGCAACCATGGTA  CTTGAAGTATGGGAGCCGACTCCTTGGCATAGTAGCTGCTTTCTT  TGCTATACTCTTCGGGCTCTGGAACGTGTTCTCCATCATCACT  TAGTGTTCATGCCTCGTCGCCGGGATCTTGCAGATGGTTGCAGG  ATTTGTGGTTATGCTGCTGGAAGCTCCCTGTTGTTTTGTTTT  GGCAGGTTAACGAGATTGCAGAGAAAGTCGAGAGCAAGCCCCT  GTACTTTAGGGCAGGGCTGTATATCGCCATGGCCATCCCTCCTAT  TATTCTCTGCTTCGGCCTGGCTTCCCTTTTTGGTTCAGGTTTGATA  TTCGGAAGTGGAGTTGTGTATGGTATGATGGCACTTGGCAAGAA  CAAGCACATCTTCTTGTGCGAAATTATATCGCTAGCGGTGGGAG  CGGCGGAAGCGGCGGT</p>	5'EcoRI 3'XbaI



**Table 9: Sequences of mouse Flower mutants**

Gene name	Sequence for synthesis ( <b>Kozak</b> – Gene <b>mutation</b> (no stop codon))	Restriction sites
FweA (N ter. YRWL to AAAA)	<b>GCCGCCACC</b> ATGAGCGGCTCGGGCGCCGCGGAGCGGCCGCGGG CCCAGCCCCGCCGGCACAGGAAGAGGGGCATGACTTGGTGG <b>GCAG</b> <b>CGGCTGCC</b> TGCCGCCTGGCGGGAGTGCTAGGAGCGGTGTCCTGT GCCATCTCTGGACTCTTCAACTGCGTCACTATCCACCCTCTGAAC ATCGCAGCTGGCGTGTGGATGATCATGAACGCCTTCATCCTGTTG TTGTGCGAGGCTCCCTTCTGCTGCCAGTTTGTGGAGTTTGCAAAC ACAGTAGCTGAGAAGGTTGACCGGCTGCGCTCCTGGCAGAAGGC TGTCTTCTACTGCGGGATGGCCATCGTCCCCATCGTCATGAGCCT CACCTGACTACACTGCTGGGCAATGCCATCGCCTTTGCCACGGG GGTGCTGTATGGACTGTCTGCCCTGGGCAAAAAGGGCGATGCCA TTTCTTATGCTCGGATCCAGCAGCAGAGACAGCAGGCAGATGAG GAGAAGCTGGCGGAGACTTTCGAGGGGGAACTGGGTGGGAGCG GCGGAAGCGGCGGT	5'EcoRI 3'XbaI
FweA (C ter. YARI to AAAA)	<b>GCCGCCACC</b> ATGAGCGGCTCGGGCGCCGCGGAGCGGCCGCGGG CCCAGCCCCGCCGGCACAGGAAGAGGGGCATGACTTGGTGGTACC GCTGGCTGTGCCGCCTGGCGGGAGTGCTAGGAGCGGTGTCCTGT GCCATCTCTGGACTCTTCAACTGCGTCACTATCCACCCTCTGAAC ATCGCAGCTGGCGTGTGGATGATCATGAACGCCTTCATCCTGTTG TTGTGCGAGGCTCCCTTCTGCTGCCAGTTTGTGGAGTTTGCAAAC ACAGTAGCTGAGAAGGTTGACCGGCTGCGCTCCTGGCAGAAGGC TGTCTTCTACTGCGGGATGGCCATCGTCCCCATCGTCATGAGCCT CACCTGACTACACTGCTGGGCAATGCCATCGCCTTTGCCACGGG GGTGCTGTATGGACTGTCTGCCCTGGGCAAAAAGGGCGATGCCA TTTCT <b>GCTGCCGACGC</b> CAGCAGCAGAGACAGCAGGCAGATGAG GAGAAGCTGGCGGAGACTTTCGAGGGGGAACTGGGTGGGAGCG GCGGAAGCGGCGGT	5'EcoRI 3'XbaI
FweA (N and C ter. YXXφ to AAAA)	<b>GCCGCCACC</b> ATGAGCGGCTCGGGCGCCGCGGAGCGGCCGCGGG CCCAGCCCCGCCGGCACAGGAAGAGGGGCATGACTTGGTGG <b>GCAG</b> <b>CGGCTGCC</b> TGCCGCCTGGCGGGAGTGCTAGGAGCGGTGTCCTGT GCCATCTCTGGACTCTTCAACTGCGTCACTATCCACCCTCTGAAC ATCGCAGCTGGCGTGTGGATGATCATGAACGCCTTCATCCTGTTG TTGTGCGAGGCTCCCTTCTGCTGCCAGTTTGTGGAGTTTGCAAAC ACAGTAGCTGAGAAGGTTGACCGGCTGCGCTCCTGGCAGAAGGC TGTCTTCTACTGCGGGATGGCCATCGTCCCCATCGTCATGAGCCT CACCTGACTACACTGCTGGGCAATGCCATCGCCTTTGCCACGGG GGTGCTGTATGGACTGTCTGCCCTGGGCAAAAAGGGCGATGCCA TTTCT <b>GCTGCCGACGC</b> CAGCAGCAGAGACAGCAGGCAGATGAG GAGAAGCTGGCGGAGACTTTCGAGGGGGAACTGGGTGGGAGCG GCGGAAGCGGCGGT	5'EcoRI 3'XbaI
FweB (N ter. YRWL to AAAA)	<b>GCCGCCACC</b> ATGAGCGGCTCGGGCGCCGCGGAGCGGCCGCGGG CCCAGCCCCGCCGGCACAGGAAGAGGGGCATGACTTGGTGG <b>GCAG</b> <b>CGGCTGCC</b> TGCCGCCTGGCGGGAGTGCTAGGAGCGGTGTCCTGT GCCATCTCTGGACTCTTCAACTGCGTCACTATCCACCCTCTGAAC ATCGCAGCTGGCGTGTGGATGATCATGAACGCCTTCATCCTGTTG TTGTGCGAGGCTCCCTTCTGCTGCCAGTTTGTGGAGTTTGCAAAC ACAGTAGCTGAGAAGGTTGACCGGCTGCGCTCCTGGCAGAAGGC TGTCTTCTACTGCGGGATGGCCATCGTCCCCATCGTCATGAGCCT CACCTGACTACACTGCTGGGCAATGCCATCGCCTTTGCCACGGG GGTGCTGTATGGACTGTCTGCCCTGGGCAAAAAGGGCGATGCCA TTTCT <b>GCTGCCGACGC</b> CAGCAGCAGAGACAGCAGGCAGATGAG GAGAAGCTGGCGGAGACTTTCGAGGGGGAACTGGGTGGGAGCG GCGGAAGCGGCGGT	5'EcoRI 3'NheI

FweB ( $\Delta$ Exon3)	<p>GCCGCCACCATGAGCGGCTCGGGCGCCCGGAGCGGCCGCGGG                  CCCAGCCCCGCCGGCACAGGAAGAGGGCATGACTTGGTGGTACC                  GCTGGCTGTGCCGCTGGCGGGAGTGCTAGGAGCGGTGTCCTGT                  GCCATCTCTGGACTCTTCAACTGCGTCACTATCCACCCTCTGAAC                  ATCGCAGCTGGCGTGTGGATGATC</p>	5'EcoRI 3'NheI
------------------------	---	-------------------

For all the following Fwe isoform constructs designed, the background vector was pMAX, unless specified. All constructs were made with a linker sequence between the gene and fluorescent tag with the sequence 5'- AGCGGTGGGAGCGGCGGAAGCGGCGGTTCT- 3' that encodes for amino acids Ser-Gly-Gly-Ser-Gly-Gly-Ser-Gly-Gly-Ser (where Ser and Gly stands for Serine and Glycine respectively).

Using standard cloning procedure, the different Flower isoforms of mouse, human and drosophila were made by tagging mTFP or Halo either at the N- or C-terminus.

All clones obtained from the above-mentioned procedures were confirmed by sequencing the plasmids with respective forward and reverse primers which was done by Microsynth Seqlab.

Following is the table of the plasmids cloned and used in this study and their respective plasmid number designated in the laboratory (Table 10).

**Table 10: Flower isoform constructs generated and used in this study**

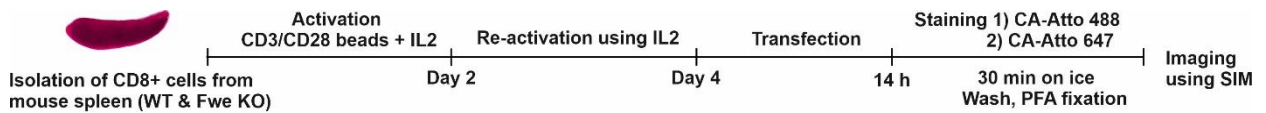
Plasmid	JRE lab plasmid number
1. pMAX-mFweA-mTFP	#1762
2. pMAX-mFweB-mTFP	#A676
3. pMAX-mFweD-mTFP	#A677
4. pMAX-mFweE-mTFP	#A678
5. pMAX-hFWE1-mTFP	#A667
6. pMAX- hFWE2-mTFP	#A669
7. pMAX- hFWE3-mTFP	#A671
8. pMAX- hFWE4-mTFP	#A673
9. pMAX- dFwe <sup>Ubi</sup> -mTFP	#A700
10. pMAX- dFwe <sup>LoseA</sup> -mTFP	#A674
11. pMAX- dFwe <sup>LoseB</sup> -mTFP	#A675
12. pMAX-mFweA-Halo	#1009
13. pMAX-mFweB-Halo	#1021
14. pMAX-mFweD-Halo	#1022

15. pMAX-mFweE-Halo	#1023
16. pMAX-hFWE1-Halo	#1015
17. pMAX- hFWE2-Halo	#1016
18. pMAX- hFWE3-Halo	#1017
19. pMAX- hFWE4-Halo	#1018
20. pMAX- dFwe <sup>Ubi</sup> -Halo	#1024
21. pMAX- dFwe <sup>LoseA</sup> -Halo	#1019
22. pMAX- dFwe <sup>LoseB</sup> -Halo	#1020
23. pMAX-Halo-mFweA	#1012
24. pMAX-Halo-mFweB	#A721
25. pMAX-Halo-mFweD	#A722
26. pMAX-Halo-mFweE	#A723
27. pMAX-mTFP-mFweA	#A719
33. pMAX-mFweA(YRWL to AAAA)-mTFP	#A735
33. pMAX-mFweA(YARI to AAAA)-mTFP	#A736
33. pMAX-mFweA(YRWL and YARI to AAAA)-mTFP	#A737
34. pMAX-mFweB(YRWL to AAAA)-mTFP	#A738
35. pMAX-mFweB( $\Delta$ Exon3)-mTFP	#A739
32. pMAX-mFweA(E74A)-mTFP	#A704
33. pMAX-mFweA(Y104A)-mTFP	#A715
34. pMAX-dFwe <sup>Ubi</sup> (Y109A)-mTFP	#A716

### 3.2.13 anti-RFP antibody labelling

In order to study the endocytosis of Syb2-mRFP positive vesicles, coupling of the anti-RFP antibody (Genway Biotech; GWB-3BF397) to Alexa 647 fluorophore was performed using Alexa Fluor™ 647 Antibody Labelling Kit (Life technologies; A20186). The conjugation was performed by adding freshly prepared 10  $\mu$ L sodium bicarbonate solution (1 M) to 100  $\mu$ l anti-RFP antibody (1 mg/ml). The alkalized mixture was then added to the vial containing Alexa Fluor dye (Alexa 647), mixed and incubated for 1 h at RT in dark by rotation. During incubation of the dye with antibody, the purification column was prepared by adding 1.5 ml resin to the column and spinning it down at 1100 x g for 3 min to obtain the column bed. The incubated reaction mixture was then added to the column and centrifuged for 5 min at 1100 x g. The eluate obtained contained the conjugated antibody ready to be used (Chang et al., 2016).

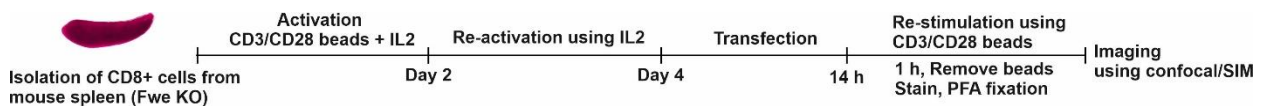
### 3.2.14 Flower topology using Halo tag constructs:



**Figure 15: Representation of Halo tag-Atto staining procedure**

Day 4 activated Flower KO CTLs (4 million cells/transfection) were transfected with 2 µg of respective Flower-Halo or Halo-Flower constructs. After 14 h of transfection, cells were washed twice with 1 x PBS (in 1.5 ml Eppendorf tube). Cells were then stained with 500 nM CA-Atto488 (1 mM stock) in 100 µl of 1 x PBS for 30 min on ice. 300 µl of 1 x PBS was added to stop the reaction and was washed by centrifugation at 1100 rpm for 10 min (4 times wash). Cells were then stained with 200 nM CA-SiR (1 mM stock) in 100 µl of 1 x PBS for 30 min on ice. 300 µl of 1 x PBS was added to stop the reaction and cells were washed by centrifugation at 1100 rpm for 10 min (4times wash) (Figure 15). Then cells were added onto poly-L-ornithine coated coverslips, were fixed using 4% PFA, quenched with 0.1 M glycine, and washed 3 times with PBS before they were mounted onto glass slides.

### 3.2.15 Localization studies



**Figure 16: Representation of staining procedure for localization study**

To study Flower isoform localization at the plasma membrane, day 4 activated CTLs ( $4 \times 10^6$  cells/ transfection) were transfected with 2 µg of respective Fwe-mTFP constructs. After 14 h, CD3/CD28 dynabeads were added in the ratio of 1: 0.8 (cells: beads) and incubated at 37° C for 1 h. The beads were then removed using magnetic holders, washed once at 4 °C and stained with anti-CD8 antibody coupled to Alexa 647 (1:100) to mark the plasma membrane on ice (to prevent endocytosis of CD8 receptor). The cells were washed and then added onto poly-L-ornithine coated coverslips, were fixed using 4% PFA, washed and mounted onto glass slides and imaged using confocal microscope (Figure 16).

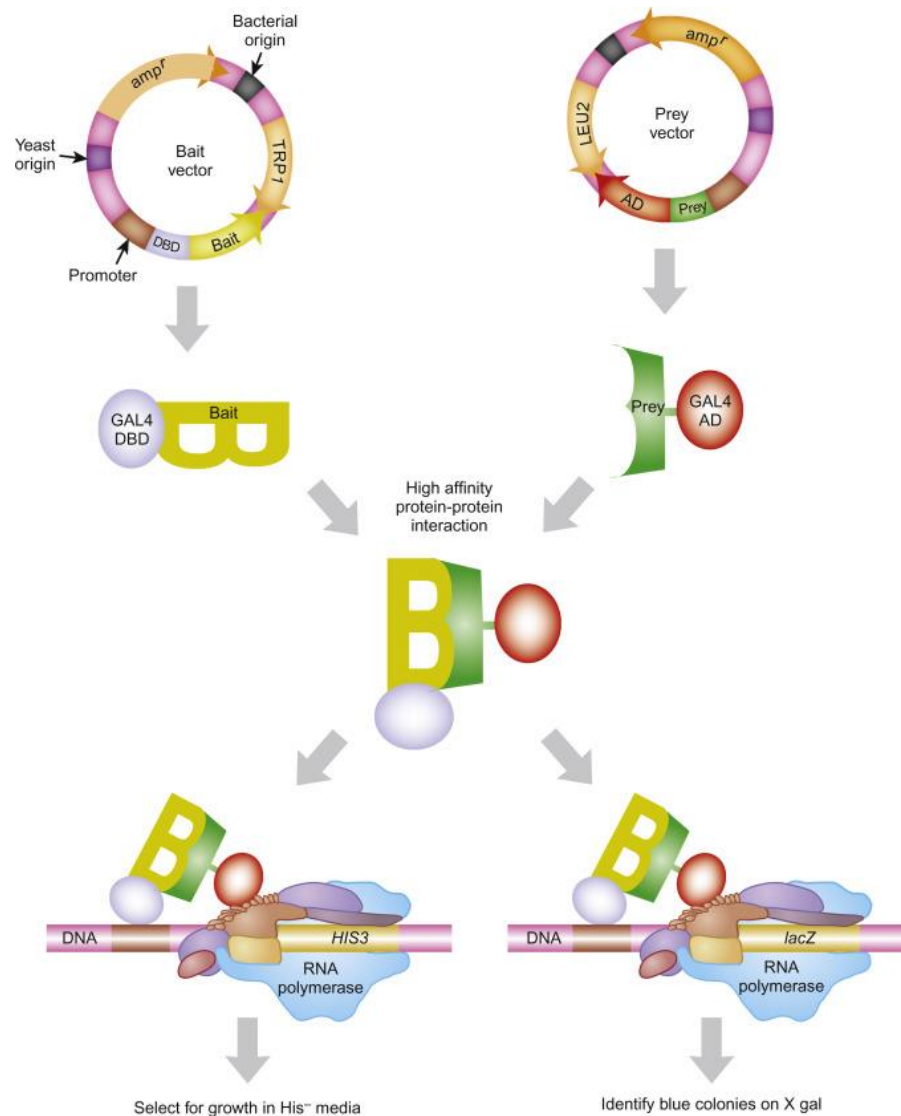
For colocalization study with ER marker protein, day 4 activated CTLs were transfected with 2 µg of respective Fwe-mTFP constructs and ER-mScarletI (Addgene #137805). The rest of the procedure was performed as described above. Images were acquired using SIM. For colocalization analysis, Manders' coefficients were determined using the JACoP plugin of ImageJ v1.46 (Bolte and Cordelieres, 2006).

### 3.2.16 High pressure freezing and freeze substitution for electron microscopy

To localize endogenous Flower protein, mouse CTLs were isolated from WT and Flower KO mouse as described above (Section 3.2.1). Additionally, Flower KO CTLs were electroporated with pMAX-FweA-mTFP. Cells were settled on 0.01% poly-L-ornithine and 30  $\mu\text{g/ml}$  anti-CD3 $\epsilon$  antibody coated 1.4 mm sapphire discs in flat specimen carriers to form an artificial immunological synapse and vitrified in a high-pressure freezing system (Leica EM PACT2/RTS). All samples were further processed in an automatic freeze-substitution apparatus (Leica AFS2). In brief, all samples were transferred into the pre-cooled ( $-130^{\circ}\text{C}$ ) freeze-substitution chamber of the AFS2. The temperature was increased from  $-130$  to  $-90^{\circ}\text{C}$  over 2 h. Cryo-substitution was performed from  $-90^{\circ}\text{C}$  to  $-70^{\circ}\text{C}$  over 20 h in anhydrous acetone and from  $-70^{\circ}\text{C}$  to  $-60^{\circ}\text{C}$  over 20 h with 0.3% (w/v) uranyl acetate in anhydrous acetone. The samples were infiltrated with increasing concentrations (30, 60 and 100% for 1 h each) of Lowicryl (3:1 K11M/HM20 mixture) with 0.3% uranyl acetate. After 5 h of infiltration with 100% Lowicryl, samples were UV polymerized at  $-60^{\circ}\text{C}$  for 24 h and for additional 15 h while the temperature was raised linearly to  $5^{\circ}\text{C}$ . Ultrathin sections were cut using a Leica EM UC7 and collected on pioloform-nickel grids (Chitirala et al., 2019). Postembedding immunogold electron microscopy was done according to the user's manual (Aurion). In brief, the ultrathin sections were first treated with blocking solution (Aurion) for 30 min at RT to block nonspecific protein binding sites. Then, the primary rabbit polyclonal anti-Flower antibody was diluted to 25  $\mu\text{g/ml}$  in incubation solution (PBS, pH7.4 with 0.1% BSAc (Aurion)) and applied for 2 hours. After several wash steps with incubation solution, the primary antibody was detected with goat anti-rabbit secondary antibody conjugated to 10 nm gold particles (Aurion). Following multiple wash steps with PBS immune complexes were fixed with 2% glutaraldehyde in PBS for 15 min at RT. After contrasting with uranyl acetate and lead citrate sections were analysed with a Tecnai12 Biotwin electron microscope (Thermo Fisher).

### 3.2.17 Yeast two hybrid assay (Y2H)

The Y2H technique is an *in vivo* approach to study protein-protein interactions in living yeast cells (Fields et al., 1989). Y2H system is based on the yeast transcription factor GAL4. In brief, the protein of interest called the bait and the presumed interaction partner (prey) are fused to the DNA-binding domain (BD) and activation domain (AD) of GAL4, respectively. If the two proteins interact, the BD and AD of GAL4 are brought into close proximity and GAL4 binds to DNA, recognizing the upstream activation sequence (UAS) and binds to its specific promoter. This activates the expression of reporter genes that are responsible for nutrition and growth selection. The reporter genes namely HIS3 (Histidine biosynthesis), ADE2 (Adenine biosynthesis), MEL1 ( $\alpha$ -Galactosidase) and LacZ ( $\beta$ -galactosidase) are important for the selection of the yeast colonies in respective selective environment to confirm protein interactions (Figure 17).



**Figure 17: Principle of Yeast two hybrid study**

The bait vector for yeast two-hybrid analysis consists of DNA binding domain (DBD) and the bait protein (the protein of interest). The prey vector has activation domain (AD) and for the prey (presumed interaction) protein. When the two plasmids are expressed in the same yeast cell and if the bait and prey proteins interact, the reporter gene is expressed. There are two possible reporter systems shown. Interaction of bait and prey leads to expression of the reporter gene *HIS3* and thereby the yeast cells will be able to make histidine and grow in media without histidine. In the second system, interaction leads to activation of the *lacZ* gene from *E. coli* and hence the yeast cells turn blue on plates containing X-gal (Clark, Pazdernik and McGehee, 2019).

The experiment was carried out in the yeast strains Y187 and AH109 of *Saccharomyces cerevisiae*. The vectors pGBKT7 and pGADT7 contain the bait and prey proteins fused to the BD and AD of GAL4 with selection markers TRP1 and LEU3 (coding for Tryptophan and Leucine amino acids). Thus, yeast cells can only grow in selection medium tryptophan (-W) or Leucine (-L) if bait and prey proteins interact. One colony from each plate was picked and suspended in 1 ml of YPD broth and incubated for 5 h at 30 °C in a shaker. Yeast mating was done and centrifuged at 3000 rpm at 4 °C for 5 min. The pellet was suspended in 100 µl of residual broth. 50 µl of the suspension was plated onto -LW and -ALWH (-Alanine, Leucine, Tryptophan, Histidine). ALWH

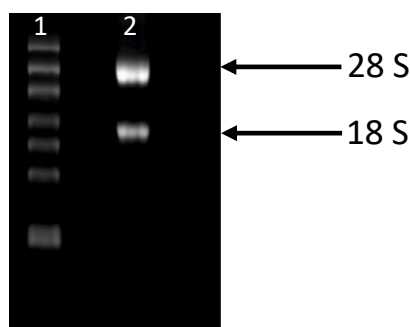
plates were treated with 100µl ATZ (10 mM stock) and 60 ng/ml of aureobasidin just prior to use. Mating efficiency was confirmed by growth of yeast colonies in -LW plates and protein interaction was demonstrated by growth on -ALWH plates. Protein interaction between bait and prey leads to GAL4 BD-AD close proximity, initiating the transcription of reporter genes in the nucleus. pGADT7\_pSE1111, pGBKT7\_pSE1112 and empty bait and prey plasmids were used as negative controls.

### **β-galactosidase assay:**

To analyze the expression of reporter genes MEL1 (α-Galactosidase) and LacZ (β-galactosidase) after interaction, qualitative β-galactosidase assay was performed (Breedon and Nasmith, 1985). Yeast cells were transferred and streaked in a triangular shape onto fresh -ALWH plates and incubated for 48 h at 30 °C. Whatmann filter paper was then cut in the same shape and placed upon the streaked grown yeast colonies to allow the cells to stick on the filter paper. These filter papers with replica yeast colonies were then cracked open by dipping into liquid nitrogen for 2 min and treated with incubation solution containing a mixture of β- Mercaptoethanol, Z buffer (Composition – Materials: Table 5) and X-Gal. The reaction was allowed to take place at room temperature in dark and the appearance of blue colour confirmed the positive interaction of the proteins compared to the empty colourless control. Presence of the galactosidase reporter genes results in the conversion of the yellow dye X-Gal into the blue dye 5 Gal5'-dibromo-4,4-dichloro-indigo and galactose.

### **3.2.18 Cloning of bait and prey proteins in yeast-two hybrid vectors**

**RNA isolation:** For AP2mu subunit (prey) cloning, the gene was amplified from cDNA produced from activated Day 3 CTLs. The cDNA synthesis was done from the isolation of total RNA. Briefly 5 x 10<sup>6</sup> activated cells were washed twice with 1 x PBS and resuspended in 1 ml trizol solution. Isolation was carried out as recommended by the manufacturer's protocol (Thermo Fisher Scientific) under clean and RNase free conditions. Briefly, cells were lysed using a clean piston and the entire procedure was performed on ice. Cells were then centrifuged at 12000 x g for 10 min at 4 °C, and the supernatant was transferred to a new eppendorf tube. 200 µl chloroform (per 1 ml trizol) were added to the supernatant, mixed and incubated for 2-3 min at RT and centrifuged at 12000 x g for 15 min at 4 °C. Two layers are seen at this stage; the top aqueous phase that contains the RNA was carefully transferred to a fresh tube. 500 µl isopropanol (per 1 ml trizol) was added and incubated for 10 min at RT, to precipitate the RNA and the sample was then centrifuged at 12000 x g for 10 min at 4 °C. The supernatant was discarded and the RNA pellet was washed with 1 ml 70% ethanol (per 1 ml trizol) then centrifuged at 7500 x g for 5 min at 4 °C. The RNA pellet was allowed to air-dry at RT until transparent. The pellet was then dissolved in 30 µl DEPC-treated water (Chitirala et al., 2019).



**Figure 18: Quality check of isolated RNA on an agarose gel.**

Lane 1: RNA ladder; Lane 2: RNA sample isolated from activated day 3 CTLs run on a gel for quality check

The quality and integrity of the RNA was determined by measuring the absorbance of the sample using an Eppendorf Plus biophotometer. Samples were dissolved in RNase-free water and measured at 260/280 nm. Reading of 2.0 designates high quality of the RNA. To confirm the quality and non-degradation of the RNA, the sample was run on an agarose gel. The presence of two bands exhibiting the different subunits of the ribosomal RNA (28S and 18S) confirmed the integrity of the RNA (Figure 18).

**cDNA synthesis:** For cDNA (complementary DNA) synthesis, SuperScript II kit from Thermo Fisher Scientific was used to synthesize cDNA from the isolated RNA from activated CTLs by reverse transcription. 1  $\mu$ l total RNA, 1  $\mu$ l random primers (1  $\mu$ M) and 1  $\mu$ l dNTPs (10 mM) were mixed and kept for 5 min at 65 °C to linearize the RNA secondary structures and immediately placed on ice. Then 4  $\mu$ l first strand buffer (5x), 1  $\mu$ l RNaseOUT (RNase inhibitor), 2  $\mu$ l DTT (0.1 M stock) and 1  $\mu$ l SuperScript II reverse transcriptase were added to the mixture and incubated for 1 h at 42 °C to obtain the cDNA (Chitirala et al., 2019).

The following primers were then used to amplify the AP2mu subunit from the cDNA: Forward primer 5' ATCGGAGGCTTATTCATC 3' with NdeI restriction site and reverse primer 5' TCAGCAGCGGGTTTCATA 3' with XhoI restriction site. The PCR product was checked on an agarose gel to determine the right molecular weight and eluted for cloning into the yeast-hybrid vector pGADT7. After the standard cloning procedure, the construct was confirmed by sequencing. In order to clone the Flower (bait) nucleotide into the pGKT7 vector background, the following primers with respective restriction sites (Table 11) were used:



**Table 11: Primers used for cloning Flower peptides into yeast vectors**

Bait	Primer	Restriction site
<b>N-terminal Flower (1-31aa)</b>		
Forward Primer	ATGAGCGGCTCGGGCGCC	EcoR1
Reverse Primer	TCAGCGGCACAGCCAGCG	Sal1
<b>C-terminal Flower (140-171aa)</b>		
Forward Primer	GGCAAAAAGGGCGATGCC	EcoR1
Reverse Primer	TCACAGTTCCCCCTCGAA	Sal1

pMAX-FweA-mTFP (Chang et al., 2018) was used as a template to amplify the respective nucleotide sequence. A stop codon was inserted into the reverse primer. The PCR product was then cloned into the yeast-hybrid vector pGKT7. After the standard cloning procedure, the construct was confirmed by sequencing. For cloning of Flower loop (82-100aa), nucleotide annealing was performed as follows: top strand 5' ACAGTAGCTGAGAAGGTTGACCGGCT GCGCTCCTGGCAGAAGTGAG 3' with EcoR1 restriction site and bottom strand 5' TCACTT CTGCCAGGAGCGCAGCCGGTCAACCTTCTCAGCTACTGTG 3' with sal1 restriction site was synthesized and 10 µl of the top and bottom primers were mixed and were subjected to 95° C for 10 min. The temperature in the block was switched off and the primer mix was allowed to cool down slowly until the block reached 25 °C in order to obtain annealing of the primers. The annealed DNA was then cloned into the yeast-hybrid vector pGKT7. After the standard cloning procedure, the construct was confirmed by sequencing.

### 3.2.19 Semi-quantitative PCR

The total RNA of naive and activated WT and Flower KO CTLs were extracted with TRIzol (Thermo Fisher Scientific) and reverse transcribed (SuperScript II; Thermo Fisher Scientific) using random hexamer primers. Semi-quantitative PCR was performed using specific primers as shown below (Table 12). Data were normalized to HPRT1. For positive control, the above mentioned procedure was also performed for WT mouse whole brain. Genomic DNA was used as negative control.

**Table 12: Primers used for RT-PCR**

Primer name	Sequence (5' to 3')	Expected size (bp)
<b>FweA1</b>		605
Exon2 Forward Primer	ATCTCTGGACTCTTCAACT	
3'UTR Reverse Primer	GAGTTCATCCCATCCATAG	
<b>FweA2</b>		616
Exon2 Forward Primer	ATCTCTGGACTCTTCAACT	
3'UTR Reverse Primer	ACTCATCTAATAAGCCACTG	
<b>FweB</b>		496
Exon2 Forward Primer	ATCTCTGGACTCTTCAACT	
3'UTR Reverse Primer	ACACATATCCACTACAACC	
<b>FweC</b>		451
Exon2a Forward Primer	GAACACAAGCAACTCCTC	
3'UTR Reverse Primer	CACCTGTTATTGGATGAGT	
<b>FweD</b>		446
Exon1b Forward Primer	TTGCTAAATCCTGGGTGTCC	
Exon5 Reverse Primer	TCACAGTTCCCCCTCGAAAG	
<b>FweE</b>		376
Exon3 and 3' Forward Primer	CTGATTATGGACAGGACTG	
3'UTR Reverse Primer	ATAGTCAAGGGCATATCCA	
<b>HPRT1</b>		465
Forward Primer	TACTGCGGGCATGGT	
Reverse Primer	CAACCATGCTACACTGAT	

### 3.2.20 Structured Illumination Microscopy (SIM)

Structured Illumination Microscopy (SIM) is a super-resolution technique that uses a combination of optical manipulations and computational algorithms to obtain optical sections and two-dimensional images that feature improved resolution. The SIM setup I used was a Zeiss Elyra PS1 (Zeiss, Oberkochen). The setup is equipped with solid-state lasers emitting at 405 nm, 488 nm, 561 nm and 642 nm. Following immunostaining, the images were acquired using 63x Plan-Apochromat (NA 1.4) objective using different laser excitations at 488, 561, and 642 nm for exciting samples. Z-stacks were measured with a typical step size of 200 nm covering about 7  $\mu$ m of the cell. Prior to analysis and presentation, the acquired raw images were processed to obtain higher resolution using Zen software (Zen 2012; Carl Zeiss). Further analysis was done using ImageJ v1.46 software.

### 3.2.21 Endocytosis of CG and Flower Rescue experiment

Activated day 5 WT and Flower KO CTLs were transfected with Syb2-mRFP plasmid as a CG marker and after 12-16 h,  $0.1 \times 10^6$  cells in 150  $\mu$ l AIMV + 10 mM HEPES containing medium were allowed to settle down onto the glass bottom of a microscopic chamber coated with 0.01mg/mL poly-L-ornithine (Sigma). Subsequently  $0.02 \times 10^6$  P815 target cells in 50  $\mu$ l AIMV containing 2  $\mu$ l anti-CD3 antibody (stock- 1 mg/mL) and 2  $\mu$ l of Alexa conjugated anti-RFP647 antibody was added for visualizing Syb2 endocytosis. For Flower rescue experiments, CTLs from Flower KO mice were transfected with respective isoforms or mutants in pMAX-Fwe-mTFP background for live imaging. All live-cell imaging experiments were done at 37 °C using a confocal microscope (Zeiss, LSM 780).

### 3.2.22 Confocal microscopy

Live imaging was performed using Zeiss laser scanning microscope 780 (LSM 780). Movies and images were acquired with a 63 x Plan-Apochromat immersion objective with a NA of 1.4. Different wavelengths were used for exciting samples, namely 488, 561 and 633 nm, and a pinhole size of 1 airy unit (AU) was used. To cover the range of the cell, confocal z-stacks were taken with a step size of 1  $\mu$ m and scanning speed of 1s/plane. Maximum intensity projections were calculated from the collected data and analysed as a function of time (t). Further analyses were done using ImageJ software. The analysis for the of accumulation of endocytosed CGs at the IS over time was performed by calculating the percentage of total fluorescence of the anti-RFP647 antibody at the IS using the formula:

$$\% \text{ fluorescence accumulated at the IS} = \frac{\text{fluorescence at the IS}}{\text{fluorescence in the entire cell}} \times 100$$

To study the localization of Flower at the plasma membrane, day 5 activated Flower KO CTLs were transfected with isoforms or mutants in pMAX-Fwe-mTFP background and were bead stimulated for 1 h at 37 °C at 5% CO<sub>2</sub>. The beads were removed, cells were washed at 4 °C and re-suspended in ice cold PBS, fixed with 4% PFA and stained with anti-CD8 antibody coupled to Alexa 647 for 30 min on ice. The cells were washed and mounted onto glass slides. The cells were imaged using confocal microscopy and line plot analysis was performed using ImageJ software.

Analysis of fluorescence intensity for the different Fwe-TFP fusion constructs were done by marking a ROI over the entire cell and over the nuclear area. The intensity of the selected ROIs was measured using ImageJ software and the cytoplasmic fluorescence of the cell was calculated using the formula:

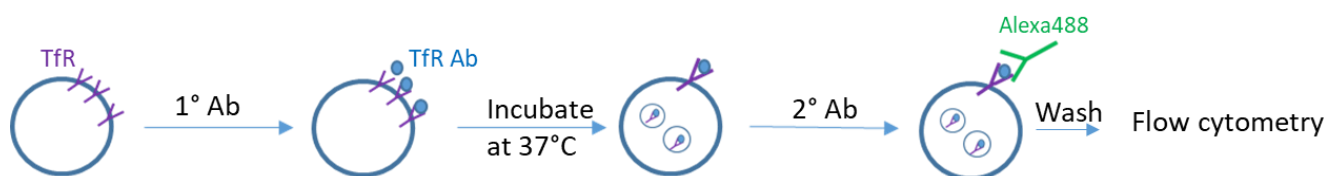
$$\text{Fluorescence intensity} = \frac{(\text{Intensity of total cell} - \text{Intensity in nucleus})}{(\text{Area of total cell} - \text{Area of nucleus})}$$

### 3.2.23 Total Internal Reflection Fluorescence Microscopy (TIRF-M)

CTLs isolated from WT and Flower knock-out mice were transfected with respective Flower isoforms. After 12-16 h of transfection,  $0.1-0.2 \times 10^6$  cells were resuspended in 30  $\mu$ l of calcium-free extracellular buffer solution (2 mM HEPES, 140 mM NaCl, 4.5 mM KCl, and 2 mM  $MgCl_2$ ) and allowed to settle for 2-3 min on anti-CD3 $\epsilon$  antibody (30  $\mu$ g/ml) coated cover slips. Cells were then perfused with extracellular buffer containing 10 mM  $Ca^{2+}$  to trigger vesicle movement towards the immunological synapse formed with the cover slip. Cells were imaged with the TIRF-M setup from Visitron Systems GmbH (Puchheim, Germany) with a custom built IX83 (Olympus) equipped with the Olympus autofocus module, a 488 nm 100 mW laser and a solid-state 100 mW laser emitting at 561 nm, a UAPON100XOTIRF NA 1.49 objective (Olympus), the evolve-EM 515 camera (Photometrics), the iLAS2 illumination control system (Roper Scientific SAS, France) and a filter cube containing Semrock (Rochester, NY, USA) FF444/520/590/Di01 dichroic and FF01-465/537/623 emission filter. Cells were imaged for 10 min at room temperature with either 488 nm or 561 nm excitation. Acquisition frequency was maintained at 10 Hz and the exposure time was 100 ms. The images were analysed using Visiview software (Version: 4.0.0.11, Visitron GmbH) and ImageJ v1.46 software.

### 3.2.24 Transferrin Receptor 1 (TfR1) flow cytometric internalization assay

Activated day 5 WT and Flower Knockout CTLs were washed with PBS and incubated at 37 °C for 2 h in serum-free AIMV medium. The cells were then washed with cold PBS and incubated with purified rat anti-mouse TfR1 (R17217) for crosslinking or Rat IgG2a isotype control for 30 min on ice. Cells were then washed and resuspended in cold PBS and an aliquot was stained with AlexaFluor 488 goat anti-rat IgG2a antibody to measure the baseline TfR1 expression. The remaining cells were placed at 37 °C for 15 and 30 min and internalization was stopped by incubating cells on ice and washing with ice cold PBS. The cells were stained with the fluorescent coupled secondary antibody, followed by flow cytometry analysis (FACS, BD FACSAria III) (Figure 19). Data were analysed using FlowJo software (Celeza-Switzerland). For control, WT CTLs were pre-treated with 15  $\mu$ M pitstop2 (ab120687; Abcam; 30 mM stock) or pitstop2 negative control (ab120688; Abcam; 30 mM stock) for 3 min at room temperature in serum-free AIMV, followed by normal staining procedure with TfR1 staining. % TfR1 internalized was calculated as follows:  $(MFI \text{ at zero min} - MFI \text{ at specified time point}) \times 100 / MFI \text{ at zero min}$ , where MFI stands for Mean fluorescent intensity.



**Figure 19: Schematic diagram showing a brief procedure of Tfr1 internalization assay**

### 3.2.25 Immunocytochemistry

CD8<sup>+</sup> T lymphocytes from WT and Flower KO mice were activated for 5 days with beads and IL2 as described above. Prior to staining, 12 mm coverslips were coated with poly-L-ornithine (0.01%) for 20 min. Beads were removed from activated CTLs, washed with isolation buffer and resuspended in AIMV medium. 80  $\mu$ l CTLs ( $0.5 \times 10^6$ ) were put on poly-L-ornithine coated glass coverslips and were allowed to adhere to the coverslip for 10 min at 37 °C with 5% CO<sub>2</sub>. The cells were then fixed with ice-cold 4% PFA immediately for 20 min. Fixed cells were washed twice with PBS and quenched using PBS containing 0.1 M glycine for 3 min. The cells were washed twice with PBS and kept at 4 °C. Cells were then ready for immunolabeling.

For immunostaining, fixed cells were permeabilized with PBS containing 0.1% Triton X-100 for 20 min and were blocked using blocking solution (PBS with 0.1% Triton X-100, 2% BSA) for 30 min. The antibody dilutions were prepared in blocking buffer. The primary antibody was added and cells were incubated for 1 h at RT before washing 5 times (5 min each) with PBS (0.1% Triton X-100). Coverslips were then incubated with the respective secondary antibody in blocking buffer, for 45 min at RT. The cells were washed and mounted onto glass slides in mounting medium. Coverslips were allowed to dry for about 15-30 min and then kept at 4 °C, ready to be imaged.

### 3.2.26 Software used

CorelDRAW 2019, version 21.0.0.593, Corel Corporation

ImageJ 1.52p (Wayne Rasband, National Institutes of Health, USA) (Schneider et al., 2012)

JACoP (Just Another Colocalization Plugin) from ImageJ (Bolte and Cordelieres, 2006).

Microsoft Office 2019

SigmaPlot Version 13, Systat Software, Inc.

SnapGene Viewer 5.1, GSL Biotech LLC

Zeiss Efficient Navigator (Zen) 2012, Carl Zeiss

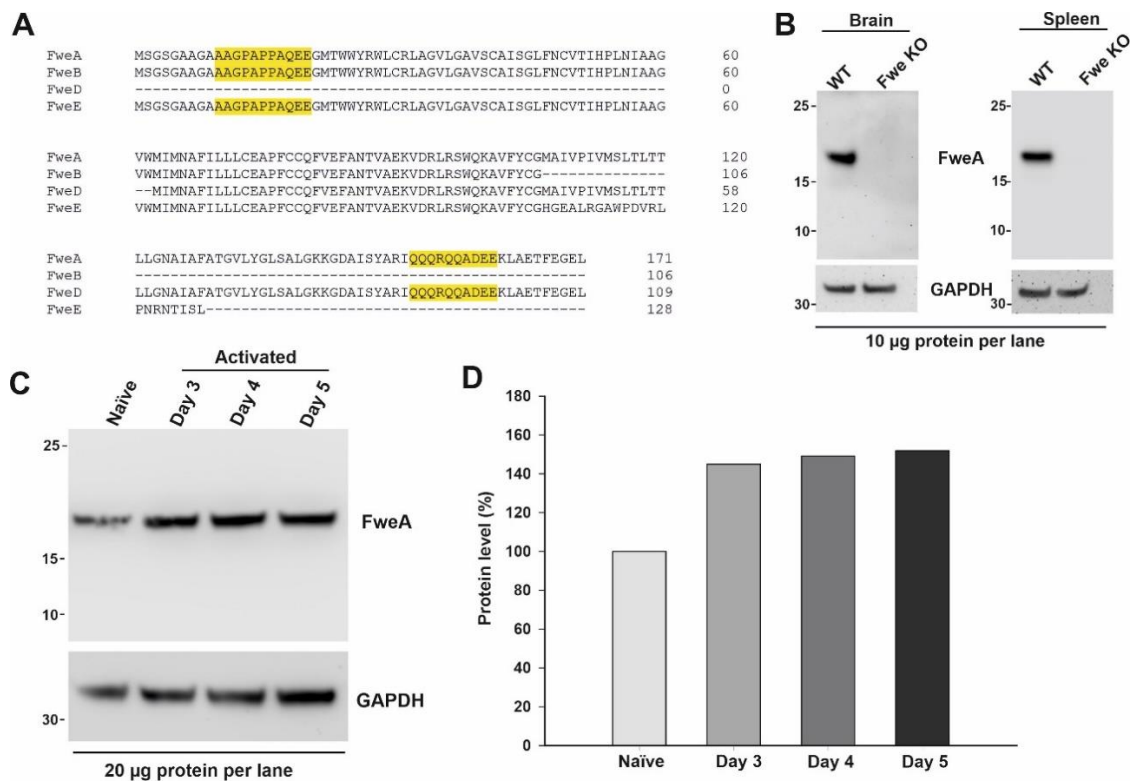
BD FACS Diva software v6.1.3

FlowJo\_v10.6.0

## 4. Results

### 4.1 Flower is expressed in the mouse spleen and primary cultures of CD8<sup>+</sup> T cells

The protein expression of murine Flower was first analysed using western blotting of whole brain and spleen proteins using rabbit polyclonal anti-Flower antibody that binds to epitopes at the N (amino acid 10-20) and the C (amino acid 152-161) termini of mouse Flower (Fwe) protein (Chang et al., 2018) (Figure 20A, sequence marked in yellow). Therefore, we expect the antibody to detect all four isoforms of mouse Fwe. The lysate from Fwe KO mouse was used as a negative control. The Fwe protein was detected as a 19 kDa band in WT mouse and was absent in Fwe KO brain and spleen lysates (Figure 20B).



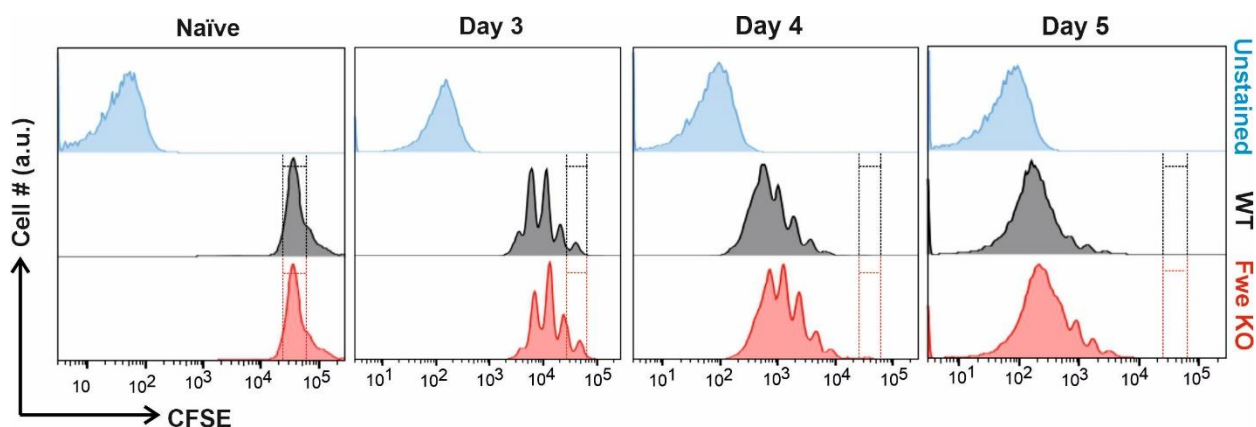
**Figure 20: Flower protein is expressed in mouse primary cytotoxic T lymphocytes (CTLs) and is upregulated after activation**

(A) Sequence alignment of murine Flower (Fwe) isoforms using Clustal Omega was done and epitope binding site of polyclonal anti-Fwe antibody is marked in yellow. Note that the antibody can detect all four isoforms of mouse Fwe. (B) Western blot analysis of lysates from brain and spleen of wild-type (WT) and Flower-deficient (Fwe KO) mice were used and probed using anti-Fwe antibody and anti-GAPDH antibody was used as a loading control. 10 µg of the lysate was loaded into each lane. FweA protein band of 19 kDa was detected only in WT lysates. (C) Primary CD8<sup>+</sup> T cells were isolated from WT mice and activated for 5 days using anti-CD3/CD28 dynabeads and 100 U of Interleukin 2 (IL2). Western blot analysis was done on lysates of naive and day 3, 4 and 5 activated CD8<sup>+</sup> T cells and probed using anti-Flower antibody. 19 kDa FweA band was detected in naive and activated CTLs. 20 µg of protein was loaded per lane and GAPDH was used as loading control. (D) Quantification of Flower protein expression in naive cells and after different days of activation (% normalized to GAPDH) by densitometry.

CD8<sup>+</sup> T cells were then isolated from mouse spleen and the cells were activated for 5 days using CD3/CD28 dynabeads and 100 U Interleukin2 (IL2). Western blot analysis showed the expression of Fwe on naive (day 0) and activated mouse CD8<sup>+</sup> T cells (Figure 20C) and was upregulated over different days of activation (Figure 20D, 100% for naive, 144% on day 3, 147% on day 4 and 151% on day 5). Although all splice variants could be detected as mRNA (details are described in an upcoming chapter, Fig. 27), notably only the largest form of Fwe isoforms that is FweA (19 kDa) was detected in western blot, whereas the other isoforms were undetectable (FweB-12 kDa, FweD-12 kDa, FweE-14 kDa). Since the expression of FweA protein band was seen dominating in the lysates, the lower molecular weight protein bands could be masked and undetected. Presumably, the weak endogenous expression of the other mouse Fwe isoforms in the tissues and primary cells could also explain the detection limit in the western blot analysis.

## **4.2 Flower KO CTLs show similar proliferation rates and CTL subset profile to Wild type CTLs**

Having detected the expression of Fwe protein, we wanted to investigate whether the Fwe KO CTLs show differences in division state and CTL subset transition during activation. Since proliferation of CTLs is an important factor for the fitness and overall integrity of the cells, CFSE staining of WT and Fwe KO CTLs was done to compare division staging in parent and daughter cells. The CFSE dye was used to monitor distinct generations of proliferating cells by dye dilution. Flow cytometry analysis showed a staining of almost all day 0 CD8<sup>+</sup> T cells (naive, non-activated and undivided cells) with CFSE dye in both WT and KO CTLs which then could be followed over the different days of activation. On day 3, four generations of cells were seen in Fwe KO CTLs as well as WT cells. Obviously at day 4 and day 5 cells may further proliferate. Due to the dilution effect of the dye, a clear counting of generations was no longer possible but still there were no differences between Fwe KO and WT (Figure 21).

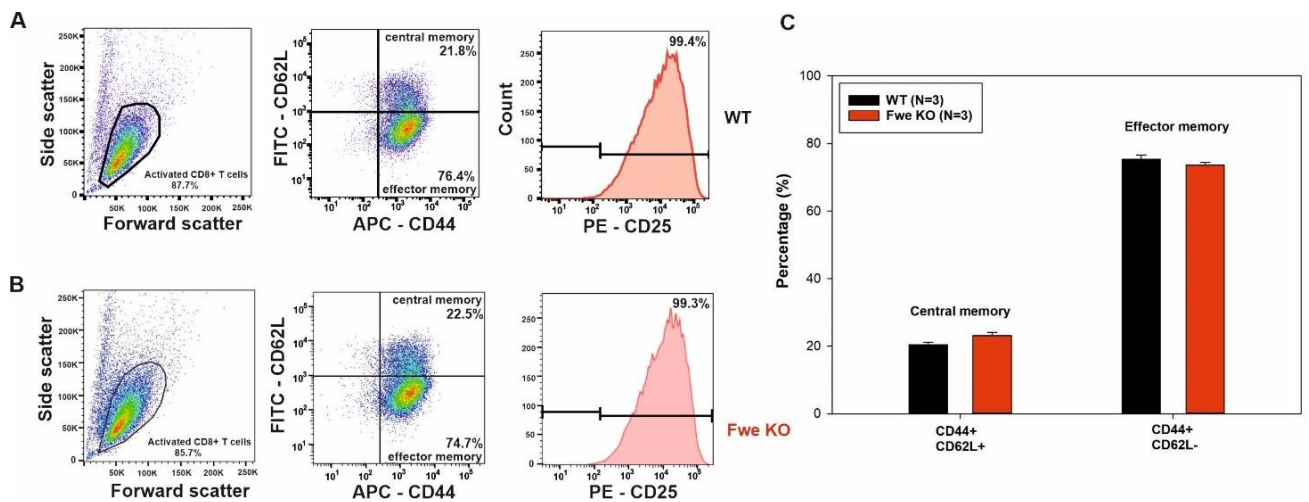


**Figure 21: Fwe KO CTLs show similar proliferation stages compared to WT cells**

Day0 (naive) primary CD8<sup>+</sup> T cells from WT (black) and Fwe KO (red) were labelled with 5  $\mu$ M of CFSE and then were cultured for 5 days using anti-CD3/CD28 dynabeads and 100 U IL2. Flow cytometric analysis was done on day 3, 4 and 5 to determine the intensity of CFSE staining using excitation of 488 nm. The histogram gating was done based on CD8<sup>+</sup> T cells of 85 to 90% live population. The different peaks in the histogram represent different cell generations stages. Gating in dotted lines represents the initial undivided cell population. Unstained cells (blue) were used as baseline control for auto-fluorescence.

The cells were then analyzed for the different CTL subsets using CD (Cluster of differentiation) markers expressed on the surface of CTLs. The CD62L<sup>+</sup> and CD62L<sup>-</sup> cells represent naive and effector populations, CD44<sup>+</sup> is a marker for effector memory cells and CD62L<sup>+</sup>/ CD44<sup>+</sup> double positive cells represent central memory cells. Since all the subsequent experiments were performed on day 5, the CTL subset staining was performed on this day. WT and Flower KO CTLs showed similar subset profiles on the day 5 that mainly consisted of the effector memory population (76.4% in WT and 74.7% in Fwe KO cells) and some remaining central memory cells (21.8% in WT and 22.5% in Fwe KO cells) (Figure 22A, 22B). The general activation state of the cells was analyzed using anti-CD25 antibody (marker for IL2 receptor) and was also found to be similar between WT (99.4%) and Fwe KO (99.3 %). We conclude from these experiments that the Flower protein does not play a major role in proliferation and differentiation of CTLs.



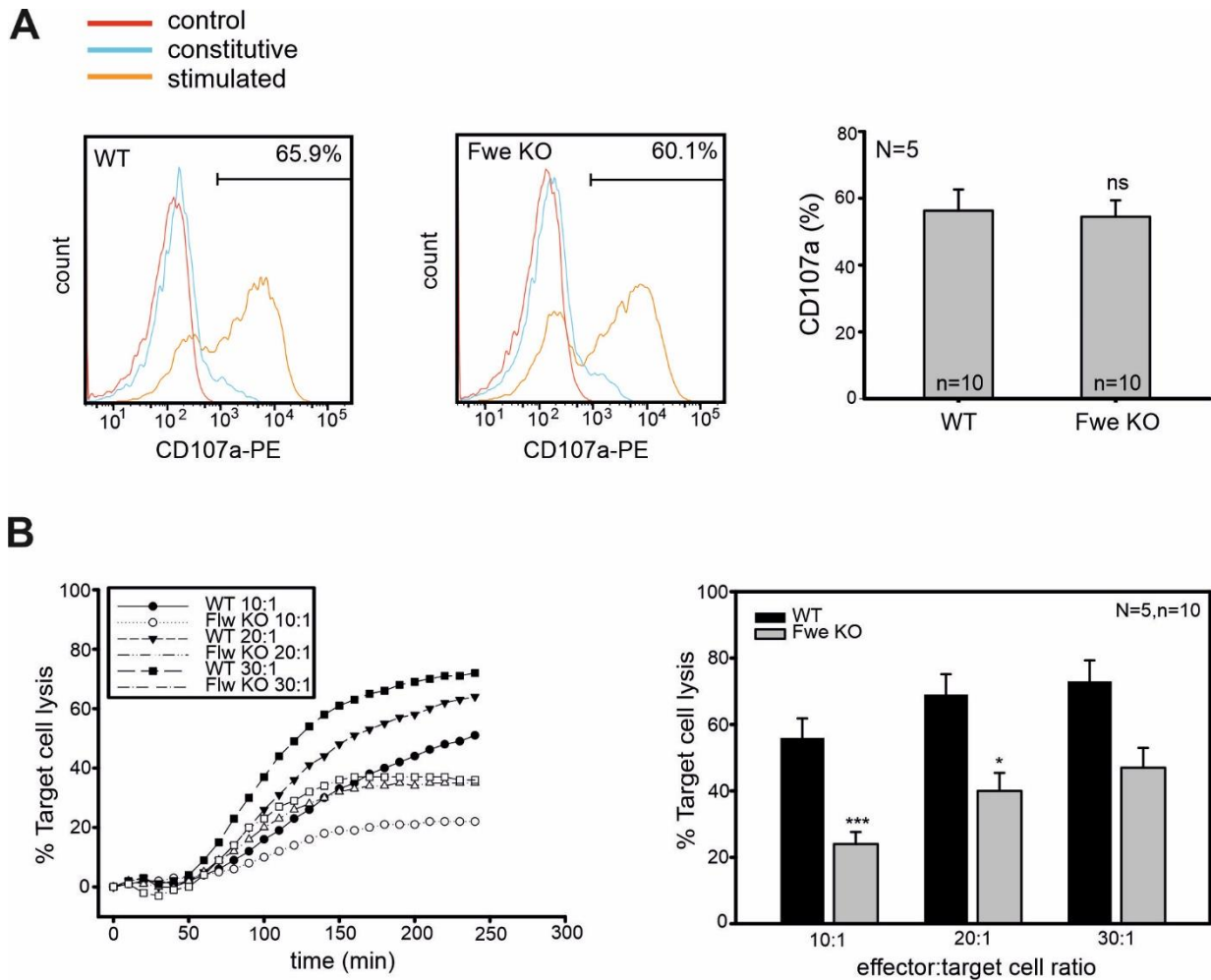


**Figure 22: Fwe KO CTLs show similar CTL subsets compared to WT cells**

Flow cytometry analysis of day 5 activated CTLs to study the subtype population using surface markers CD62L and CD44. (A) CD8<sup>+</sup> T from WT were activated for five days and stained using CD62L-FITC, CD44-APC and CD25-PE antibodies. Healthy CTLs were first selected based on forward and sideward scatter (left panel). Those cells were plotted according to the surface markers CD62L and CD44 (middle panel) resulting in the detection of 76.4% of effector memory and 21.8% of central memory cells. In addition, the general activation state of cells was analyzed using the surface marker CD25 (right panel). (B) same as (A) for Fwe KO cells. 74.7% were effector memory and 22.5% central memory cells. All gating was done in comparison to unstained control (not shown). (C) Quantification and average percentage of effector and central memory cells between WT and Fwe KO CTLs from three independent experiments (N=3; values shown as mean ± SEM).

### 4.3 Loss of Flower reduces the killing efficacy of CTLs but does not affect exocytosis of CGs directly

Since Flower KO CTLs showed similar phenotype in proliferation and subset population, next we wanted to understand the function of Flower protein in granule exocytosis. A degranulation assay was performed to study the fusion of lysosomes and cytotoxic granules (CGs) by measuring the surface expression of LAMP1 (lysosome-associated membrane protein 1 or CD107a) by flow cytometry (Betts et al., 2003; Chang et al., 2019). The CD107a surface-expression in WT and Fwe KO derived CTLs, which had been stimulated with 10 µg/ml of anti-CD3ε antibody (Figure 23A, orange line in WT and Fwe KO), was compared. There was no significant difference in the two groups, with 57% and 55% of LAMP1 surface expression, respectively.



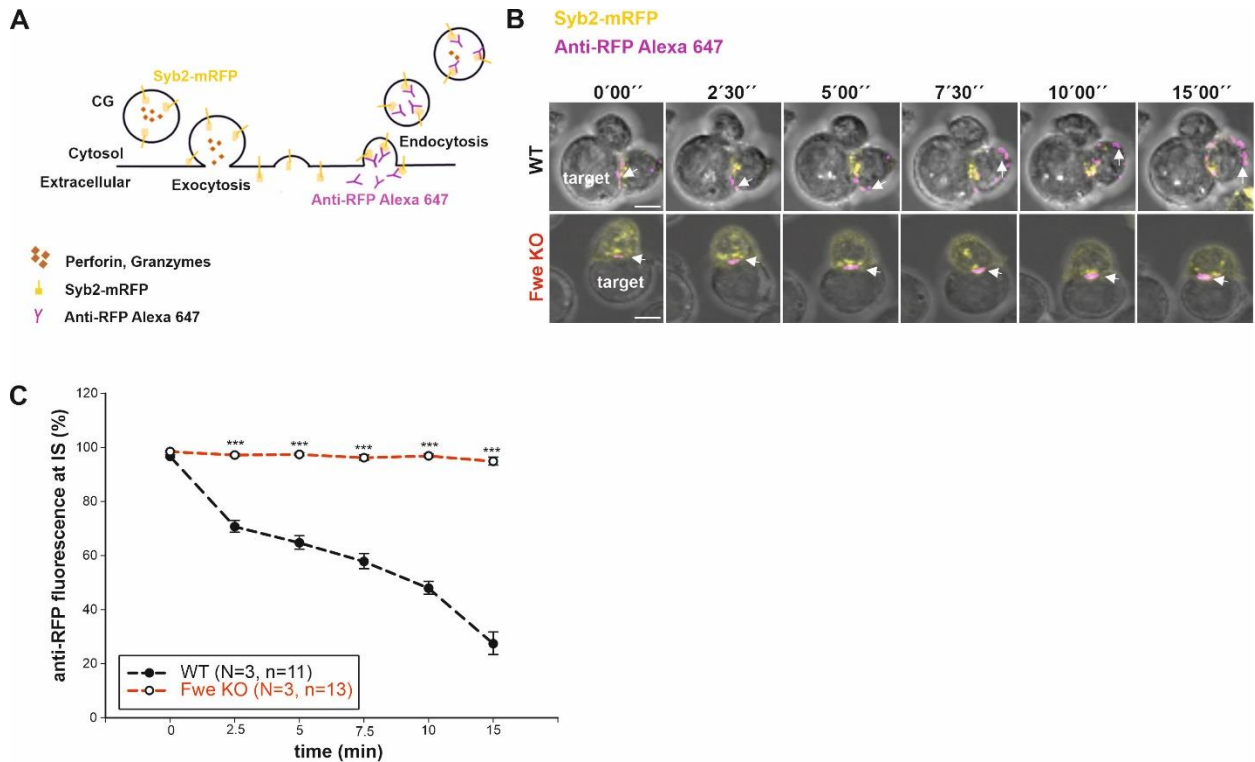
**Figure 23: Exocytosis of CG granules is unaffected, but the killing efficiency is decreased in Fwe KO CTLs**

(A) Flow cytometry-based degranulation assays of WT and Fwe KO CTLs showing constitutive (blue) and 10  $\mu$ g anti-CD3 $\epsilon$  stimulated (orange) surface expression of CD107a. Cells in the absence of CD107a-PE antibody served as controls (red). One representative experiment is shown. Statistical analysis (right side) of the average percentage of cells exhibiting CD107a fluorescence at the plasma membrane after stimulation ( $N = 5$ ;  $n = 10$ ). ns,  $P > 0.05$ . (B) Real-time calcein release-based killing assay of different CTL: P815 target cell ratios from WT and Fwe KO mice. Killing was measured every 10 min for 4 h. Data are given as mean  $\pm$  SEM from five independent experiments performed in duplicates ( $N = 5$ ,  $n=10$ ). One-tailed unpaired Student's  $t$  test: \*,  $P < 0.05$ ; \*\*\*,  $P < 0.001$  (data already published in Chang et al., 2018).

The unchanged surface expression of LAMP1 is a strong argument that the overall exocytotic capacity of CTLs is not Flower-dependent. But this result does not test if the exocytosed lytic granules are functional. To directly check functionality, we performed a real-time killing assay with varying T:target cell ratios. A decrease in the fluorescence intensity of preloaded fluorophore calcein in target cells was used as a read-out for necrosis of the target cells (Kummerow et al., 2014). A significant decrease in killing efficiency (measured by the percentage of target lysis) in Fwe KO CTLs compared to that of WT was seen, especially at the low T:target cell ratio of 1:10 (Figure 23B). These results show that although Flower does not affect CG exocytosis, it plays a major part in the killing by effector CTLs.

#### **4.4 Flower KO blocks endocytosis of Synaptobrevin2 but does not affect Transferrin receptor (TfR1) uptake**

The decrease in killing seen in Flower KO CTLs might be due to inefficient endocytosis of CG membrane proteins which could result in limited availability of components required for serial killing of target cells. In order to test whether Flower has a function in CG material endocytosis, real-time confocal imaging was performed on activated day 5 CTLs transfected with Syb2-mRFP. It is known that Syb2 is localized in CG membranes (Matti, 2013), and that the mRFP of our overexpressed fusion-protein is directed to the lumen of CG. Therefore, we expected that exocytosis would lead to a presentation of mRFP at the cell surface where an anti-RFP antibody coupled to Alexa647 fluorophore (that was added to the extracellular medium) could bind with it. Hence, endocytosis could be quantified as the uptake of the fluorescent anti-RFP antibody (Figure 24A). Live cell imaging was started when P815 target cells were added. Retrospectively time 0'00" was set when the first signal from the anti-RFP-Alexa647 antibody appeared inside or at the surface of a CTL (Figure 24B, C). In WT and Flower KO cells, polarization of CG granules (marked by Syb2-mRFP, yellow) to the IS was seen. Uptake of mRFP-647 antibody, via endocytosis at the IS, into the cytosol of the cell (yellow Syb2-mRFP puncta co-localized with magenta RFP647 puncta) could be seen in WT cells (within 2.5 min) but not in Flower KO CTLs (Figure 24B, C). Fwe KO CTLs showed an accumulation of the Syb2-mRFP-Alexa 647 antibody at the IS over a period of 15 min (Figure 24B, bottom row), but no uptake occurred. The anti-RFP fluorescence at the IS showed a steep decrease in WT cells (mean intensity of  $96.7\% \pm 0.5$ ,  $70.9\% \pm 2.2$ ,  $64.9\% \pm 2.5$ ,  $58\% \pm 2.8$ ,  $48\% \pm 2.3$  and  $27.5\% \pm 4.1$  at time points 0, 2.5, 5, 7.5, 10 and 15 min; black curve) remained high (mean intensity of  $98.5\% \pm 0.4$ ,  $97.2\% \pm 0.5$ ,  $97.5\% \pm 0.6$ ,  $96.2\% \pm 1$ ,  $97\% \pm 0.6$  and  $95\% \pm 1.5$  at time points 0, 2.5, 5, 7.5, 10 and 15 min; red curve) in Fwe KO cells (Figure 24C). These data indicate that loss of Flower protein leads to a block in endocytosis of CG related material.

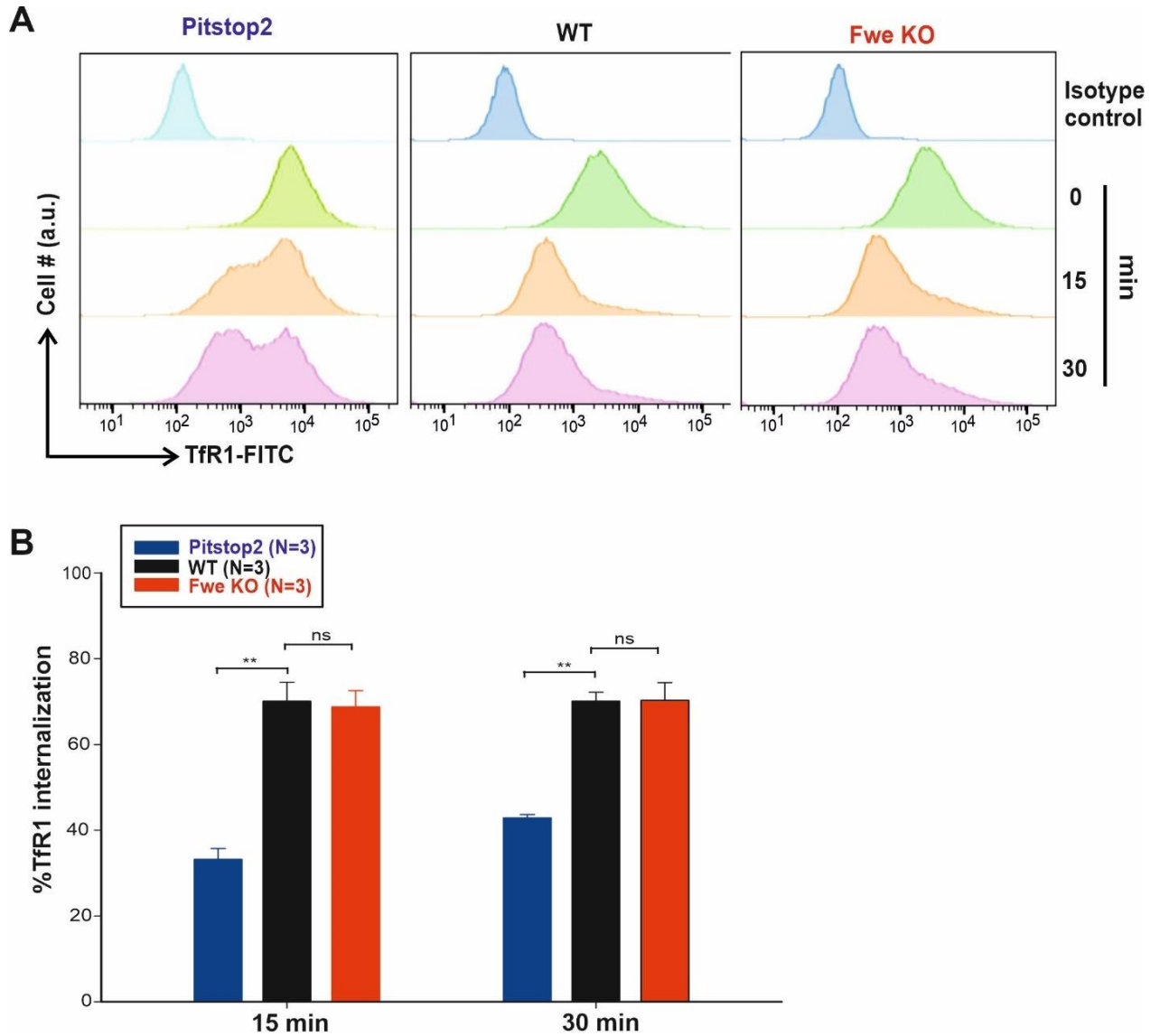


**Figure 24: Fwe KO CTLs show a block in Syb2 endocytosis**

(A) Schematic diagram depicting the principle of the quantification of Syb2 endocytosis using Alexa 647 coupled anti-RFP antibody added to the medium. (B) Time-lapse live snapshots over 15 min of Syb2-mRFP (yellow) transfected CTLs conjugated to P815 target cells in the presence of anti-RFP647 antibody (magenta) in the medium. The endocytosis of Syb2 (arrows) is shown in WT (upper panel) and Flower-KO (lower panel) cells. Scale bar: 5  $\mu$ m. (C) Quantitative analysis of the redistribution of endocytosed Syb2 (anti-RFP647) from the IS into the cytosol. IS was defined by one third of CTL volume facing towards the target cell. Time zero is defined as the appearance of the first fluorescent Syb2 signal at the IS. Data given as mean  $\pm$  SEM; One-way Analysis of Variance (ANOVA), \*\*\*  $p < 0.001$ .

In order to examine if loss of Flower specifically reduces endocytosis of material which is related to CGs such as Syb2, we analysed if the endocytosis of other CG-independent plasma membrane proteins is also defective in the Fwe KO. We chose the Transferrin receptor1, which is well known to be taken up after binding its target, via clathrin mediated endocytosis (Mayle et al., 2012). For the original experiment, TfR1 receptors were cross-linked with a functional anti-TfR1 antibody. The cells were maintained at 37  $^{\circ}$ C. The surface expression of TfR1 was probed 15 and 30 min after treatment, using a secondary antibody coupled to FITC. Pitstop2 (15  $\mu$ M), a potent inhibitor of clathrin mediated endocytosis, was used as a positive control (to test the phenotype of a block of transferrin receptor uptake (Figure 25A, left panel). A significant decrease in receptor-mediated endocytosis was seen in Pitstop2 treated cells after 15 and 30 min (Figure 25B, 33%  $\pm$  2.5, 43%  $\pm$  0.8 at 15 and 30 min, dark blue bar). No comparable block was observed in Flower KO cells.

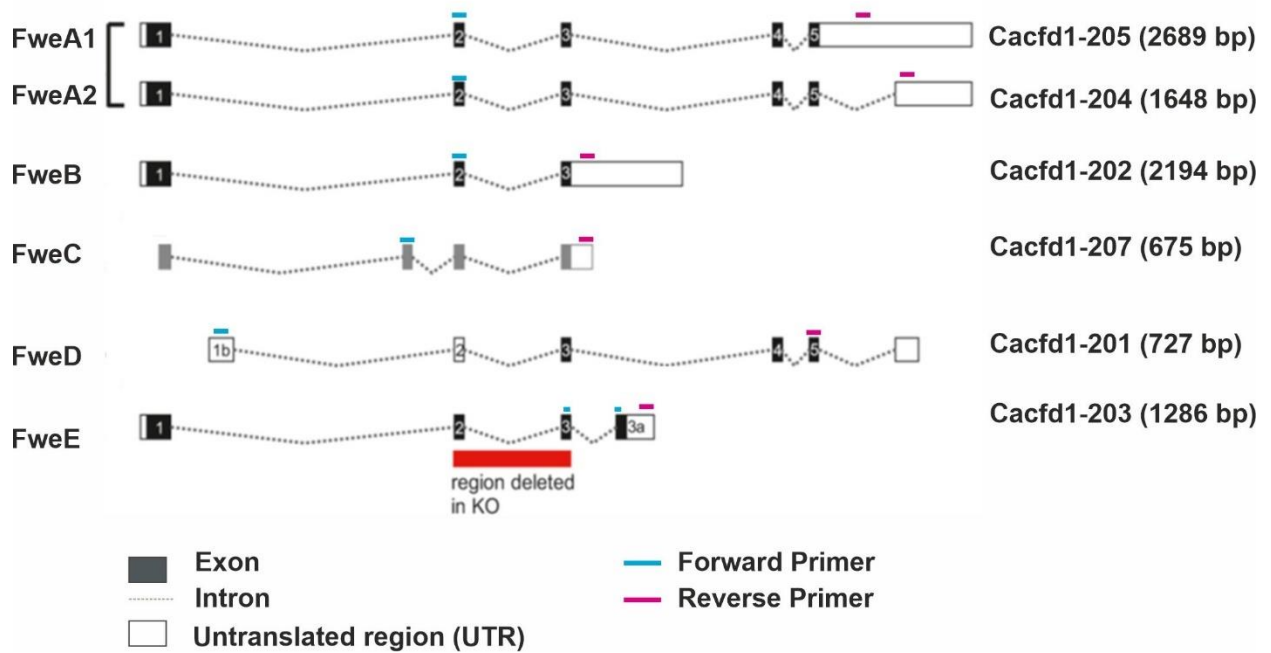
Since loss of Flower did not show any defect in the constitutive receptor-mediated endocytosis, we suggest a very specific role of Flower in endocytosis of CG proteins.



**Figure 25: Fwe KO CTLs do not show defect in Tfr1 internalization**

(A) Representative flow cytometric histogram analysis showing remaining Tfr1 expression on the surface of day 5 activated CTLs after Tfr1 endocytosis run 15 and 30 min in WT and Fwe KO CTLs. Isotype control (light blue histogram) was used as baseline gating. Pitstop2 was added to WT cells independently to block endocytosis and Tfr1 expression was measured. (B) Quantification of pooled mean fluorescence intensity of Tfr1 internalization from pitstop2 treated, WT and Fwe KO cells. Error bars represent mean  $\pm$  SEM; One-way Analysis of Variance (ANOVA), \*\* $p < 0.01$ , ns  $p > 0.05$ .

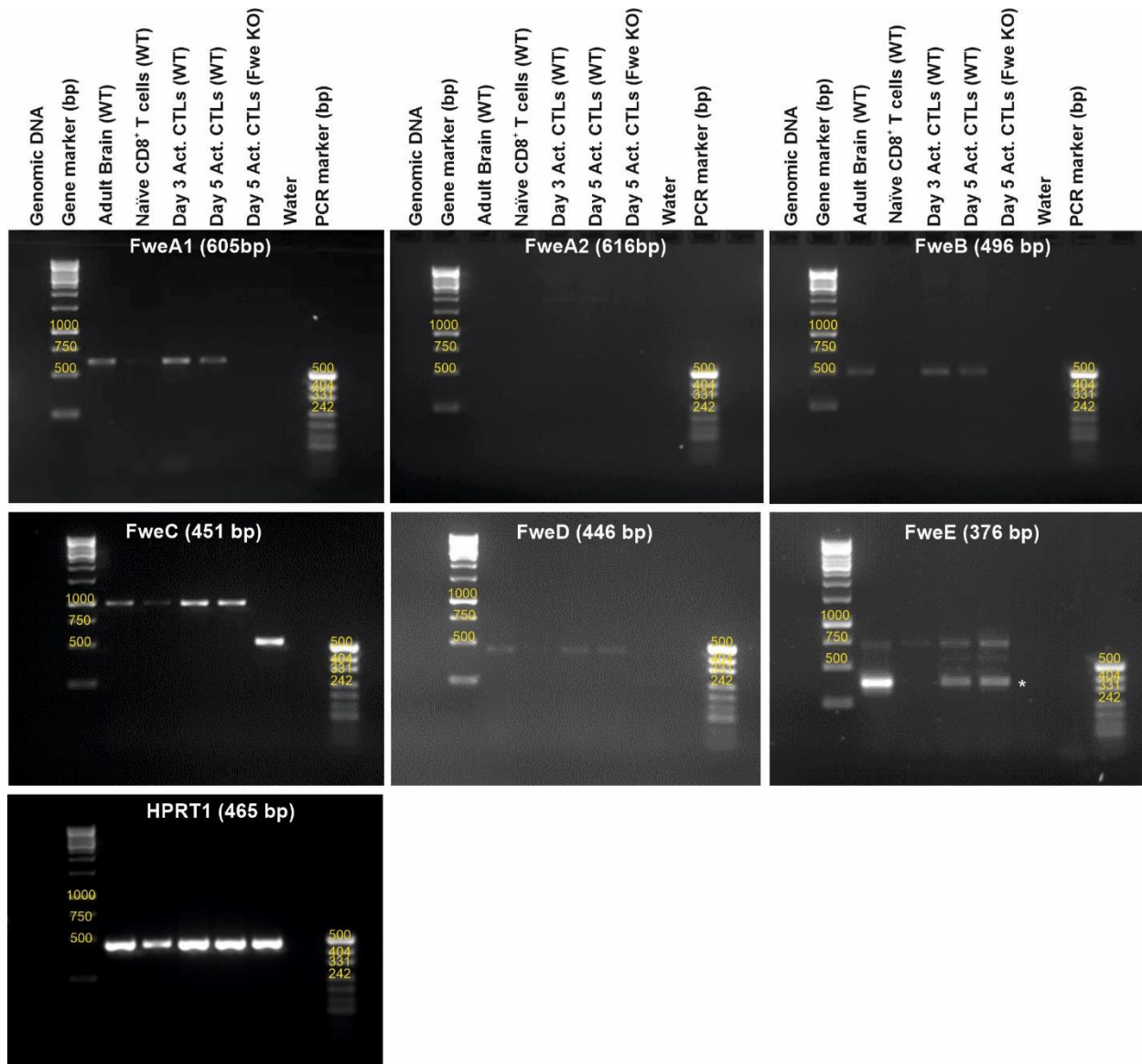
## 4.5 Mouse CTLs express 5 splice variants of murine Flower protein



**Figure 26: Murine Flower transcript variants**

Schematic depiction of the murine Flower gene locus showing protein-coding alternative splice transcripts. The exon sequence is portrayed as black boxes, whereas white boxes represent untranslated sequences (UTR). Exons are marked by a number, whereas alternative exons have been labelled by a number followed by a letter. The size of the transcript is shown next to each variant. A red line marked shows the common exon that was targeted for deletion to generate the Flower KO mouse used during this thesis. The small blue and pink line about each transcript indicated the position of the primer designed for RT-PCR.

The murine Flower gene (5930434B04Rik (accession number: MGI:1924317)) (Flicek et al., 2010) encodes six different transcripts namely A1, A2, B, C, D and E, which are translated into four protein isoforms. At the exon level, FweA1 and A2 translate into the same amino acids but differ in their nucleotide sequence. FweB lacks Exon4 and 5. FweC lacks a start codon and contains an extra Exon between exons1 and 2. The start codon of FweD begins at exon3 and is similar to FweA at the exon level. FweE is similar to FweB but contains an extra short exon 3a which is not conserved among the splice variants. The major similarity among the 6 splice variants is the presence of conserved Exon 3 (Figure 26).

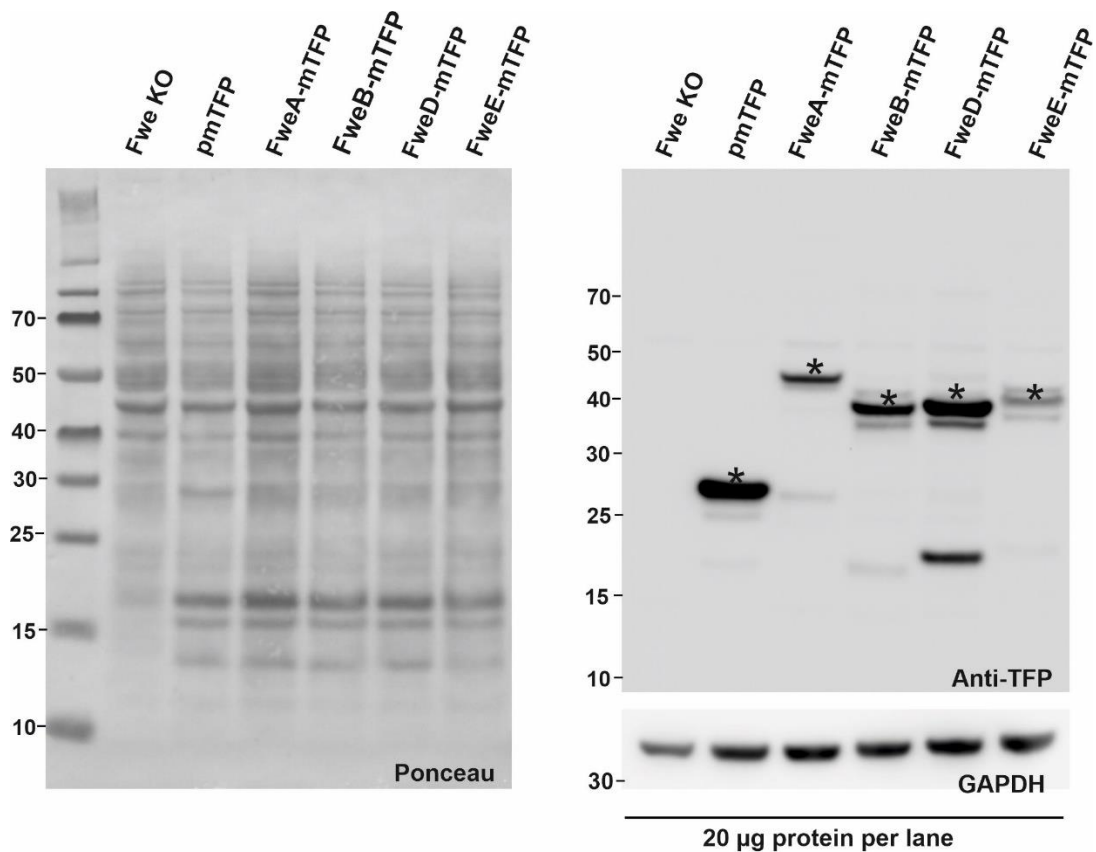


**Figure 27: Except for FweA2, mRNA for all murine splice variants is present in primary cytotoxic T lymphocytes**

Representation RT-PCR gel images showing the expression of murine Flower splice variants from cDNA template isolated from WT naive and 5 days activated mouse CTLs. cDNA from brain and Fwe KO day 5 cells were used as control. The expected size of the PCR product is indicated for each splice variant. HPRT1 was used as a loading control. \* Indicates PCR band of expected size for FweE PCR.

To analyse the transcription of the murine Flower splice variants in mouse CD8<sup>+</sup> T cells, RT-PCR was performed on cDNA of naive and activated day 3 and 5 CTLs. The primers for the RT-PCR were designed specifically at characteristic exon-intron borders to identify and differentiate the different splice variants (Figure 26, marked in blue and pink). cDNA from mouse whole brain was used as positive controls and cDNA from day 5 Fwe KO CTLs were used as negative controls. The PCR result showed an upregulation of all splice variants from naive to activated CTLs. Fwe A2 was not expressed under any condition (Figure 27).

Since the antibody did not detect the isoforms of Flower endogenously at the protein level in western blot (Figure 20), it is unclear if the different mRNAs are translated into protein or if the antibody can only detect the full-length product. The protein detection limit could also be due to the dominant FweA expression or low expression of the other isoforms. Nevertheless, to further characterise the function of putative splice variants we cloned expression plasmids for all splice variants (A1, B, D and E) tagged with C-terminal TFP (teal-fluorescent protein) and expressed them in day 4 CTLs. After 12-14 h of transfection with the respective splice variants, the cells were lysed and used for western blotting. Empty vector containing mTFP (pmTFP (26 kDa)) was used as a control. The fusion protein of all splice variants was detected at the correct protein size (FweA-mTFP: 46 kDa, FweB-mTFP: 39 kDa, FweD-mTFP: 39 kDa, FweE-TFP: 41 kDa) using anti-TFP probing (Figure 28, marked \*). These constructs were later used for endocytosis rescue experiments.



**Figure 28: Expression of Flower isoforms-mTFP fusion constructs in mouse CTLs**

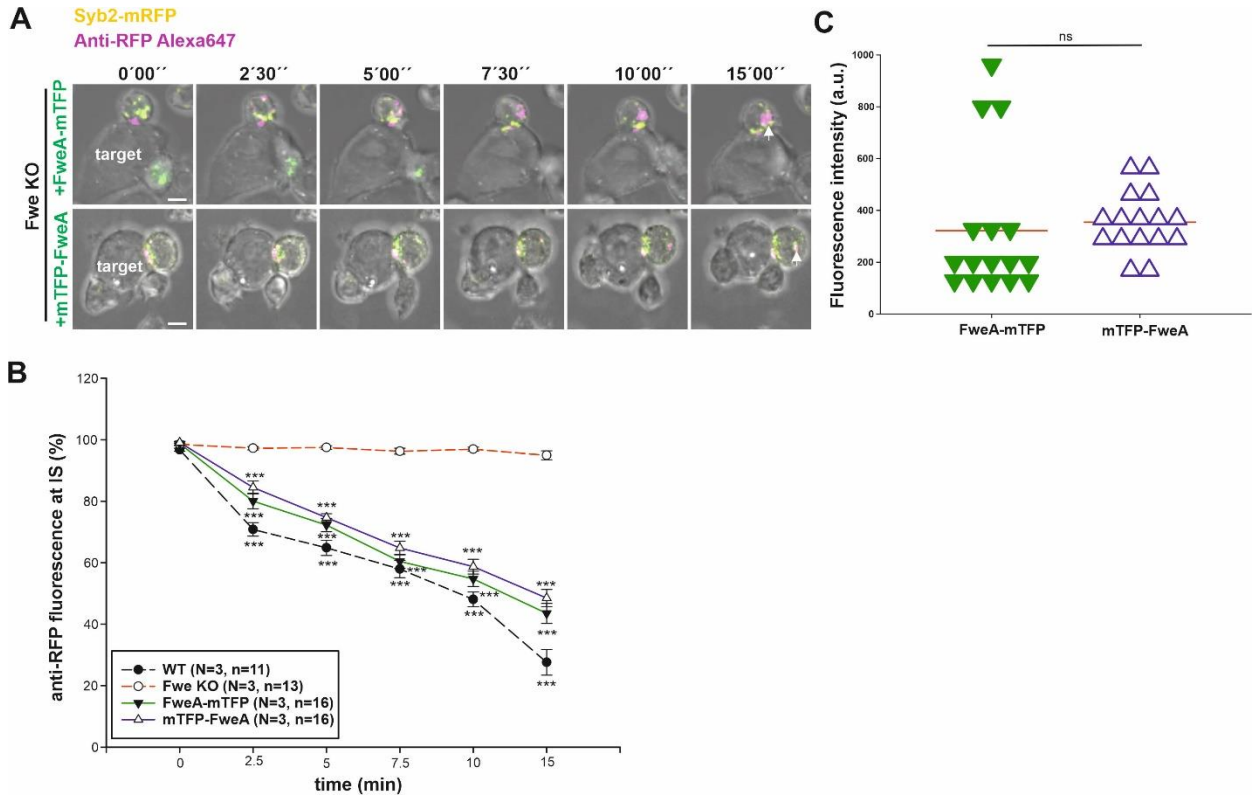
Western blot analysis of day 5 activated Fwe KO CTLs transfected with Flower isoforms fusion constructs tagged to mTFP. The blot was probed with anti-TFP antibody against the mTFP protein. GAPDH was used as loading control. \* Represents protein bands of expected size. Ponceau staining on the left was done to show proper protein run of the lysates during electrophoresis.



#### 4.6 FweA tagged at either the N- or C-terminus was able to rescue endocytosis of Syb2 in Flower KO CTLs

To test if the phenotype of endocytosis block in Fwe KO (Figure 24) could be rescued by reintroduction of FweA, the previously described fusion constructs (Figure 28) and in independent experiments also an N-terminal fusion protein was overexpressed in Flower KO CTLs together with Syb2-mRFP. After 14 h of expression, cells were conjugated to target cells and real time imaging was done to analyse endocytosis as described (Figure 24). Since it was shown previously that the N- and C-termini of FweA faces the cytosol of the CTL (Chang et al., 2018), the marker antibody cannot bind to mTFP of Fwe protein. Therefore, we used the RFP647 antibody, which is specific to the Syb2-mRFP binding site, to quantify endocytosis of FweA. Expression of the FweA fusion constructs resulted in the internalization of anti-RFP647 antibody-positive puncta (magenta) towards the cytosol and was no longer seen accumulated at the plasma membrane. This indicated the reversal of the endocytic defect by expression of FweA fusion plasmids in Flower KO CTLs (Figure 29A, arrow pointed). Quantification of the anti-RFP antibody-positive puncta at the IS was then calculated over 15 min. A decrease in the fluorescence of anti-RFP647 antibody-positive puncta was observed at the IS over time in mTFP-FweA transfected (mean intensity of  $99.1\% \pm 0.3$ ,  $84.5\% \pm 2$ ,  $74.6\% \pm 1.2$ ,  $64.8\% \pm 2.1$ ,  $58.7\% \pm 2.4$  and  $48.5\% \pm 2.8$  at time points 0, 2.5, 5, 7.5, 10 and 15 min; Figure 29B, dark blue) and FweA-mTFP transfected (mean intensity of  $98.7\% \pm 0.5$ ,  $80\% \pm 2.5$ ,  $72.2\% \pm 2.1$ ,  $60.4\% \pm 2.3$ ,  $54.8\% \pm 2.5$  and  $43.5\% \pm 3.2$  at time points 0, 2.5, 5, 7.5, 10 and 15 min; Figure 29B, dark green) CTLs. Both constructs were able to rescue the block of endocytosis over 15 min to WT levels (Figure 29B) and also showed similar expression levels (Figure 29C, mean intensity of 354.8 for mTFP-FweA vs 321.5 for FweA-mTFP) showing that the mTFP tag at either the N- or C-terminus does not interfere with rescue.

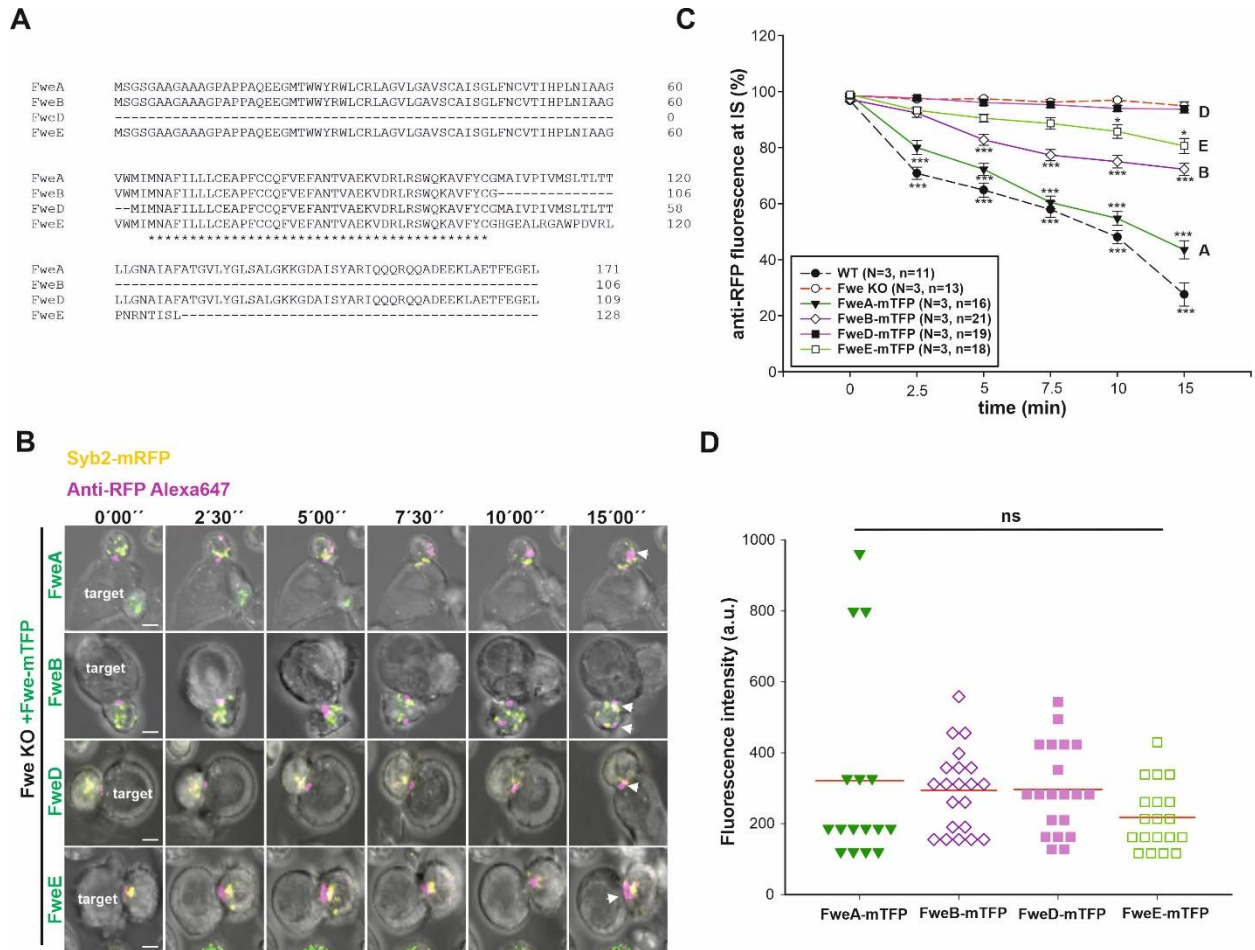
We conclude from these experiments that the loss of endocytosis of Syb2 in Fwe KO CTLs is directly related to the loss of Flower protein.



**Figure 29: FweA tagged with mTFP at either N- or C-terminus can rescue block in Syb2 endocytosis** (A) A sequence of images acquired over 15 min, of Syb2-mRFP (yellow) and FweA-mTFP (green, upper panel) or mTFP-FweA (green, lower panel) transfected Fwe KO CTLs conjugated to P815 target cells in the presence of anti-RFP647 antibody (magenta) in the medium. The endocytosis of CGs (arrow pointed) is shown. Scale bar: 5  $\mu$ m. (B) Quantitative analysis of the redistribution of endocytosed Syb2 (anti-RFP 647) from the IS to the cytosol. Time zero is determined as the appearance of the first endocytic signal at the IS. Data given as mean  $\pm$  SEM; One-way Analysis of Variance (ANOVA) was done against Fwe KO as control, \*\*\*  $p < 0.001$ . (C) Fluorescence intensity of mTFP expression in the cell in both groups were calculated and plotted. Data given as mean in red line. ns  $p > 0.05$ .

#### 4.7 Not all mouse Flower isoforms are able to rescue endocytosis of cytotoxic granule material

Since both N- and C-terminus tagged FweA constructs were able to rescue endocytosis, for further experiments with fusion isoforms we choose the C-terminus mTFP tagged Flower constructs (Figure 28). Fusion constructs of Fwe B, D and E with C-terminus tagged TFP were transfected along with Syb2-mRFP in Fwe KO CTLs. The Flower variant C was not included in the study as this variant does not contain a start codon ATG (that codes for the amino acid methionine) (Figure 26).



**Figure 30: The Flower splice-variants differ in their ability to rescue Syb2 endocytosis in Flower KO CTL**

(A) Protein sequence alignment of mouse Flower isoforms by Clustal Omega. \* Indicate conserved aminoacids. (B) Time-lapse live snapshots over 15 min of Syb2-mRFP (yellow) of all four Fwe-mTFP isoforms (green) transfected into Fwe KO CTLs conjugated to P815 target cells in the presence of anti-RFP647 antibody (magenta) in the medium. The accumulation and endocytosis of CGs (arrow pointed) transfected with the different Fwe isoforms is shown. Scale bar: 5  $\mu$ m. (C) Quantitative analysis of redistribution of endocytosed Syb2 (anti-RFP647) from the IS into the cytosol for FweA (green), FweB (purple), FweD (pink), FweE (light green). Time zero is determined as the appearance of the first endocytic signal at the IS. Data given as mean  $\pm$  SEM; One-way Analysis of Variance (ANOVA) was done against Fwe KO as control, \* $p < 0.05$ , \*\* $p < 0.01$ , \*\*\*  $p < 0.001$ . (D) Fluorescence intensity of mTFP expression in the cell of the four isoforms. Data given as mean in red line; ns  $p > 0.05$ .

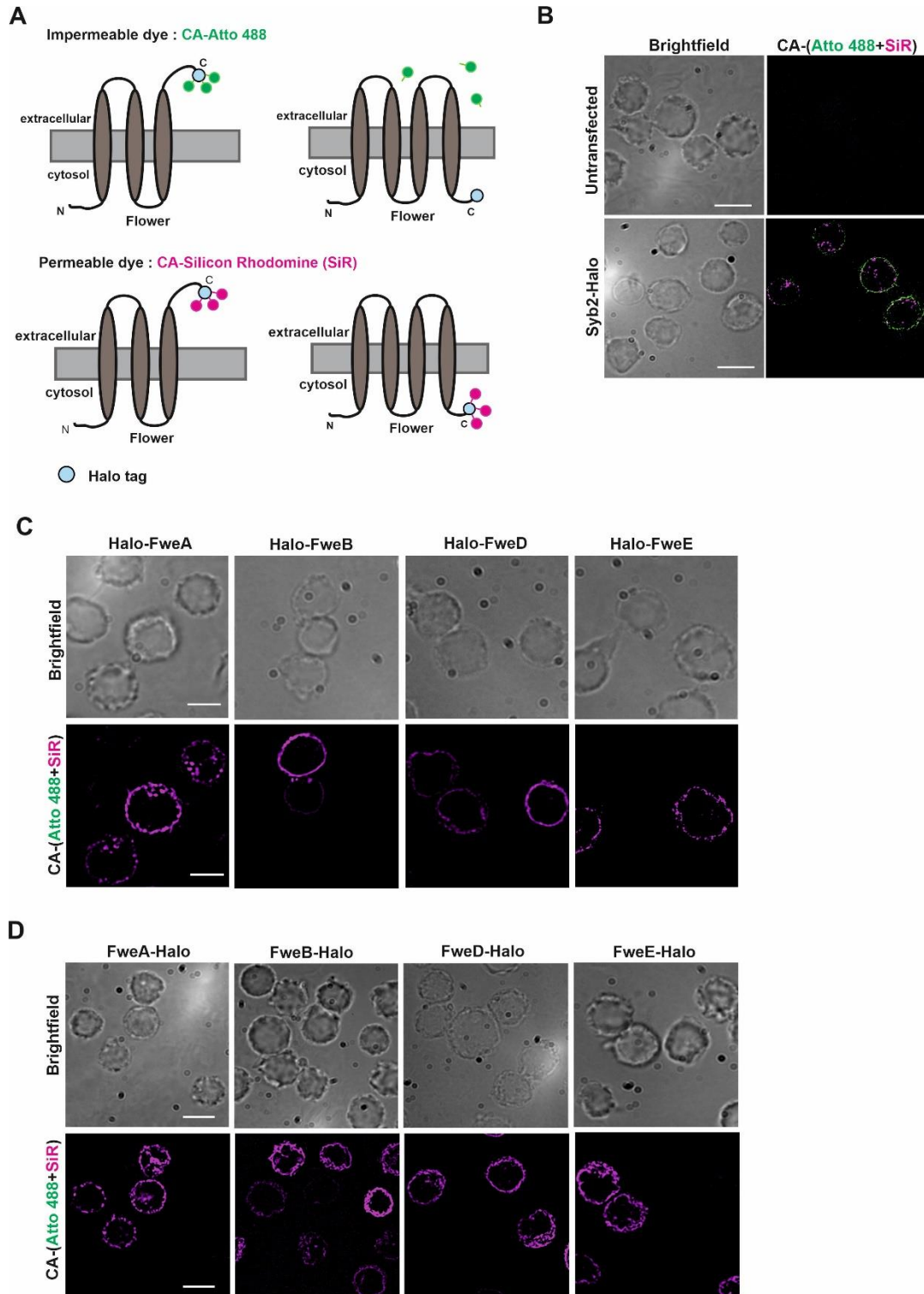
Live imaging of endocytosis rescue with Fwe B showed a partial rescue (Figure 30B, panel 2, arrow) with the fluorescence intensity of anti-RFP647 at IS (mean of  $97.2\% \pm 0.6$ ,  $92.3\% \pm 1.6$ ,  $82.8\% \pm 1.9$ ,  $77.3\% \pm 2$ ,  $75\% \pm 2.2$  and  $72.2\% \pm 2.1$  at time points 0, 2.5, 5, 7.5, 10 and 15 min; Figure 30C, purple) slightly decreasing overtime. There was also a delay in start of endocytosis of around 5 min in comparison to WT cells ( $82\%$  in B to  $64\%$  in WT at 5 min, Figure 30C). FweD showed no rescue of endocytosis at all (Figure 30B, panel 3, arrow) (mean of  $98.5\% \pm 0.6$ ,  $97.7\% \pm 0.8$ ,  $96.1\% \pm 0.9$ ,  $95.3\% \pm 0.9$ ,  $94\% \pm 1.08$  and  $93.7\% \pm 1.4$  at time points 0, 2.5, 5, 7.5, 10 and 15 min; Figure 30C, pink). FweE showed a minimal rescue (Figure 30B, panel 4, arrow) compared

to WT (mean of  $98.9\% \pm 0.5$ ,  $93.3\% \pm 1.1$ ,  $90.5\% \pm 1.4$ ,  $88.6\% \pm 2$ ,  $85.7\% \pm 2.4$  and  $80.6\% \pm 2.7$  at time points 0, 2.5, 5, 7.5, 10 and 15 min; Figure 30C, light green). ). In order to make sure that the difference in rescue by different isoforms is not due to differences in expression level, the mTFP fluorescent intensity of the cell was analysed. There was no significant difference seen in expression level among different Flower isoforms (mean fluorescence (arbitrary units) 293.7 in FweB , 296.4 in FweD and 218 in FweE; Figure 30D) in comparison to FweA isoform (mean 321.4; Figure 30D). The above data shows that not all Flower isoforms rescued Syb2 endocytosis and thus each of the isoforms (Figure 30A) may have a specific role in CTL function.

#### **4.8 Flower topology in the plasma membrane determined by Halo tag fusion constructs**

Flower has been reported to possess 3 or 4 transmembrane domains based on various prediction software and was is partially localized to the plasma membrane, a result which was confirmed by immunostaining and surface biotinylation (Chang et al., 2018). The orientation of N- and C-termini is still not clear. To understand the topology of the Flower protein at the plasma membrane, Flower splice variants were tagged to Halo at either the C- or the N-terminus and transfected at day 5 into CTLs. Subsequently, cells were stained with either Chloroalkane (CA, HALO substrate) Atto488 dye (membrane impermeable) or CA-Silicon Rhodamine (SiR) (membrane permeable) to check the topology of Flower. Since CA-Atto488 is membrane impermeable but CA-SiR is permeable this approach should allow us to decide between an odd (1 or 3) or even (2 or 4) transmembrane model (Figure 31A).

Syb2-Halo transfected cells used as controls (Figure 31B) show clear membrane staining by CA-Atto488 dye indicating that Syb2 was present at the plasma membrane with its C-terminus facing the extracellular space (Figure 31B). Surprisingly, none of the N- and C-terminal Halo tagged Flower splice variants from mouse, showed a signal, leading to the conclusion that neither the N- nor the C-terminus is facing the extracellular space (Figure 31C). This interpretation is strengthened by a second finding that CA-SiR always gives a clear membrane signal. Thus, the above results show that the N- and C-termini of Flower might be oriented towards the cytosol at the plasma membrane in the resting condition which is in favour of the even (2 or 4) transmembrane-domain-model.



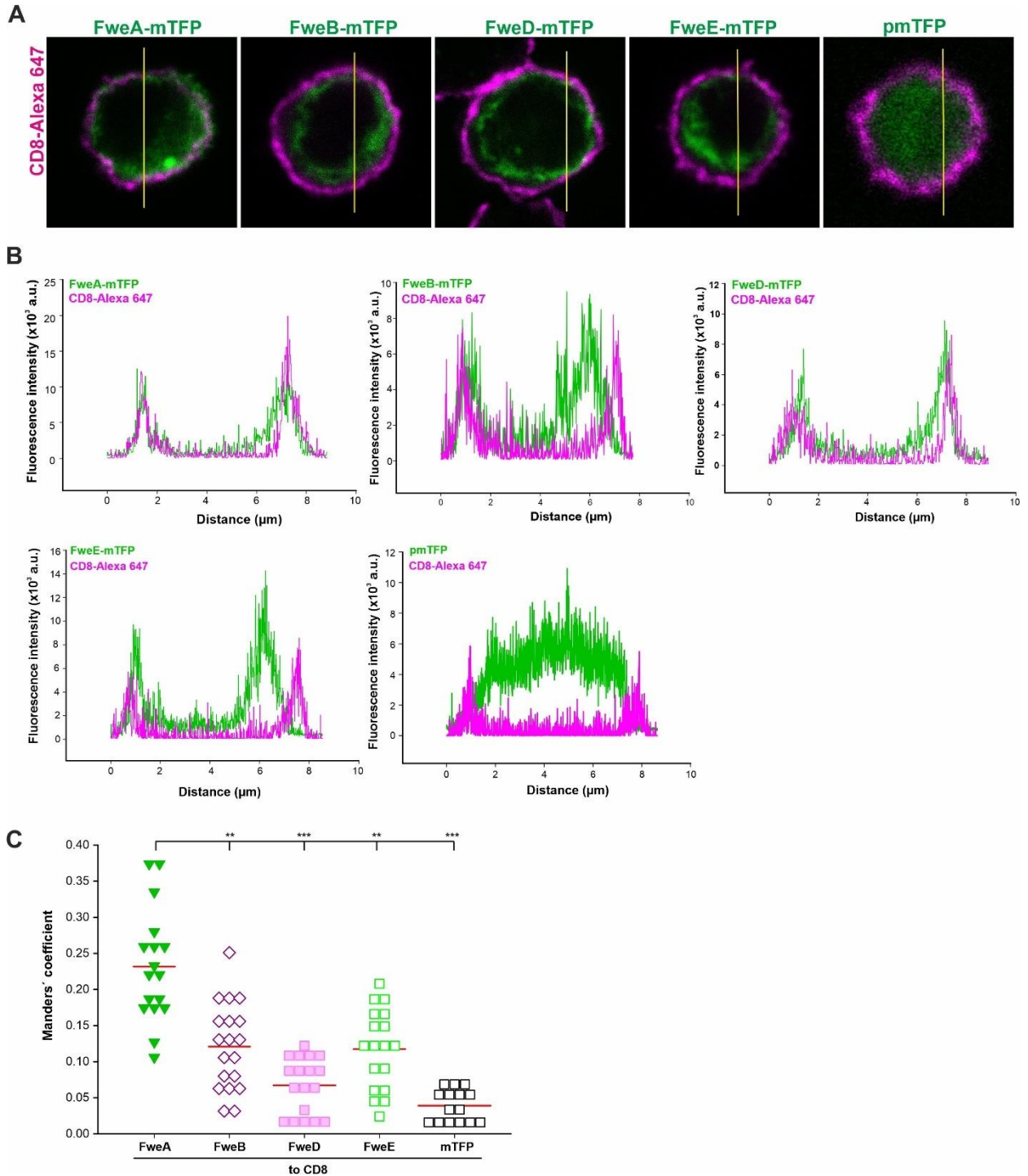
**Figure 31: Both N- and C-termini of Flower splice variants are facing the cytoplasm of a CTL**

(A) Schematic diagram showing the procedure followed in this experiment. (B) SIM image of activated day 5 CTLs transfected with Syb2-Halo (positive control). After 14 h cells were stained with CA-Atto488 dye (green) to mark the Halo tag facing the extracellular space. After several washes CA-SiR (magenta) was added to stain all transfected cells. Un-transfected cells were used as negative controls and treated in a similar manner. Scale bar: 5  $\mu$ m. (C) and (D) SIM image of activated day 5 CTLs transfected with mouse Fwe isoforms with Halo tag fused at the (C) N-terminus or (D) C-terminus. After 14 h, the cells were stained with CA-Atto488 dye (green) to bind to the Halo tag if facing the extracellular space. After washing CA-SiR (magenta) was added to stain all HALO tags. Scale bar: 5  $\mu$ m.

## **4.9 FweA is localized to plasma membrane upon bead activation**

Originally it was assumed that Flower could be a membrane protein (Yao et al., 2007). Recent findings also proposed a Flower localization on intracellular vesicles and a small proportion at the plasma membrane (Chang et al., 2018). Since different isoforms of Flower in our hands rescued the Flower KO phenotype in varying degrees, we next tested whether the degree of rescue may correlate with plasma membrane localization.

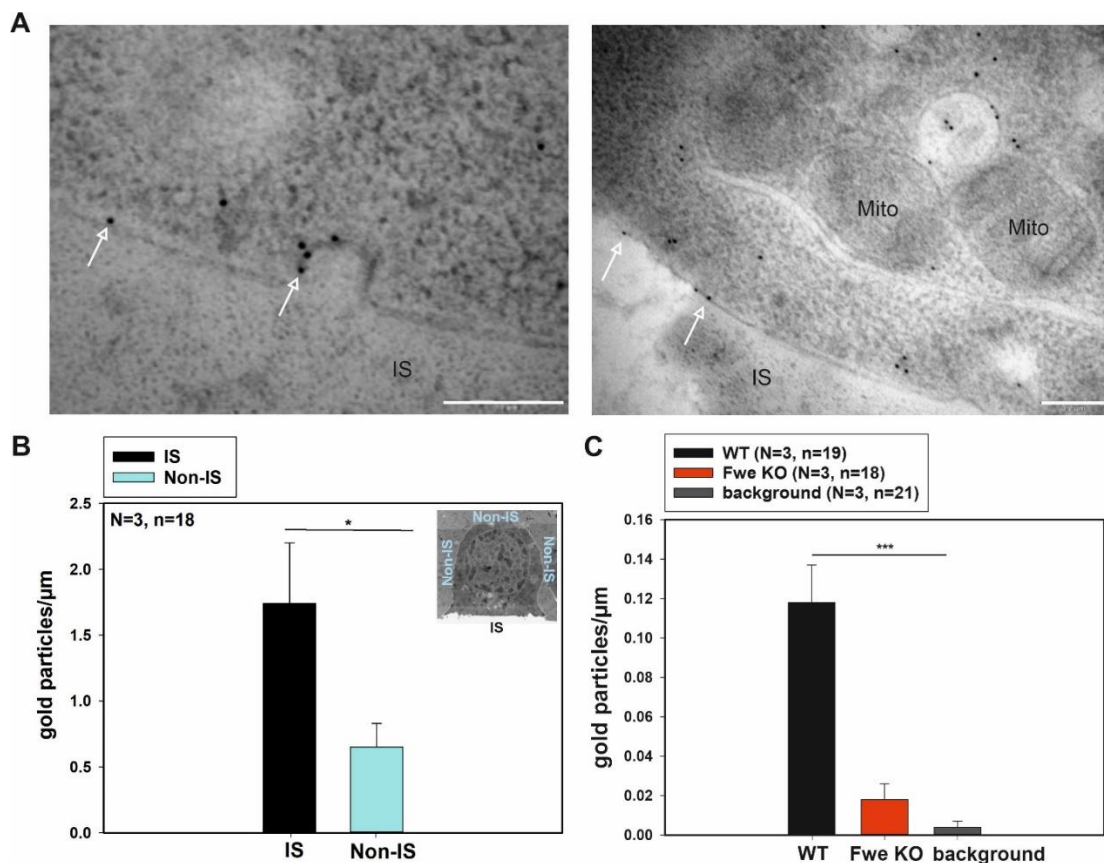
Activated CTLs were transfected with four mouse Fwe isoforms as TFP-tagged fusion proteins and the localization was microscopically determined. Transfected CTLs were bead-activated for 1 h using CD3/CD28 dynabeads at 37 °C. Beads were removed and the cells were stained with CD8-Alexa647, a surface marker, to visualize the membrane. Confocal images and line plot analysis show that only FweA colocalizes with the CD8 signal while FweB, D and E showed minimal co-localization (Figure 32A, B). Manders' coefficient analysis showed significant increase of FweA localization with CD8 surface marker (Manders: 0.232) in comparison to the other isoforms (Manders: B- 0.121, D- 0.07 and E: 0.117) (Figure 32C). The above results indicate that the only the FweA isoform is targeted to the plasma membrane on bead activation, which may explain the stronger rescue seen with FweA.



**Figure 32: FweA is localized to the plasma membrane after CD3/CD28 bead stimulation**

(A) Confocal images showing activated Fwe KO CTLs transfected with mouse Fwe isoforms and stained with plasma membrane marker, CD8-Alexa 647. Note the colocalization of FweA with CD8 seen in white. Scale bar: 2  $\mu\text{m}$  (B) Line profile of the fluorescence intensity from Figure A (yellow line) to compare the peaks of colocalization between Fwe isoforms and CD8. (C) Manders coefficients of co-localization between Fwe and CD8 (N = 2). \*\*  $p < 0.01$ , \*\*\*  $p < 0.001$ .

To further validate apparent FweA localization at the plasma membrane, we performed post-embedding immunogold electron microscopy (Immuno-EM) experiments. Immunolabeling was performed on 100 nm thin resin sections of FweA-mTFP transfected Fwe KO CTLs added onto anti-CD3 $\epsilon$  antibody coated sapphire discs to mimic IS formation. The binding of the primary antibody against FweA was detected with a secondary goat-anti-rabbit antibody conjugated to 10 nm gold particles. Immuno-EM data clearly showed the presence of FweA on the plasma membrane (Figure 33A, arrow pointed) and Fwe was also seen on membrane invaginations consistent with endocytosis of FweA itself . Quantification analysis showed a significant increase in the number of gold particles at the IS (1.74 particles/ $\mu$ m) in comparison to the rest of the plasma membrane (0.65 particles/ $\mu$ m) (Figure 33B). An independent immuno-EM experiment showed significant increases in gold particles at the plasma membrane in WT compared to KO CTLs (Figure 33C, 0.118 for WT vs 0.018 for KO) thus confirming the membrane localization of endogenously expressed FweA.



**Figure 33: FweA is present at the plasma membrane of CTLs**

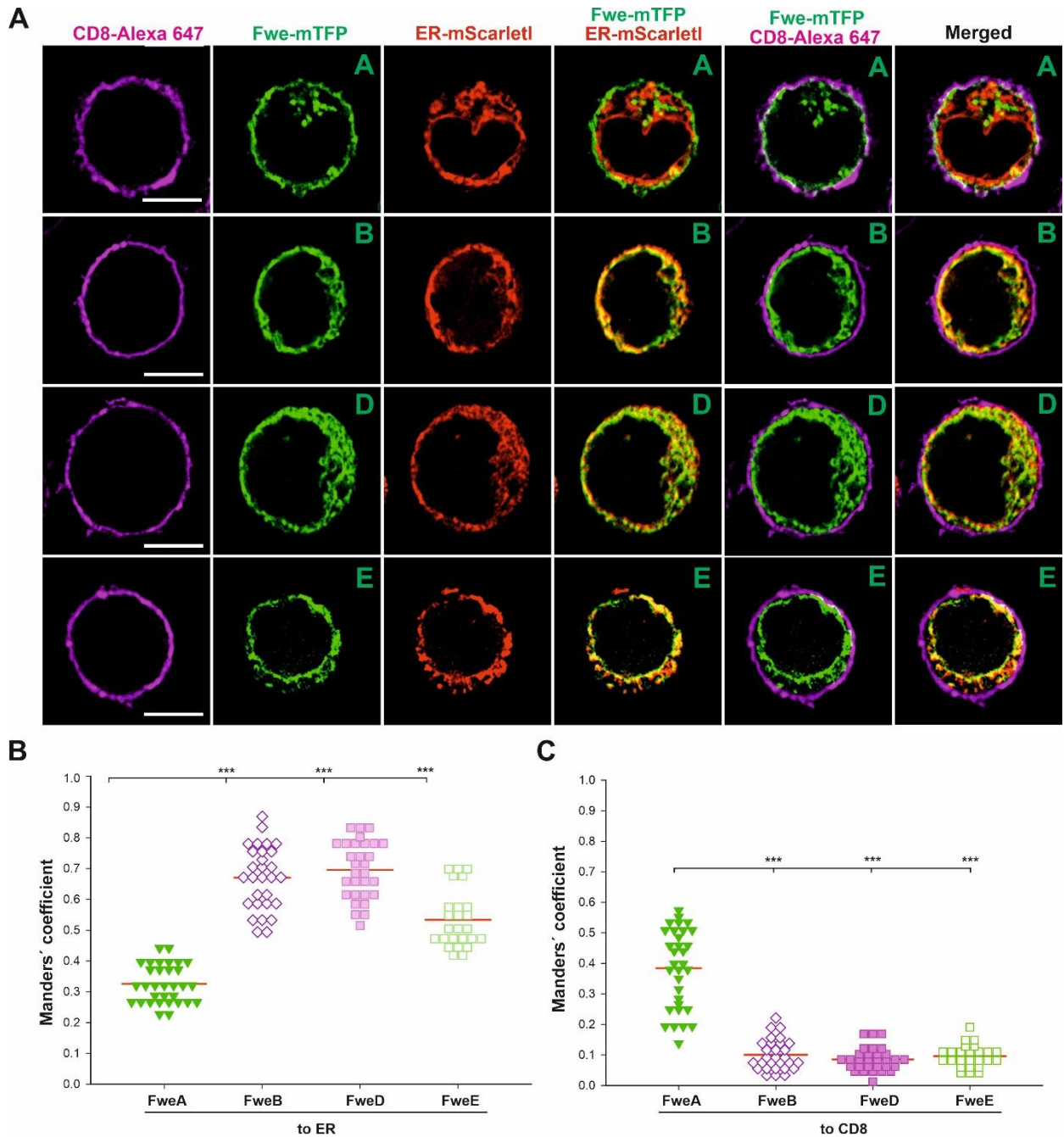
(A) Two immuno electron micrographs showing magnified regions of immunological synapses. Flower immunogold labelling is localized at the plasma membrane of the IS of Fwe KO activated CTLs transfected with FweA-mTFP. White arrow represents the Fwe bound immunogold particles at the plasma membrane. IS: Immunological synapse; Mito: mitochondria; Scale bar: 2  $\mu$ m (B) Quantitative analysis of gold particle distribution at the IS and non-IS regions of the cell. Inset shows an overview image of activated CTL settled on anti-CD3 $\epsilon$  coated sapphire disc with IS and non-IS regions marked. \* $p < 0.01$  (C) Quantitative analysis of Flower marking gold particles at the plasma membrane of WT and Fwe KO CTLs. \*\*\* $p < 0.001$ .



#### **4.10 The Flower rescuers of endocytosis show vesicular localization while the non-rescuers localize to the ER**

Apart from the difference in the natural truncations and plasma membrane localization of mouse Fwe isoforms, the reason for varying rescue-abilities remained unknown. To address this question, we decided to look at the localization of the Flower isoforms after bead activation to determine if there are any differences in the localization of Fwe positive structures in the cell. To study localization of the isoforms, CTLs were transfected with respective Fwe-mTFP isoforms and ER-mScarletI (possessing KDEL signal sequence for visualization of ER). After 14 h, the cells were bead activated as described previously (Section 4.9). The cells were stained for surface marker CD8-Alexa 647 and settled on poly-L-ornithine coated coverslips.

The FweA isoform showed a clear vesicular pattern with several punctate structures (Figure 34A; panel 1) that did not colocalize with the ER. Notably, we observed a plasma membrane localization of FweA with CD8 surface marker, confirming its role in the endocytic pathway. FweB, D and E were associated with the ER-signal in tubular structures (Figure 34A; panel 2, 3 and 4). Manders' coefficient of colocalization of Fwe non-rescuers with the ER was significantly higher than that of FweA (Manders' of Fwe to CD8: FweA- 0.325; FweB- 0.67; FweD- 0.695; FweE- 0.533) (Figure 34B). Comparison of the localization of Fwe isoforms with that of CD8 surface marker clearly shows an enrichment of FweA at the plasma membrane (Manders' of Fwe to CD8: FweA- 0.384; FweB- 0.10; FweD- 0.085; FweE- 0.095; Figure 34C) which confirms the data from section 4.9 (Figure 32). These data indicate that the rescuers of endocytosis show vesicular localization and may reach the plasma membrane via vesicular transport to aid CG endocytosis while the non-rescuers do not reach the plasma membrane and are reside at the ER.



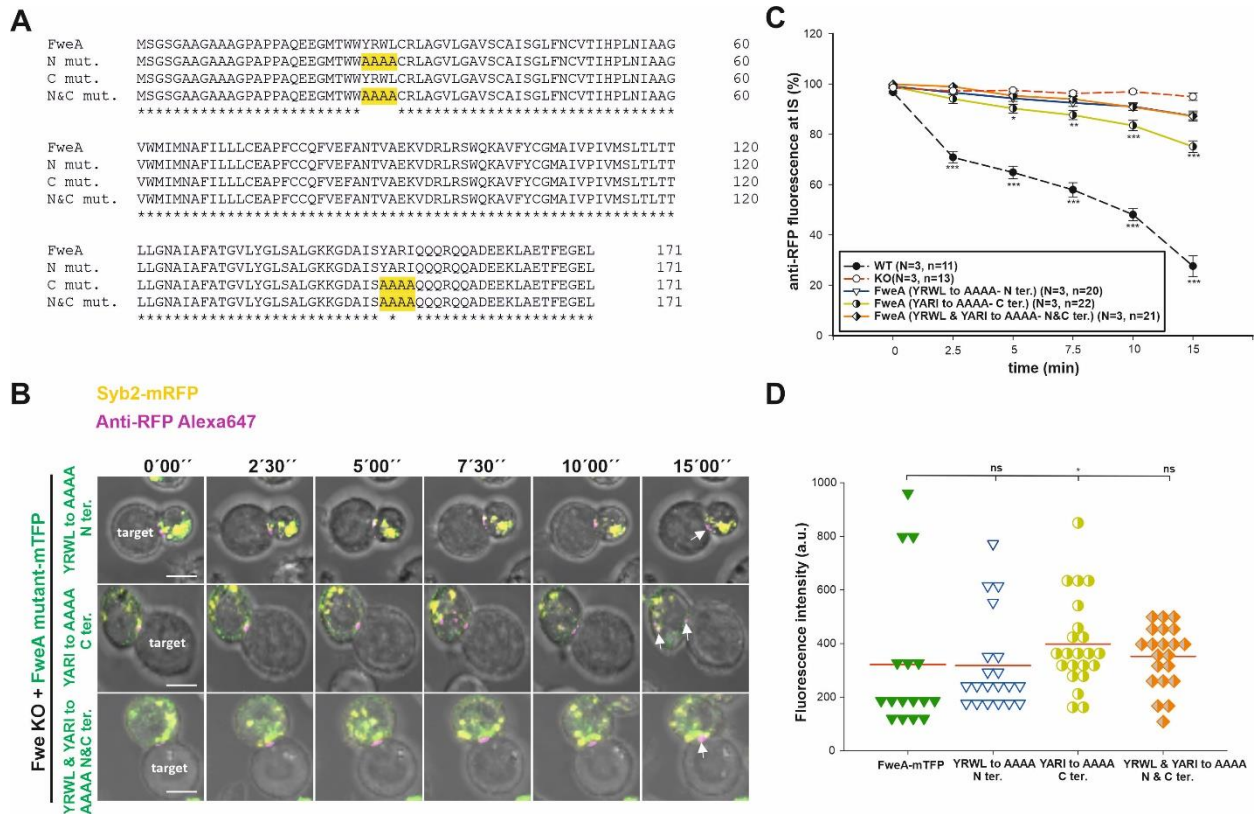
**Figure 34: Vesicular localization versus ER localization between Flower rescuers and non-rescuers of endocytosis**

(A) Single plane SIM images of activated Fwe KO CTLs transfected with Fwe-mTFP isoforms and ER-mScarlet-I. After 14 h, cells were bead activated for 1 h and stained with CD8-Alexa 647 surface marker. The cells were settled on poly-L-ornithine coated coverslips, fixed with 4% PFA and imaged using SIM. Scale bar: 5  $\mu$ m. (B) Manders' coefficients of co-localization analysis between Fwe isoforms and ER marker (N = 2). \*\*\*  $p < 0.001$ . (C) Manders' coefficients of co-localization analysis between Fwe isoforms and CD8 surface marker (N = 2). \*\*\*  $p < 0.001$ .

#### 4.11 The N- and C-terminal YXX $\phi$ motifs are important for Syb2 endocytosis

Since the major structural difference between FweA and its splice variants is the absence of N- and C-terminal parts of the protein, we next wanted to check if any particular sequence at these termini might be involved in promoting Syb2 uptake. The YXX $\phi$  endocytosis signal motif was reported to be an important recognition site for AP2 $\mu$  adaptor protein (Pandey et al., 2010). By sequence analysis we found two motifs within Flower namely YRWL (26-29 aa) and YARI (147-150 aa) at the N- and C-terminus respectively which correspond to the YXX $\phi$  motif. Therefore, we mutated the respective amino acids to Alanine moiety, either individually or together in FweA-TFP and tested for rescue by these constructs (Figure 34A, highlighted in yellow). Flower KO CTLs were transfected with Syb2-mRFP and FweA-mTFP constructs with YXX $\phi$  mutation. Anti-RFP647 antibody was added to the extracellular medium as an endocytosis indicator.

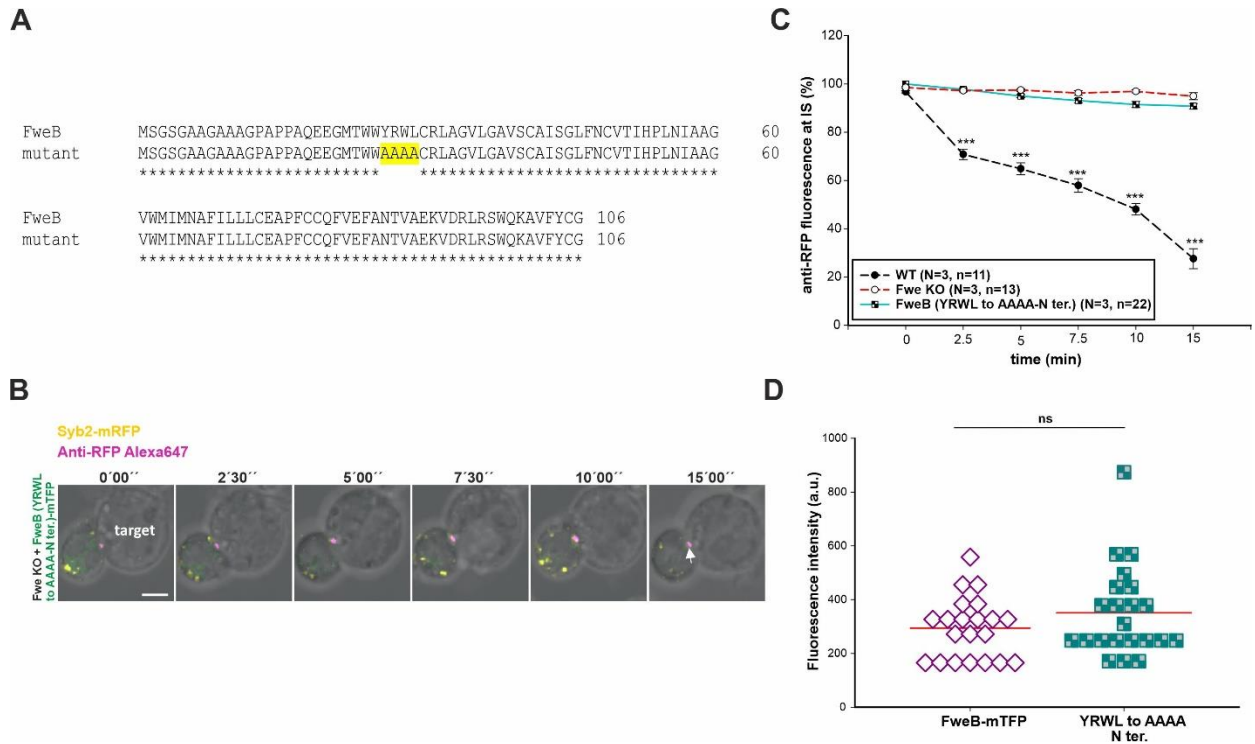
FweA (N-terminal YRWL>AAAA) mutation did not rescue Syb2 endocytosis (Figure 35B, panel 1, arrow). Quantification of anti-RFP647 intensity (mean of 99%  $\pm$  0.3, 96.6%  $\pm$  0.7, 94.3%  $\pm$  1.1, 92.5%  $\pm$  1.4, 91.1%  $\pm$  1.5 and 87.3%  $\pm$  2 at time points 0, 2.5, 5, 7.5, 10 and 15 min; Figure 35C, blue) showed arrest of the fluorescence at the IS. The FweA (C-terminal YARI>AAAA) mutation resulted in a partial endocytosis of Syb2 (Figure 35B, panel 2, arrow) and showed a mild rescue similar to that observed for FweB (Figure 30). Quantification of anti-RFP647 intensity (mean of 99%  $\pm$  0.4, 94%  $\pm$  1.8, 90.2%  $\pm$  1.7, 87.6%  $\pm$  1.8, 83.5%  $\pm$  2.1 and 75.1%  $\pm$  2.2 at time points 0, 2.5, 5, 7.5, 10 and 15 min; Figure 35C, greenish yellow) showed partial arrest of the fluorescence at the IS. Mutation of both N- and C-terminal motifs (Figure 35B, panel 3, arrow) showed no rescue, as expected. Quantification of anti-RFP647 intensity (mean of 99.9%  $\pm$  0.1, 99%  $\pm$  0.4, 95.3%  $\pm$  0.7, 94%  $\pm$  1.03, 90.8%  $\pm$  1.3 and 87.2%  $\pm$  1.4 at time points 0, 2.5, 5, 7.5, 10 and 15 min; Figure 35C, orange) showed arrest of the fluorescence at the IS. The protein expression was similar for all constructs (Figure 35D) with a slight increase for the double mutant. The results convincingly confirm the importance of both the N-terminal YRWL (26-29aa) and C-terminal YARI (147-150aa) sequence for endocytosis of Syb2. Substitution of amino acids within these regions to Alanine at both leads to a dramatic reduction of endocytosis.



**Figure 35: Mutation of the C- and N-terminal amino acid motifs YRWL (26-29 aa) and YARI (147-150 aa) mutant of FweA cannot rescue the block of Syb2 endocytosis**

(A) Sequence alignment of mouse FweA isoform with indicated mutations (yellow) of YRWL>AAAA and YRWL>AAAA. (B) Time-lapse live snapshots over 15 min of CTLs transfected with Syb2-mRFP (yellow) and Fwe-mTFP (YRWL>AAAA) and YARI>AAAA mutant constructs (green). CTLs are conjugated with P815 target cells in the presence of anti-RFP647 antibody (magenta) in the medium. The accumulation and endocytosis of Syb2 (arrow pointed) transfected with the different FweA mutants are shown. Scale bar: 5  $\mu$ m. (C) Quantitative analysis of the redistribution of endocytosed Syb2 (anti-RFP647) from the IS into the cytosol over 0 to 15 min for FweA-YRWL>AAAA mutant at N-terminus (blue), YARI>AAAA mutant at C-terminus (greenish yellow), YRWL>AAAA and YARI>AAAA double mutant (orange) is shown. Time zero is defined as the appearance of the first endocytic signal at the IS. Data given as mean  $\pm$  SEM; One-way Analysis of Variance (ANOVA) was done against Fwe KO as control, \* $p < 0.05$ , \*\* $p < 0.01$ , \*\*\*  $p < 0.001$ . (D) Fluorescence intensity of mTFP expression in the cell of FweA and the mutants was calculated and plotted. Data given as mean in red line; \* $p < 0.05$ , ns  $p > 0.05$ .

In order to confirm the importance of the YRWL motif in Syb2 uptake further, we tested whether the partial rescue of FweB which we observed earlier (Figure 30) was also dependent on the YRWL motif. Therefore, FweB was mutated correspondingly (YRWL>AAAA) (Figure 36A, yellow highlighted) and expressed in Flower KO CTLs. As expected, the rescue failed (Figure 36B, arrow). Quantification of RFP647 fluorescence (mean of 100%  $\pm$  0, 97.7%  $\pm$  0.6, 95%  $\pm$  0.7, 93.1%  $\pm$  1, 91.5%  $\pm$  1.2 and 90.8%  $\pm$  1.1 at time points 0, 2.5, 5, 7.5, 10 and 15 min; Figure 36C, teal colour) showed persistent accumulation at the IS. The expression level of FweB and mutated FweB was similar (Figure 36D). All these experiments show the importance of N- and C-terminal YXX $\phi$  motifs in endocytosis of CGs.



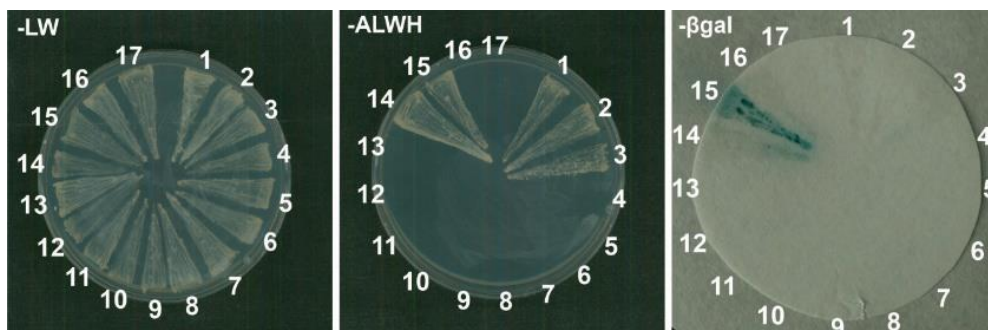
**Figure 36: YRWL>AAAA (26-29 aa) mutation of FweB prevents partial FweB-rescue of Syb2 endocytosis**

(A) Protein sequence of mouse FweB and the YRWL>AAAA mutant. (B) Time-lapse live snapshots over 15 min of Flower KO CTLs transfected with Syb2-mRFP (yellow) and FweB-mTFP YRWL>AAAA mutant construct (green). Cells were conjugated with P815 target cells in the presence of anti-RFP647 antibody (magenta) in the medium. The accumulation of mRFP signal at the IS (arrow pointed) is indicated. Scale bar: 5  $\mu$ m. (C) No distribution of endocytic vesicles (anti-RFP647) into the cytosol over 0 to 15 min in FweB-YRWL>AAAA mutant (teal) could be observed. Time zero is defined as the appearance of the first endocytic signal at the IS. Data given as mean  $\pm$  SEM; One-way Analysis of Variance (ANOVA) was done against Fwe KO as control. ns  $p > 0.05$  (D) Fluorescence intensity of mTFP expression in the cell between the FweB and mutant were calculated and plotted. Data given as mean in red line; ns  $p > 0.05$ .

#### 4.12 The YXX $\phi$ motif does not interact with AP2mu subunit in yeast

The YXX $\phi$  motif of N- and C-terminus showed a strong effect on the rescue of endocytosis in Flower KO CTL. To determine if interaction of this motif with AP2mu subunit occurs (Jadot et al., 1992; Ohno et al., 1995; Owen and Evans, 1998; Traub and Bonifacino, 2013), we used the yeast two hybrid protein interaction assay. The N-terminal (1-33aa) and C-terminal (140-171aa) of FweA was cloned in the bait vector pGBKT7 and AP2mu in prey vector pGADT7. A part of exon 3 (81-99aa) which did not possess a potential motif was also used as a negative control. The mating strategy was done with proper positive and negative controls (Figure 37, table). The N-terminal motif showed self-activation with control prey vectors, resulting in yeast growth in -ALWH plates and was unsuitable for the mating process as the  $\beta$ -galactosidase ( $\beta$ Gal) assay was negative (Figure 37, top row). Self- or auto-activation is seen when proteins activate the reporter genes without the presence of an interacting protein partner.

The C-terminal and the exon3 short fragment was suitable for further interaction studies since it showed no growth in empty prey vectors . Thus, the two bait proteins C-terminal and exon 3 did not show any interaction with the AP2mu subunit (Figure 37, table). Since our functional results concerning the importance of the motif for endocytosis were convincing, we speculate that the YXX $\phi$  motif of Flower binds to a yet unknown adaptor protein.



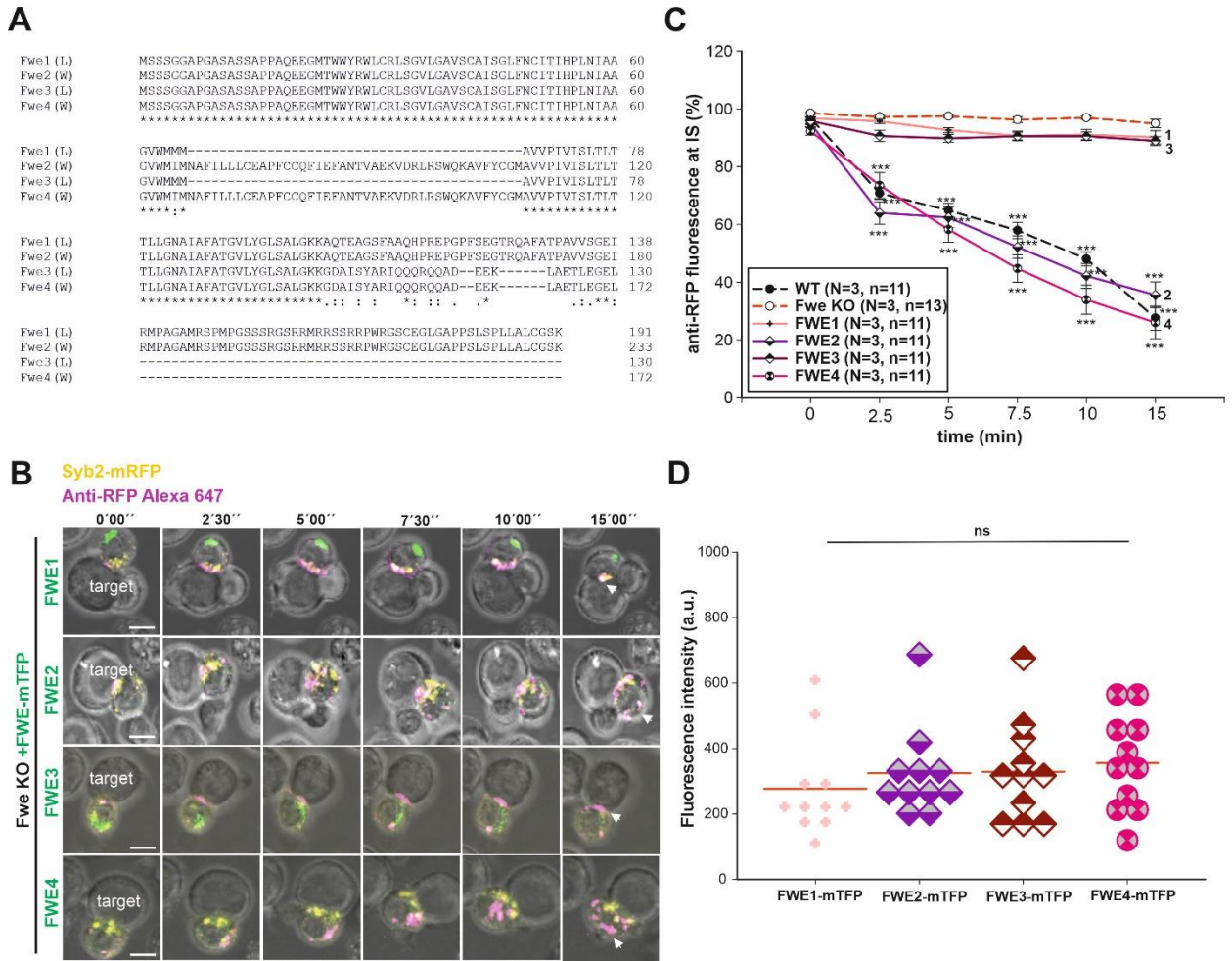
Mating	Bait (pGBKT7) (-W)	Prey (pGADT7) (-L)	-ALWH	βGal
1.	FlowerA (1-33aa)	AP2mu	+	-
2.	FlowerA (1-33aa)	pGADT7	+	-
3.	FlowerA (1-33aa)	pSE1111	+	-
4.	FlowerA (Ex3(81-99aa))	AP2mu	-	-
5.	FlowerA (Ex3(81-99aa))	pGADT7	-	-
6.	FlowerA (Ex3(81-99aa))	pSE1111	-	-
7.	FlowerA (140-171aa)	AP2mu	-	-
8.	FlowerA (140-171aa)	pGADT7	-	-
9.	FlowerA (140-171aa)	pSE1111	-	-
10.	FlowerA (140-171aa) YARI to AAAA mutant	AP2mu	-	-
11.	FlowerA (140-171aa) YARI to AAAA mutant	pGADT7	-	-
12.	FlowerA (140-171aa) YARI to AAAA mutant	pSE1111	-	-
13.	pGBKT7	AP2mu	-	-
14.	pSE1112	AP2mu	+	-
15.	Ribeye(B)	Ribeye(B)	+	+
16.	Ribeye(B)	pGADT7	-	-
17.	pGBKT7	Ribeye(B)	-	-

**Figure 37: Yeast two hybrid assay shows no interaction of YXX $\phi$  based motifs in FweA with AP2mu.**

Top panel shows an overview of the summary plates of yeast growth on the -LW and -ALWH plates and the  $\beta$ -galactosidase ( $\beta$  Gal) assay of the individual yeast hybridizations. In the table below, yeast mating with the respective FweA constructs (bait) used are listed and evaluated with a positive (+) and negative (-) sign with regard to their growth on -LW and -ALWH medium and the  $\beta$ Gal assay. AP2mu was used as the prey protein for interaction. pSE1111 and pSE1112 are irrelevant prey and bait vectors (Tai et al., 1999; Magupalli et al., 2008). pGBKT7 (bait) and pGADT7 (prey) empty vectors were used as control mating pairs to rule out the state of self-activation.

### 4.13 The Exon 3 of Human Flower is important in Syb2 endocytosis

Since the characterisation of murine Flower protein indicate a dominant role of the N- and C-termini in endocytosis, we tested for a similar role in endocytosis for human Flower (hFWE) protein. The ability of splice variants of human Flower protein to rescue endocytosis in Flower KO CTLs. *C9ORF7* (also known as *CACFD1*) encodes hFWE and generates four protein-coding splice variants (hFWE1–hFWE4) (Ensembl number: ENSG00000160325). The hFWE gene has six exons, which are alternatively spliced to generate four hFWE isoforms (Figure 38A). The major difference between the splice variants is the presence or absence of exon3 (Figure 38A). Endocytosis rescue experiments with hFWE variants showed that hFWE2 and 4 (Figure 38B, panel 2 and 4, arrow) were able to rescue the Syb2 endocytosis block but hFWE1 and 3 (Figure 38B, panel 1 and 3, arrow) could not. Quantification of RFP647 fluorescence for hFWE2 (mean of 94.9% ± 1, 64% ± 3.8, 62.4% ± 3.6, 52.1% ± 3.8, 42.1% ± 4.9 and 35.5% ± 4.5 at time points 0, 2.5, 5, 7.5, 10 and 15 min; Figure 38C, dark purple) and hFWE4 (mean of 98.8% ± 0.6, 85.6% ± 3, 69.5% ± 2.6, 61.2% ± 2.5, 54.9% ± 3.5 and 45.4% ± 3 at time points 0, 2.5, 5, 7.5, 10 and 15 min; Figure 38C, baby pink) showed less accumulation at the IS. The RFP647 intensity accumulated at the IS was higher in hFWE1 (mean of 96.7% ± 0.6, 95.7% ± 0.8, 92.6% ± 0.9, 90.6% ± 1.7, 91% ± 1.8 and 90.1% ± 2.3 at time points 0, 2.5, 5, 7.5, 10 and 15 min; Figure 38C, pale pink) and hFWE3 (mean of 95.8% ± 1.3, 90.6% ± 1.9, 89.8% ± 1.3, 90.5% ± 1.3, 90.5% ± 1.5 and 88.9% ± 1.5 at time points 0, 2.5, 5, 7.5, 10 and 15 min; Figure 38C, deep red) isoforms. The expression levels of the respective constructs, based on the mTFP fluorescence intensity, was similar in all four splice variants (Figure 38D; mean 276.5, 324.2, 328.7, 355.2 for hFWE1 ,2, 3, 4 respectively). These results are consistent with a role for Exon 3 of human Flower rescue of Syb2 endocytosis and subsequent function in CTLs.

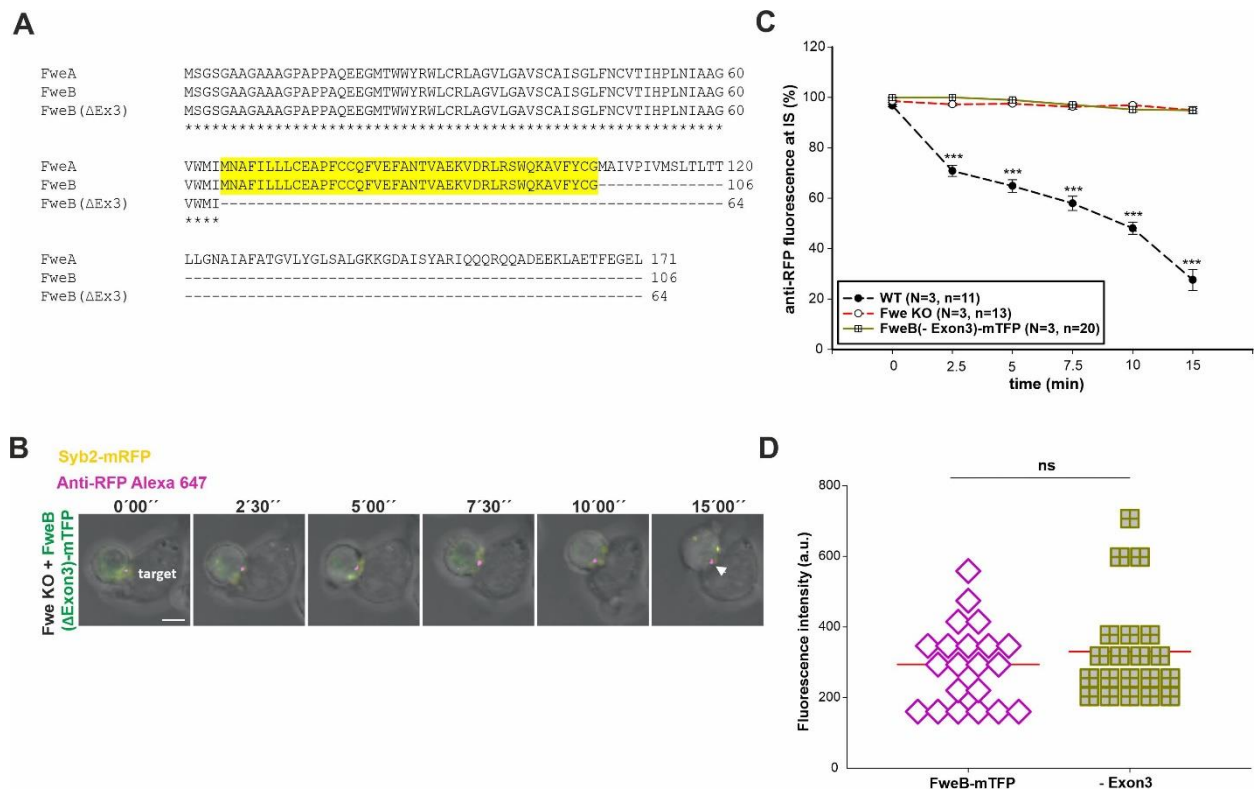


**Figure 38: Isoforms lacking Exon3 in human FWE could not rescue the block of Syb2 endocytosis**  
 (A) Protein sequence alignment of the 4 human FWE isoforms by Clustal Omega. \* Indicate conserved aminoacids. (B) Time-lapse live snapshots for over 15 min of Syb2-mRFP (yellow) plus the four hFWE-mTFP isoforms (green) transfected Fwe KO CTLs conjugated to P815 target cells in the presence of anti-RFP647 antibody (magenta) in the medium. The accumulation and endocytosis of CGs (arrow pointed) transfected with the different hFWE isoforms are shown. Scale bar: 5  $\mu$ m. (C) Quantitative analysis of endocytosis and accumulation of Syb2 (anti-RFP647) at the IS during 0 to 15 min in hFWE1 (pale pink), hFWE2 (dark purple), hFWE3 (deep red) and hFWE4 (pink) transfected cells in comparison to WT and Fwe KO is shown. Time zero is determined as the appearance of the first endocytic signal at the IS. Data given as mean  $\pm$  SEM; One-way Analysis of Variance (ANOVA) was done against Fwe KO as control; \*\* $p < 0.01$ , \*\*\*  $p < 0.001$ . (D) Fluorescence intensity of mTFP expression in the cell between the four isoforms were calculated and plotted. Data given as mean in red line; ns  $p > 0.05$ .



### 4.14 Exon 3 is an important part of murine Flower for Syb2 endocytosis

Based on the hFWE rescue phenotype, the major difference between the rescuers and non-rescuers is Exon3. The Exon 3 sequence is highly conserved among various species. hFWE4 shows 96% sequence similarity (Clustal Omega) to FweA isoform. In order to confirm the importance of Exon3 in mouse Flower, a deletion mutant was made by removing the exon3 portion of FweB (Figure 39A, yellow highlight).



**Figure 39: Deletion of Exon3 in mFweB isoform could not rescue the block of Syb2 endocytosis**

(A) Protein sequence alignment of the FweB isoform and Exon3 deletion mutant by Clustal Omega. \* Indicate conserved aminoacids. (B) Time-lapse live snapshots for over 15 min of Syb2-mRFP (yellow) plus the four FweB (ΔExon3)-mTFP isoform (green) transfected Fwe KO CTLs conjugated to P815 target cells in the presence of anti-RFP647 antibody (magenta) in the medium. The accumulation of CGs (arrow pointed) transfected with the deletion mutant is shown. Scale bar: 5 μm. (C) Quantitative analysis of endocytosis and accumulation of Syb2 (anti-RFP647) at the IS during 0 to 15 min for the deletion mutant (deep yellow) transfected cells in comparison to WT and Fwe KO is shown. Time zero is defined as the appearance of the first endocytic signal at the IS. Data given as mean ± SEM; One-way Analysis of Variance (ANOVA) was done against Fwe KO as control; ns p > 0.05. (D) Fluorescence intensity of mTFP expression in the cell for the deletion mutant was calculated and plotted. Data given as mean in red line; ns p > 0.05.

Since FweB could partially rescue the phenotype, we wanted to check if exon3 mutant would still maintain the partial rescue or completely abolish this effect. Endocytosis rescue experiment was thus performed with the exon3 mutant of the FweB variant. The mutant failed to rescue (Figure 39B, arrow, ) and Syb2 endocytosis was similar to that of Flower KO cells. Quantification of RFP647 fluorescence (mean of  $100\% \pm 0.1$ ,  $100\% \pm 0$ ,  $99\% \pm 0.3$ ,  $97.1\% \pm 0.5$ ,  $95.2\% \pm 0.9$  and  $94.9\% \pm 0.7$  at time points 0, 2.5, 5, 7.5, 10 and 15 min; Figure 39C, deep yellow) showed accumulation at the IS. The expression of the mutant construct was similar to FweB levels and showed no significant difference in the TFP intensity (Figure 39D; mean 330). These results show that Exon3 of murine Flower is important for endocytosis of Syb2 though we cannot rule out that lack of protein function is due to improper folding of the mutated protein.

#### **4.15 The conserved tyrosine residue in exon3 of mouse Flower is mainly responsible for aiding Syb2 endocytosis**

Flower (in this case termed Cacfd1, ENSMUSP00000015632) is a member of a family of small (less than 200 residues) proteins called Cg6151-P that are conserved from fungi to humans (SMART accession number: SM01077). The fungal members have a characteristic ICP (Inhibitors of Cysteine Peptidases) sequence motif. Certain members are marked as putative clathrin-coated vesicle proteins. Other family members include the Golgi membrane proteins TVP18 that may be involved in vesicular trafficking pathways (Yao et al., 2009). The alignment of Cg6151-P with mostly yeast and fungi proteins is shown in the Figure 40A (SMART program: <http://smart.embl-heidelberg.de>). Interestingly, the homologous regions of mouse Flower (AA 33-142) start at the beginning of transmembrane domain 1 (TM1) and end at TM4. E74, P76 and Y104 namely, E (Glutamic acid), P (Proline) and Y (tyrosine) in the exon3 of mouse Flower were found to be the only highly conserved amino acids in all species containing the Cg6151-P region (Figure 40, highlighted in yellow and marked \*).

----Results----

Candida lipolytica (TVP18) (19-130aa)	IGVLCII-----LCIALGIANIFHASLV-II-----FSIICIVQGLVVVFEI*PFLLRICPVTE	53
Saccharomyces (TVP18) (30-141aa)	FGYINII-----LCIALGIANLFHVSGV-IA-----FGIISIIQGLVILFIEI*PFLLLKICPLSD	53
Aspergillus fumigatus (tvpl8) (19-133aa)	TGVLICII-----LCIALGIANIFSFVAVLR-II-----FVSLCLISGLLILFIEI*VPFLLRICPTSS	54
Candida glabrata (TVP18) (30-141aa)	FGYINIF-----LCIALGIANLFHVSVA-IA-----FGIVGIVQGLIILFIEI*PFLLLKICPLSD	53
Neurospora crassa (tvpl8) (19-131aa)	LGILSMI-----LCFALGIANIFTRFPIIIV-----FSVITLCFSFVILFVEI*PFLLRICPTSP	54
Candida sphaerica (TVP18) (32-143aa)	ISYLNII-----FCLAFGIANIFHFSAV-IV-----FSIIAIVQGLIILFIEI*VPFLLLKICPLSD	53
Schizosaccharomyces (tvpl8) (30-141aa)	LGILSIF-----LCIILGIVNLFHVTLV-VL-----FSALTIIEGVLLIFIEI*PFLSRICPVSD	53
<b>Mus musculus (mFwe) (Cacfd1) (33-142aa)</b>	AGVLGAV-----SCAISGLFNCVTIHLPLNIA-----AGVVMIMNAFILLLCEA*PFCQFVEFAN	54
Takifugu rubripes (27-136aa)	AGVLGGI-----SCAIIAGVWNCVTIHLPLNIA-----AGVVMVNAFVFLFCEA*PFCQFVEFAN	54
Culex aegypti (Flower) (35-147aa)	VGIVGGF-----FAILFGLYNCIGILLGDVGCGLV-----GGILEILAGFVVLAI*EAPCCFIFIDHVQ	57
<b>Cg6151-PA (dFwe ubi) (35-147aa)</b>	LGIVAAF-----FAILFGLWNVFSIITLVSVCGLV-----AGILQMVAGFVVMLEA*PCCFVCFQVQN	57
Caenorhabditis (flower) (33-142aa)	VAILGGF-----LSLFFGVGLGLITLSATCMV-----AIIQLQMTAGALVIAL*EAPFCQFVDFIE	54
<b>Homo sapiens (hFWE) (CACFD1) (34-143aa)</b>	SGVLGAV-----SCAISGLFNCVTIHLPLNIA-----AGVVMIMNAFILLLCEA*PFCQFIEFAN	54
Gallus gallus (35-144aa)	AGVIGGV-----SCAVAGLWNCVTINPLNIA-----AGVVMMLNAFVFLFCEA*PFCQFIEFAN	54
Xenopus tropicalis (12-119aa)	AGILGGF-----SCAVAGLWNCVTINPLNIA-----AGVLMMLNAFVFLFCEA*PFCQFVEFAN	54
Erinaceus (Cacfd1) (34 to 142aa)	SGVLGAV-----XXXXXXXXXXXXXXXXXXXXX-----XXXXXXXXXNAFILLLCEA*PFCQFVEFAN	54
Ciona savignyi (31-140aa)	AAIVCGICAI---TTFISGTFGFDGL---CIT-----SAVVMVLCNCFVLLF*EAPICCAFCEITQ	54
Monodelphis domestica (34-144aa)	AGVMGGICEQ---SLSGVGLLCLIGLPLSSND-----FFSFFSRLNAFVFLFCEA*PFCQFIEFAN	58
	* *	
Candida lipolytica (TVP18) (19-130aa)	RFSNFIRFFNQNPRAAF*IGMATIQYCSLI--FMTTSLVPAVFLTITSMCYALAAALKH	111
Saccharomyces (TVP18) (30-141aa)	NFIEFIKRFETNGWRCLFYLAMAI IQYISIA--VMATSLIVVAVGLTISISYAVAYTKH	111
Aspergillus fumigatus (tvpl8) (19-133aa)	KFDAFIRRFITNMWRAAMYGVMSVVQWLSLPLGSGASSLIVAAVFLLIASIFYALAGLKS	114
Candida glabrata (TVP18) (30-141aa)	RFIEFIKRFETNGYRCIFYTLMAIVQYCSLA--VMTTSLLVGLITLTISAVSYGIATFKH	111
Neurospora crassa (tvpl8) (19-131aa)	TFDNLIRKISTNYTRAAAYGVMAVVVFLSCL--DRTTSLVPGIFLSFTGCYALAAALKG	112
Candida sphaerica (TVP18) (32-143aa)	NFIGFVSKFDNLRALFYLVCMCAIQWCSII--VQSTSLIVVAVGLSITATVYALGAAAG	111
Schizosaccharomyces (tvpl8) (30-141aa)	KFQAFTNAFASNYRGLVYFIFSVVTFPLSCI--FMATSLIATGIVLALTGLCYTFAGIKG	111
<b>Mus musculus (mFwe) (Cacfd1) (33-142aa)</b>	TVAEKVDRLR--SWQKAVFYCGMAIVPVMMSL---TLTLLGNIAFA--TGVLYGLSALGK	109
Takifugu rubripes (27-136aa)	AIAARADKLR--PWQKALFYCGMAVVPILLKF---SFTTLFGNAIAFA--TGVLYGLSALGK	109
Culex aegypti (Flower) (35-147aa)	QIAEKADQRP--YWNRAALYCI IALPVPVILCL---GLGSLFGCGLIFV--TGMIVGMMSLKG	112
<b>Cg6151-PA (dFwe ubi) (35-147aa)</b>	EIAEKVESKP--LYFRAGLYIAMAIPPIILCF---GLASLFGSGLIFG--TGVVYGMMLGK	112
Caenorhabditis (flower) (33-142aa)	KIARFSESRA--LWHKAAIYGAMGLIPIFLCI---ELNTILGSGTIFA--SGVIYGFMALGK	109
<b>Homo sapiens (hFWE) (CACFD1) (34-143aa)</b>	TVAEKVDRLR--SWQKAVFYCGMAVVPVIVISL---TLTLLGNIAFA--TGVLYGLSALGK	109
Gallus gallus (35-144aa)	AVSARADKLR--AWQKAAFYCGMAVFPVMTL---TLTTLFGNAIAFA--TGVLYGLCDAAG	109
Xenopus tropicalis (12-119aa)	TVSEKADRLK--SWQKAAFYCGMALLPIFISF---FTTTLFGNAIAFA--SGVLVGRISML-	108
Erinaceus (Cacfd1) (34 to 142aa)	TVAEKVDRLR--SWQKAVFYCGMAVVPVIVISL---TLTLLGNIAFA--TGVLYGLSALGK	109
Ciona savignyi (31-140aa)	PISNVWDKRP--YWQKGAIVGLSILPVALCR---NIATILGVCVPPFA--AGVLYGLMSLKG	109
Monodelphis domestica (34-144aa)	TIADKADRLR--A-LRAIFYCGG--FPLGISL---NLTTPLGNIAFA--TGVLYGLSALGK	110
	*	

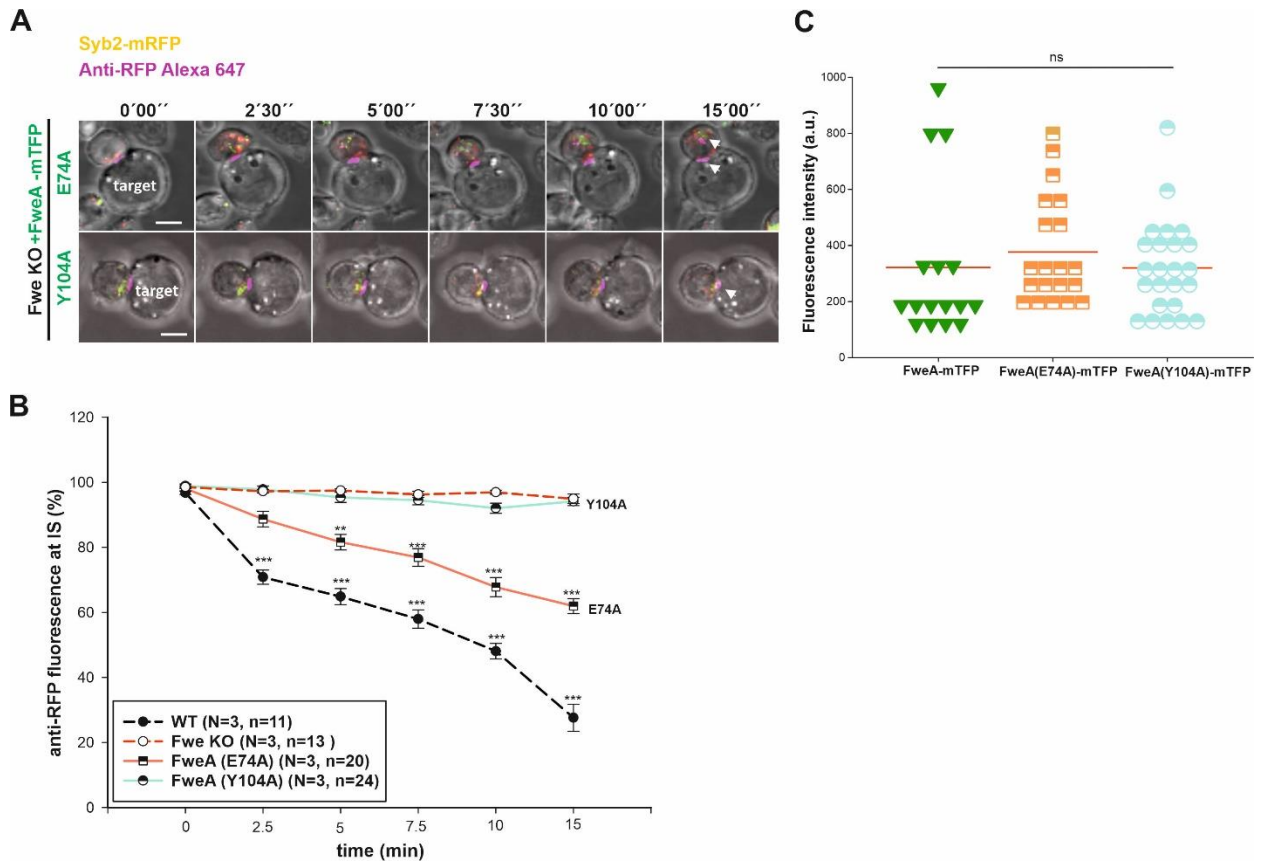
**Figure 40: Conserved Glutamate(E), Proline(P) and Tyrosine(Y) amino acids among Cg6151-P containing proteins**

Alignment of members of the Cg6151-P containing proteins in Clustal format is shown. The proteins mainly include the TVP18 Golgi membrane proteins and calcium channel Flower proteins from various species namely yeast to mammals. The highly conserved residues Glutamate (E), Proline (P) and Tyrosine (Y) are highlighted in yellow and marked with an \*.

Glutamic acid (E) was shown to be present at the selectivity filter region as in TRPV channels (Yao et al., 2009). Proline (P) is known to be an important alpha helix breaker mainly important for structural flexibility (Jacob et al., 1999) and Tyrosine (Y) was shown in some proteins to undergo phosphorylation by kinases (Nucifora and Fox, 1999; Getz et al., 2019). Based on this information, we chose to mutate E and Y in FweA, and not P as this might alter the structure of the protein and lead to misfolding. Endocytosis rescue experiments were performed on Fwe KO CTLs by overexpressing cells with either of the mutant constructs FweA (E74A) or (Y104A)-mTFP along with Syb2-mRFP and conjugated with target P815 cells. Addition of RFP-Alexa 647 showed partial rescue of Syb2 with cells expressing E74A mutant construct (Figure 41A, top row, arrow) whereas cells with Y104A showed no rescue (Figure 41A, bottom row, arrow) of endocytosis and behaved similar to KO cells. Quantification of RFP647 fluorescence for E74A mutant (mean of 98.1% ± 0.7, 88.7% ± 2.4, 81.6% ± 2.4, 77% ± 2.7, 67.8% ± 3 and 62% ± 2.3 at time points 0, 2.5, 5, 7.5, 10 and 15 min; Figure 41B, light orange) and Y104A mutant (mean of 98.8% ± 0.6, 97.8% ± 1, 95.3% ± 1.5, 94.5% ± 1.4, 92% ± 1.6 and 94.1% ± 1.3 at time points 0, 2.5, 5, 7.5, 10 and 15 min; Figure 41B, cyan) showed differences in accumulation at IS. Both the

mutant constructs showed equal expression of the mTFP fluorescence intensity (Figure 41C, mean 377.1 and 319.7 for E74A and Y104A mutant respectively).

The result indicates that the Tyrosine (104) residue is required for Flower function in endocytosis. Moreover, it can explain the importance of Exon3 for endocytosis as described earlier in this thesis (Section 4.14).

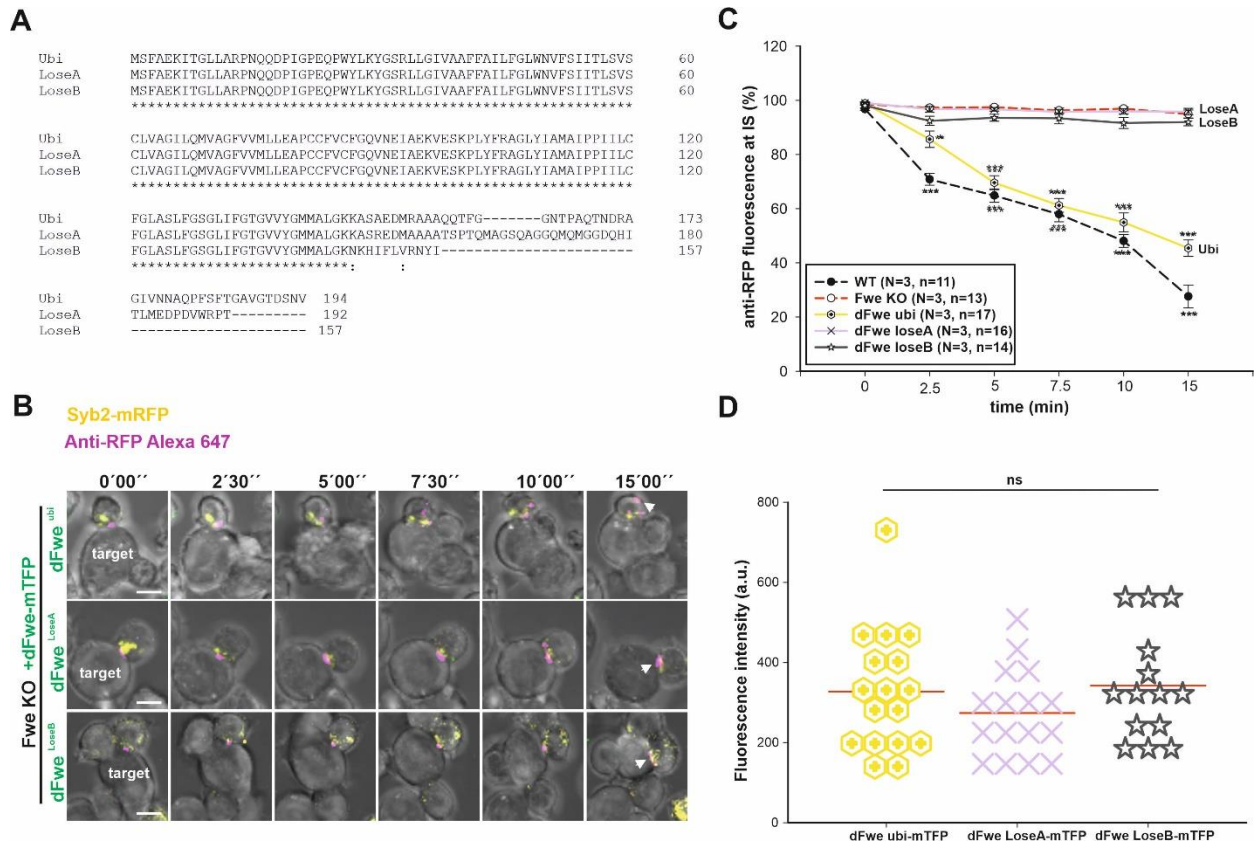


**Figure 41: Mutation of Tyrosine residue (Y104A) in FweA isoform has severe block of Syb2 endocytosis**

(A) Time-lapse live snapshots for over 15 min of Syb2-mRFP (yellow) plus the two mutants FweA(E74A) and (Y104A)-mTFP isoform (green) transfected Fwe KO CTLs conjugated to P815 target cells in the presence of anti-RFP647 antibody (magenta) in the medium. The accumulation of Syb2 (arrow pointed) transfected with the E and Y mutation are shown. Scale bar: 5  $\mu$ m. (B) Quantitative analysis of endocytosis and accumulation of Syb2 (anti-RFP647) at the IS from 0 to 15 min for the mutant E74A (orange) and Y104A (cyan) transfected cells in comparison to WT and Fwe KO is shown. Time zero is defined as the appearance of the first endocytic signal at the IS. Data given as mean  $\pm$  SEM; One-way Analysis of Variance (ANOVA) was done against Fwe KO as control; \* p < 0.01, \*\* p < 0.001. (C) Fluorescence intensity of mTFP expression in the cell for the E and Y mutant was calculated and plotted. Data given as mean in red line; ns p > 0.05.

#### 4.16 The C-terminus of drosophila Flower is important in Syb2 endocytosis

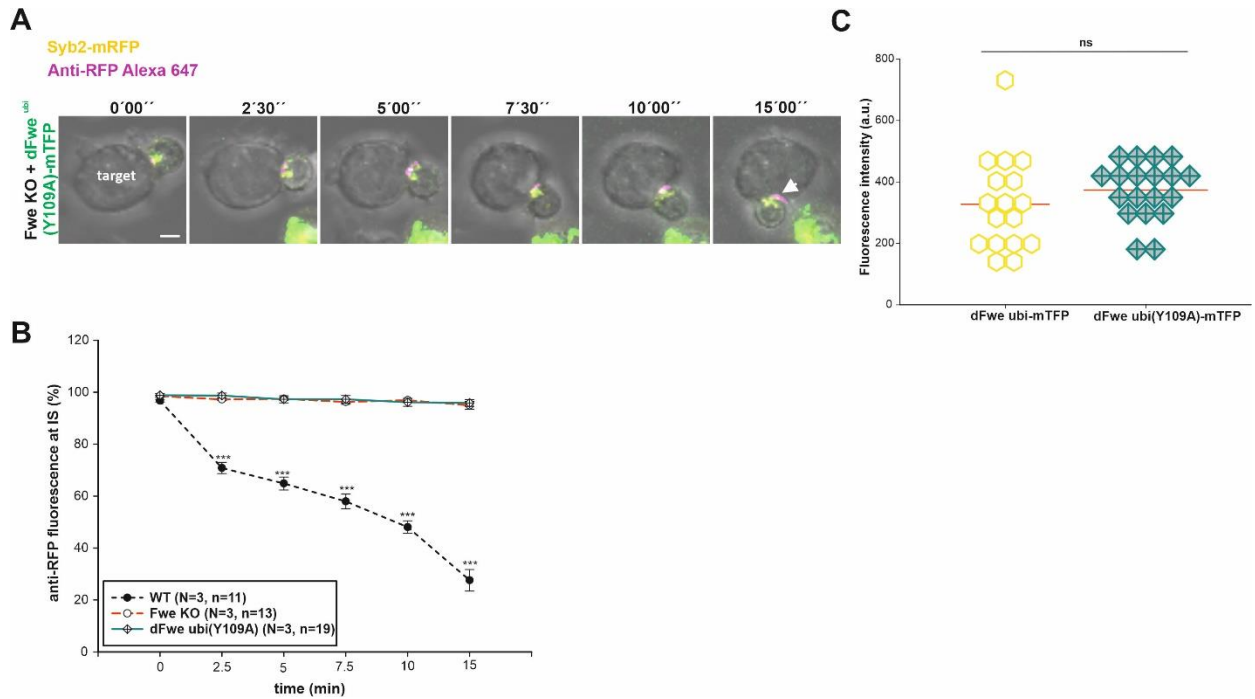
Since we have shown that loss of the C-terminus in mouse FweB dramatically reduced Syb2 endocytosis (Figure 30), we addressed the general importance of the C-terminus. Drosophila has three Flower splice variants, namely Flower Ubiquitous (Ubi), LoseA and LoseB. The 3 variants mainly differ at the C-terminus (Figure 42A). The constructs for the drosophila splice variants were cloned by using codon optimisation to match amino acid sequences similar to those of murine to enhance protein expression. Codon optimization involves recombination, without modifying the sequence of the amino acid (of drosophila Flower) and therefore can favour expression of the recombinant gene in different host organisms (Fu et al., 2020). The fusion proteins were made using mTFP as the fluorescent tag. Endocytosis rescue experiments were then performed with the respective isoforms as described previously, on Syb2-mRFP transfected Flower KO cells. dFwe<sup>Ubi</sup> was able to rescue the phenotype completely but CTLs expressing LoseA or LoseB behaved similarly to KO and did not exhibit endocytosis (Figure 42B, arrow). Quantification of RFP647 fluorescence for Fwe<sup>ubi</sup> (mean of 98.8% ± 0.6, 85.6% ± 3, 69.5% ± 2.6, 61.2% ± 2.5, 54.9% ± 3.5 and 45.4% ± 3 at time points 0, 2.5, 5, 7.5, 10 and 15 min; Figure 42C, yellow) showed less accumulation at IS. The RFP647 intensity accumulated at IS was higher in LoseA (mean of 99% ± 0.4, 96.7% ± 1, 96.6% ± 0.7, 95.8% ± 0.9, 95.8% ± 1.2 and 45.4% ± 3 at time points 0, 2.5, 5, 7.5, 10 and 15 min; Figure 42C, light purple) and LoseB (mean of 98% ± 1, 92.4% ± 1.7, 93.5% ± 1.3, 93.4% ± 2, 91.6% ± 2 and 92% ± 1.3 at time points 0, 2.5, 5, 7.5, 10 and 15 min; Figure 42C, grey) isoforms. Expression levels of the three isoforms were not significantly different (mean intensities 327.7, 273.9 and 342.3 for Ubi, LoseA and LoseB respectively; Figure 42D).



**Figure 42: dFwe<sup>ubi</sup> and not dFwe<sup>LoseA</sup> or dFwe<sup>LoseB</sup> could rescue Syb2 endocytosis**

(A) Protein sequence alignment of drosophila Flower isoforms. \* Indicate conserved amino acids. (B) Time-lapse live snapshots over 15 min of CTLs transfected with Syb2-mRFP (yellow) and the three dFwe-mTFP isoforms (green). Cells were conjugated to P815 target cells in the presence of anti-RFP647 antibody (magenta) in the medium. The accumulation and endocytosis of Syb2 (arrow pointed) transfected with the different dFwe isoforms are shown. Scale bar: 5  $\mu$ m. (C) Quantitative analysis of endocytosis and accumulation of Syb2 (anti-RFP647) at the IS from 0 to 15 min for Ubi (yellow), LoseA (grey) and LoseB (light purple) transfected cells. Time zero is determined as the appearance of the first endocytic signal at the IS. Data given as mean  $\pm$  SEM; One-way Analysis of Variance (ANOVA) was done against Fwe KO as control; \*\* $p < 0.01$ , \*\*\*  $p < 0.001$ . (D) mTFP expression in the cell measured as fluorescence intensity of the three isoforms. Data given as mean in red line; ns  $p > 0.05$ .

Since the Y104A mutation in mouse Flower showed a dramatic effect on the rescue phenotype (Figure 41), mutation of the tyrosine residue in drosophila Ubi variant (Y109A) was used as a control to analyse if the effect was consistent. An endocytosis rescue experiment was performed on KO CTLs by overexpressing cells with the mutation constructs dFwe<sup>Ubi</sup> (Y109A)-mTFP along with Syb2-mRFP and conjugated with target P815 cells. Addition of RFP647 antibody showed no rescue of Syb2 endocytosis (Figure 43A, arrow) and behaved similarly to KO cells. Quantification of RFP647 intensity (mean of  $98.8\% \pm 0.6$ ,  $98.7\% \pm 1$ ,  $97.2\% \pm 1.4$ ,  $97.2\% \pm 1.4$ ,  $96.1\% \pm 1.5$  and  $95.8\% \pm 1.3$  at time points 0, 2.5, 5, 7.5, 10 and 15 min; Figure 43B, deep cyan) showed accumulation at the IS. Expression level of the mutant construct was compared and shown to be equal in mTFP fluorescence intensity to drosophila constructs (Figure 43C, mean 373.5).



**Figure 43: Mutation of Y109A in dFwe<sup>ubi</sup> isoform cannot rescue the block of Syb2 endocytosis**

(A) Time-lapse live snapshots for over 15 min of Syb2-mRFP (yellow) along with dFwe<sup>ubi</sup>(Y109A)-mTFP mutant (green) transfected Fwe KO CTLs conjugated to P815 target cells in the presence of anti-RFP647 antibody (magenta) in the medium. The accumulation of Syb2 (arrow pointed) transfected with the Y109A mutant is shown. Scale bar: 5  $\mu$ m. (B) Quantitative analysis of endocytosis and accumulation of Syb2 (anti-RFP647) at the IS from 0 to 15 min for the mutant (deep cyan) transfected cells in comparison to WT and Fwe KO is shown. Time zero is defined as the appearance of the first endocytic signal at the IS. Data given as mean  $\pm$  SEM; One-way Analysis of Variance (ANOVA) was done against Fwe KO as control; ns  $p > 0.05$ . (C) Fluorescence intensity of mTFP expression in the cell for the Y109A mutant was calculated and plotted. Data given as mean in red line; ns  $p > 0.05$ .

Combined, the results show the importance of C-terminal among the dFwe variants but it is still unclear which part of the sequence in the C-terminus of LoseA and LoseB contribute to the non-rescuer effect. Clustal analysis using Clustal Omega software of dFwe isoforms with mouse FweA showed only 33% of conserved sequence and no motif similarity was detected at the C-terminus. Mutation of the conserved Y residue of mouse(104) and drosophila (Y109) results in a drastic loss of Syb2 endocytosis.

## 5. Discussion

In the present study, we have characterized the relevance of Flower isoforms in aiding endocytosis, specifically endocytosis of the cytotoxic granule (CG) marker protein, Synaptobrevin2 (Syb2). Since it was shown that Syb2 in CTLs is mainly located on CG and serves as the vSNARE of CG exocytosis we interpret its endocytic uptake as a kind of “cytotoxic granule endocytosis”. Our hypothesis is that mainly Syb2 and the other constituents of lytic granules may be endocytosed and this is a specific form of endocytosis that is mainly dependent on and regulated by the Flower protein at the plasma membrane. A strong argument for that interpretation is that the constitutive TfR1 internalization is unaltered in the absence of Flower.

This study further shows that endocytosis of Syb2 is dependent on Flower with some isoforms being able to support endocytosis and others not. Obviously, the ability of Flower isoforms to reach the plasma membrane is decisive for its function in endocytosis. Since natural mutations of N- and C-terminal domains lead to accumulation in the ER and a simultaneous block of endocytosis, we think these are important parts of the Flower protein. Moreover, we were able to identify a single, broadly conserved tyrosine residue, whose mutation leads to a loss of the ability of Flower function to support endocytosis.

To characterize the function of Flower protein, we made use of a Fwe KO mouse line, and carried out loss and gain of function studies following expressing several Flower mutants in a pure KO genetic background.

### 5.1 Validation of the Flower KO model

We show that FweA, the longest isoform of mouse Flower, is expressed in isolated primary cytotoxic T lymphocytes from spleen and is upregulated during activation and differentiation of CTLs. Since other upregulated proteins such as cytokines interfere with the maturation and differentiation process of CTLs (Kaech et al., 2002) we excluded a differentiation and/or proliferation defect in our Flower KO cells by measuring the proliferation rate and CTL subtype distribution in culture. Since we found no differences in those parameters between WT and Flower KO CTLs, we conclude that Flower does not have a major impact on differentiation processes in CTLs. Moreover, this result allows direct comparison of functional readouts as degranulation assays or killing assays, because the effector cell status between KO and WT was identical (Kaech et al., 2002).

The major function of CTLs is to recognize target cells and release CG granular contents, leading to lysis of infected target cells (Lancki et al., 1987). The exocytosis of CG granules was unaltered in Fwe KO cells but the immune function of CTLs was reduced (Figure 23A, B). The killing capacity of Fwe KO CTLs was reduced to half. Since Flower is thought to be involved in



endocytosis, we considered the possibility that loss of flower might reduce target cell killing via a reduction of endocytotic function. One possibility is that the loss of Flower might influence the recycling of the CG components needed for continued killing of target cells. Thus, analysis of Syb2, a membrane CG marker was used as a tool to study the endocytosis of CG component Syb2. During exocytosis of CG granule, Syb2 is targeted to the plasma membrane. We visualized the endocytosis of Syb2-mRFP in CTLs upon target cell contact by live cell confocal imaging. Flower-deficient CTLs show a reduction in Syb2-mRFP uptake resulting in its accumulation at the IS (Figure 24B, C). This defect in endocytosis could be rescued by reintroducing FweA protein. In principle, tagging of proteins at N-terminus might influence the localization signal of the protein and might lead to differences in their function (Yu et al., 2006). Interestingly, we found that the expression of FweA with mTFP tag at both N- and C-terminus was able to rescue the Syb2 block (Figure 29). Therefore, for further endocytosis experiments in Fwe KO CTLs, mTFP tag at the C-terminus was used to determine and characterize Flower isoform function.

## 5.2 Comparing the Flower splice variants among different species

The Flower gene is conserved among multicellular organisms from fungi to human. The mouse homologue of Flower (Fwe) gene (Ensembl: ENSMUSG00000015488) has six transcript variants which were shown to be expressed in low concentrations in adult tissues and results in four protein isoforms (Petrova et al., 2012) (Figure 26). A portion of sequences called exons from the primary transcripts of pre-mRNA are linked together and exported into the cytosol, to form mature mRNA. The introns found as intervening sequences are spliced out and retain in the nucleus where they are subsequently degraded (Sharp, 2005). A large number of pre-mRNAs contain exons that are alternatively included into the mature mRNA or deleted from it, which is termed alternative splicing (Stamm et al., 2005). Protein diversity is increased through alternative splicing by allowing multiple and functionally distinct proteins to be encoded by the same gene. These splice variants can be specific to developmental and pathological states, various tissues and stress conditions. In most cases, these variants serve as an on/off regulator by introducing a premature stop codon (Sorek and Amitai, 2001). In order to study the function of Fwe isoforms in primary mouse CTLs, we first checked the expression of Flower by western blotting. The polyclonal antibody generated against the Flower protein in principle should detect all 4 isoforms. Western blot analysis of brain and spleen lysates from WT mice showed a clear band at 19 kDa but could not detect any other bands at a lower molecular weight (Figure 20B). The 19 kDa protein band corresponds to the longest isoform, FweA. Further, isolated primary CTLs showed the expression of only one form of Fwe protein at 19 kDa (Figure 20C). In order to know whether the other Fwe splice variants are expressed in brain and CTLs, RT-PCR was performed and verified the transcription of 5 splice variants namely Flower A, B, C, D, E (Figure 27). FweC is missing a start codon and should not be expressed, leading to theoretically four Flower isoforms expected to be expressed in CTLs, being mFweA (171 aa), mFweB (106 aa), mFweD (109 aa) and mFweE (128aa) (Petrova et al., 2012).

The Fwe KO mouse model used here was generated by targeting the deletion of Exon 2 and 3 (Chang et., 2018). The deletion of this region had an overall effect on all the Fwe isoforms leading to complete knock-out of the protein in the entire mouse.

In this thesis the ability of each of the Flower isoforms to reverse the loss of endocytosis of Syb2 observed in Flower KO CTLs was compared. This allowed us to examine the effects of the various splice variant on Flower function in this assay. FweB is alternatively spliced until the end of Exon 3 (Figure 44, grey highlights exon/intron borders) and FweE has a specific sequence of 22 aa after Exon 3 (Figure 44, sequence in red). The 22 aa sequence is not conserved and is not present in any of the other splice variants. FweD has a start codon exactly at the beginning of Exon 3 (Figure 44) and the rest of the sequence is identical to FweA. We think that FweD was unable to rescue the endocytic block because the N-terminus that is absent in this isoform might be important for targeting the protein to the plasma membrane. Based on the rescue phenotypes, the major difference seen in the partial rescuers FweB and E compared with that of the longer isoform FweA is the region after Exon 3 at the C-terminal end (Figure 30C). FweD on the other hand, lacks the N-terminal part and showed no effect in endocytosis of CG material (Figure 30C). We therefore think that the N- and C-terminus of mouse Fwe might influence and interact with other protein complexes which might in turn help in regulating CG endocytosis.

FweA	MSGSGAAGAAAGPAPPAQEEGMTWWYRWLCRLAGVLGAVS	CAISGLFNCVTIHPLNIAAG	60
FweB	MSGSGAAGAAAGPAPPAQEEGMTWWYRWLCRLAGVLGAVS	CAISGLFNCVTIHPLNIAAG	60
FweD	-----	-----	0
FweE	MSGSGAAGAAAGPAPPAQEEGMTWWYRWLCRLAGVLGAVS	CAISGLFNCVTIHPLNIAAG	60
FweA	VWMI	MNAFILLLCEAPFCCQFVEFANTVAEKVDRLRSWQKAVFYCGMAIVPIVMSLTLTT	120
FweB	VWMI	MNAFILLLCEAPFCCQFVEFANTVAEKVDRLRSWQKAVFYCG-----	106
FweD	--M	MNAFILLLCEAPFCCQFVEFANTVAEKVDRLRSWQKAVFYCGMAIVPIVMSLTLTT	58
FweE	VWMI	MNAFILLLCEAPFCCQFVEFANTVAEKVDRLRSWQKAVFYCGHGEALRGAWPDVRL	120
	*****		
FweA	LLGNAIAFATGVLYGLSALGKK	GD AISYARIQQQRQQADEEKLAETFEGEL	171
FweB	-----	-----	106
FweD	LLGNAIAFATGVLYGLSALGKK	GD AISYARIQQQRQQADEEKLAETFEGEL	109
FweE	PNRNTISL	-----	128

**Figure 44: Protein sequence of mouse Flower isoforms**

Protein clustal analysis of mouse Flower Isoforms A, B, D and E showing the exon/intron borders in grey. Note the conserved Exon3 region marked by \* and the extra non-conserved amino acid sequence in FweE marked in red.

The Flower gene was first referred in 2009 by the group of Yao et al., where they studied the function of a calcium channel containing domain protein in wing imaginal discs of a fruit fly. In the Fly Database, the Flower gene is encoded by the symbol Dmel\dFwe (CG6151, FBgn0261722). The drosophila Fwe has 3 transcripts and encodes 3 unique polypeptides. The CG6151 locus encodes for Flower, a protein of barely characterized function with three or four transmembrane domains (Yao et al., 2009) and encodes three isoforms formed via alternative splicing- dFwe<sup>Ubi</sup>, dFwe<sup>LoseA</sup> and dFwe<sup>LoseB</sup> that differ mainly in their C-terminal part (Celniker et al., 2002). The molecular function was described initially as a calcium channel and was shown to promote synaptic vesicle endocytosis (Yao et al., 2009). This hypothesis has not been verified. In 2019 the same group reported that the Fwe protein is important in regulating two modes of endocytosis namely clathrin mediated (CME) and activity dependent bulk endocytosis (ABDE) (Yao et al., 2017). However, a different function was proposed by the group of Eduardo Moreno, who suggested that Fwe isoforms act as fitness fingerprints and that they help in developmental regulation by acting as major players in cell competition (Rhiner et al., 2010). The group showed that the isoform dFwe<sup>Ubi</sup> acts as a Winner signal and the other two isoforms dFwe LoseA and LoseB as Loser signals during cell competition. It is difficult to understand how a cell competition protein may influence endocytosis. Either Flower in drosophila has completely different functions as in CTLs or an at present unresolved mechanism links endocytosis and cell competition. To get deeper insights into the dFwe function we expressed dFwe isoforms in KO CTLs. Surprisingly dFwe<sup>Ubi</sup> could rescue endocytosis while LoseA and LoseB forms could not (Figure 42). The result clearly shows that dFwe can induce endocytosis in mammalian cells. Moreno's observation of Loser and Winner isoforms together with our finding that the Winner induces endocytosis while the Losers don't, are an argument for a causal link between both processes. It could be that the winner cells expressing Fwe rescuer isoforms endocytose certain survival factors from the extracellular space while the loser cell having Fwe non-rescuers isoforms cannot, leading to cellular competition and death of the loser cells.

Amino acid sequence alignments of mFwe and dFwe showed only a mild conservation (Figure 45) between mouse and drosophila homologs, which did not give a hint for any functional domains. What attracted our attention was the conserved tyrosine around position 104 and 109 in mouse and drosophila forms. Since tyrosine can be phosphorylated by specific phosphatases this amino acid often is involved in regulatory processes (Getz et al., 2019). Consequently, mutations of tyrosine in mFweA (Y104A) and dFwe<sup>Ubi</sup> (Y109A) completely blocked endocytosis of Syb2 (Figure 41, 43).

mFweA	-----MSGSGAAGAAAGPAPPAQEEGMTWYRWLCRLAGVLGAVSCAISGLFNCVTIHP	54
ubi	MSFAEKITGLLARPNQQDPI----GPEQPWYLKYGSRLLGIVAAFFAILFGLWNVFSIIT	56
loseA	MSFAEKITGLLARPNQQDPI----GPEQPWYLKYGSRLLGIVAAFFAILFGLWNVFSIIT	56
loseB	MSFAEKITGLLARPNQQDPI----GPEQPWYLKYGSRLLGIVAAFFAILFGLWNVFSIIT	56
	* * * * *	
mFweA	LN---IAAGVWMI <del>MNAFILLLCEAPFCCQFVEFANTVAEKVDRLRSWQKAVFYC</del> GMAIVP	111
ubi	LSVSCLVAGILQMVAGFVVMLEAPCCFVCFQGVNEIAEKVESKPLYFRAGLYIAMAIIP	116
loseA	LSVSCLVAGILQMVAGFVVMLEAPCCFVCFQGVNEIAEKVESKPLYFRAGLYIAMAIIP	116
loseB	LSVSCLVAGILQMVAGFVVMLEAPCCFVCFQGVNEIAEKVESKPLYFRAGLYIAMAIIP	116
	* ** * * * * *	
mFweA	IVMSLTLLTLLGNIAIFATGVLYGLSALGKKGDAISYARIQQQRQQADEEKLAET-----	166
ubi	IILCFGLASLFGSGLIFGTGVVYGMMALGKKASAEEMRAAAQQTFG-----GNTPAQT	169
loseA	IILCFGLASLFGSGLIFGTGVVYGMMALGKKASREDMAAAATSPTQMAGSQAGGQMOMGG	176
loseB	IILCFGLASLFGSGLIFGTGVVYGMMALGKNKHI FLVRNYI-----	157
	* * * * *	
mFweA	-----FEGEL-----	171
ubi	NDRAGIVNNAQPFSTGAVGTDSNV	194
loseA	DQHITLMEPDVWRPT-----	192
loseB	-----	157

**Figure 45: Comparison of mouse FweA protein sequence with the drosophila Fwe isoforms**

Protein Clustal analysis of mouse FweA with drosophila isoforms showing exon3 marked in green for mouse and yellow for drosophila isoforms. The conserved tyrosine (Y) amino acid that showed a drastic phenotype in failure of rescuing Syb2 endocytosis is marked in teal colour. Marked in \* are the conserved amino acid sequence among all isoforms.

### 5.3 Importance of YXX $\phi$ motif in aiding endocytosis

Screening of the mouse Flower sequence for possible interaction sites with binding partners which may aid in endocytosis led to the identification of N- and C-terminal motifs of the common signal motif YXX $\phi$ . This motif is mainly recognized by adaptor coat proteins along the endocytic and sorting pathways (Pandey, 2009). The YXX $\phi$  tyrosine-based motif represents X as any amino acid residue and  $\phi$  that denotes a residue with a large bulky hydrophobic side chain. In particular, we recognized a sequence of amino acids YRWL (26-29 aa) and YARI (147-150 aa). Mutation of these putative tyrosine- based motif sites to alanine individually or in combination was used as a strategy to identify its contribution in regulating CG endocytosis. Rescue experiments following expression of YXX $\phi$  mutants in Fwe KO CTLs showed that the YRWL/AAAA single mutant and the double mutant failed to reverse the endocytotic deficit block (Figure 35, 87% of RFP647 accumulation at IS) while the YARI/AAAA single mutant partially rescued the phenotype (Figure 35, 75% of RFP647 accumulation at IS) (Figure 35B, C). To confirm these data, the FweB isoform was used as an additional target to check the importance of this motif. Since FweB is spliced at the end of Exon3 and therefore lacks the C-terminus end, we mutated the YRWL to alanine at the N-terminus of FweB. Expression of FweB YRWL/AAAA in Fwe KO CTLs showed no rescue of Syb2 endocytosis. These results thus give us a clue that Fwe might participate in internalization and trafficking of endocytotic vesicles. The YXX $\phi$  sorting signals was previously shown to

interact with the mu ( $\mu$ ) subunit of adaptor protein complexes AP-2 by directing the target of integral membrane proteins (Bonifacino and Traub, 2003; Kirchhausen, 1999; Paing et al., 2006). AP2 belongs to the family of heterotetrameric clathrin adaptors that play a central role in many vesicular traffic pathways within the cell (Collawn et al., 1991; Trowbridge et al., 1993). AP2 was also shown to function in clathrin-mediated endocytosis (Collins et al., 2002). We could not show an interaction of the motifs YRWL and YARI in FweA with the AP2 $\mu$  subunit in the yeast two hybrid system. We take that as a strong argument that endocytosis of CG material as Syb2 might be fundamentally different from clathrin mediated endocytosis. Consistent with this observation, there are already published immunoprecipitation studies showing that Flower co-precipitates with AP2 $\mu$  in brain lysates but with AP2A1 and B in CTLs (Chang et al., 2018).

Taken together, the results are consistent with the existence of at least two independent endocytotic pathways in CTLs, a clathrin dependent and a Flower dependent one. While clathrin mediated endocytosis may account for most constitutive proteins like the TfR1 (Figure 25), Flower dependent endocytosis may account for proteins of lysosomal related organelles (LRO) such as CGs which are mainly activated by a regulated pathway. As a marker protein, we used the v-SNARE of CGs, Syb2. At least LAMP1, another LRO-protein, seems to use the same pathway (Chang et al., 2018).

Previously, it was shown that in CTLs, Syb2 is endocytosed independently from recycling endosomes and that dynamin, clathrin, and CALM proteins are necessary for this action (Chang et al., 2016). However, since TfR1 internalization is a classical and well-studied example of Clathrin-dependent endocytosis, and it is not reduced in Fwe KO cells, it is likely that clathrin-dependent internalization is not Flower-dependent. Based on these observations, a second clathrin independent pathway of endocytosis, which might also be regulated by Flower, is likely.

#### **5.4 Exon3 as the common factor that imparts specific function in Flower isoforms**

An amino acid alignment of different members of the CG6151-P protein family by various bioinformatics programs like Pfam, Smart and InterPro showed that the CG6151-P proteins are conserved among species from fungi to human. Some members of the Cg6151-P family were recognized as putative clathrin-coated vesicle proteins. The fungal members have a characteristic ICP (Natural cysteine peptidase (CP) inhibitor of the I42 family) sequence motif and others belong to the Golgi apparatus membrane protein TVP family involved in vesicular Golgi/endosome trafficking (Yao et al., 2009) (Figure 40). Interestingly, we found that the regions of mouse FweA span the beginning of TM1 to the end of TM4 (AA 33-143) (Figure 40, highlighted in teal). Clustal alignment of the specific Exon3 of FweA with other mammalian homologues showed a high conservation of this region. The CACFD1 encodes hFWE protein and encodes for four protein-

coding splice variants (hFWE1–hFWE4) (Figure 12). In a recent study in 2019, the group of Moreno et al. showed that during cell competition, two human Flower isoforms (hFWE1 and hFWE3) function and contribute as Flower-Lose proteins, whereas the other two isoforms (hFWE2 and hFWE4) act as Flower-Win proteins (Coelho et al., 2018; Moreno et al., 2019). The major difference seen between the win and lose isoforms of hFWE is the absence of Exon 3 in the lose proteins (Figure 38A). Since we already have naturally truncated mutants within the hFWE isoforms, we wanted to check its role in Syb2 rescue phenotype in Fwe KO CTLs. Rescue experiments with the hFWE isoforms showed efficient rescue of Syb2 block by hFWE 2 and 4 (Figure 38, 35% and 45% of accumulated RFP647 at the IS) but no rescue of the block by hFWE1 and 3 (Figure 38, 90% and 89% of accumulated RFP647 at the IS). Clustal analysis of FweA with FWE4 showed 96% of sequence identity. To see if loss of Exon 3 is important in CG endocytosis, we removed Exon 3 in mouse FweB isoform and saw no rescue of the Syb2 endocytosis in Fwe KO CTLs (Figure 39, 95% of accumulated RFP647 at the IS). These results show that the conserved Exon 3 region is highly important and might have interactive sites that aid CG endocytosis.

In Exon 3 of mouse Flower, three amino acid residues were found that were highly conserved among the CG6151-P proteins from various species (Figure 40). The glutamate (E) residue in the second TM domain of dFwe and mFwe was shown to play a role in ion selectivity filters of TRPV5 and 6 (Yao et al., 2009). The proline (P) residue is known for its role in protein stability (Prajapati et al., 2007) and the tyrosine (Y) residue is an important phosphorylation site for kinases (Lemmon and Schlessinger, 2010). Based on this information we decided to mutate the amino acids individually to alanine. Since proline is important for protein integrity, we decided not to mutate proline but only focus on glutamate and proline residues for rescue experiment (Figure 40). Endocytosis rescue experiment with E74A showed a partial rescue and Y104A mutant showed no rescue (Figure 41). If the respective tyrosine was mutated in dFwe<sup>Ubi</sup> (Y109A) endocytosis could also not be rescued.

The phenotype seen by E74A could be due to the function of glutamate residue as a selectivity filter thereby playing an important role in regulating calcium influx to the cell. Previous reports show that the E74Q mutant of dFwe had reduced Ca<sup>2+</sup> conductance in Fwe mutant boutons in comparison to WT Fwe (Yao et al., 2017). Our results may strengthen the interpretation that also in mouse and human Flower may act as a Ca<sup>2+</sup> channel. It was also found that dFwe (E79Q) mutant lost the ability to promote PI (4,5) P2 microdomain formation in a Ca<sup>2+</sup> dependent manner in drosophila boutons (Li et al., 2020). Since endocytosis at the IS is Ca<sup>2+</sup> dependent (Chang et al., 2016), mutation of the glutamate residue might alter the intracellular Ca<sup>2+</sup>, leading to defect in endocytic process.

The Y mutants completely failed in rescue experiments which could be due to the fact that these residues are possible regulatory sites of endocytosis presumably by tyrosine-phosphorylation.

Protein phosphorylation is a regulatory mechanism that is majorly important in many cellular processes (McCance and Huether, 2014) including endocytosis (Nuzifora and Fox, 1999). Prediction software shows the conserved tyrosine to be a part of the transmembrane region. Since Flower is involved in hexamer and multimer formation (Yao et al., 2009), alteration of this conserved tyrosine residue might interfere with the channel formation and thus lead to altered function. Therefore, more experimental strategies are needed to study the precise role of tyrosine residue of Exon3 in Flower protein to understand its function in the endocytic pathway.

## 5.5 Localization and topology of Flower

The localization of Flower protein in mouse CTLs is still unclear. Endogenous expression of Flower showed vesicular staining. The localization at the plasma membrane is still unclear as immunostaining showed weak surface staining, while surface biotinylation study showed 1.6% endogenous Flower at the plasma membrane (Chang et al., 2018). In the present work, electron microscopic analysis of the endogenous localization of Flower by immunogold labelling of WT CTLs revealed both a cytoplasmic and plasma membrane localization with more Flower at the membrane (Figure 32). These data thus add as a confirmation to the result shown in Figure 31, that upon activation and CD3/CD28 bead stimulus, FweA is localized to the plasma membrane in order to aid CG endocytosis.

Plasma membrane expression and Fwe topology analysis on activated cells (cells on poly-L-ornithine coated coverslips) using Halo tagged constructs of the isoforms stained with non-permeable Atto488 dye indicated that none of the Fwe isoforms might be present at the plasma membrane and that the N- and C-terminus of Fwe protein might face the cytosolic part of the cell (negative Atto488 stain; Figure 31). The negative staining might also mean that Flower needs a specific trigger for its localization at the plasma membrane which was confirmed by the 1 hr bead activation of cells (also to mimic target cell-based activation) after overnight transfection of CTLs with Fwe isoform constructs. FweA showed perfect membrane staining (Figure 32,33) after stimulation where the mTFP signal colocalized with the plasma membrane marker CD8 (Figure 32A, C). The Fwe non-rescuers of endocytosis showed no plasma membrane localization (Figure 32A, C) showing one of the reasons why the endocytosis rescue might have failed. The vesicular localization of the FweA rescuer versus the non-rescuers also differed after bead stimulation. Super resolution microscopic analysis of the Fwe KO CTLs expressing the Fwe isoforms with ER marker showed that the rescuers of endocytosis had vesicular localization and no colocalization with ER (Figure 34) whereas the non-rescuers showed tubular like pattern that showed maximum colocalization with the ER marker (Figure 34). It was previously shown that alternative splicing of tetraspanins, which are classic transmembrane proteins, show altered transmembrane topology, and contain deleted parts of the large extracellular loop, or generate alternative N- or C-termini. This results in structure-based forms of non-conventional tetraspanins. They therefore speculate that non-conventional tetraspanins may have roles in regulating ER exit thereby modulating

tetraspanin-enriched microdomain function (Hochheimer et al., 2019). Moreover, Flower at the ER might function by interacting with STIM and Orai channels in regulating  $Ca^{2+}$  and thereby indirectly influencing endocytosis. These results might explain the drastic phenotype seen by different Flower isoforms in regulating and aiding Syb2 positive CG endocytosis.

## 5.6 Proposed model of mouse Flower isoforms in aiding Syb2 endocytosis

From all these above results, we categorize Fwe isoforms and their mutants, as rescuers and non-rescuers based on their ability to restore Syb2 endocytosis in Flower KO CTLs. Rescuers and non-rescuers of CG endocytosis can also be determined by features found in Exon3 and the C-terminal sequence, based on the murine long isoform of Flower (see table 13).

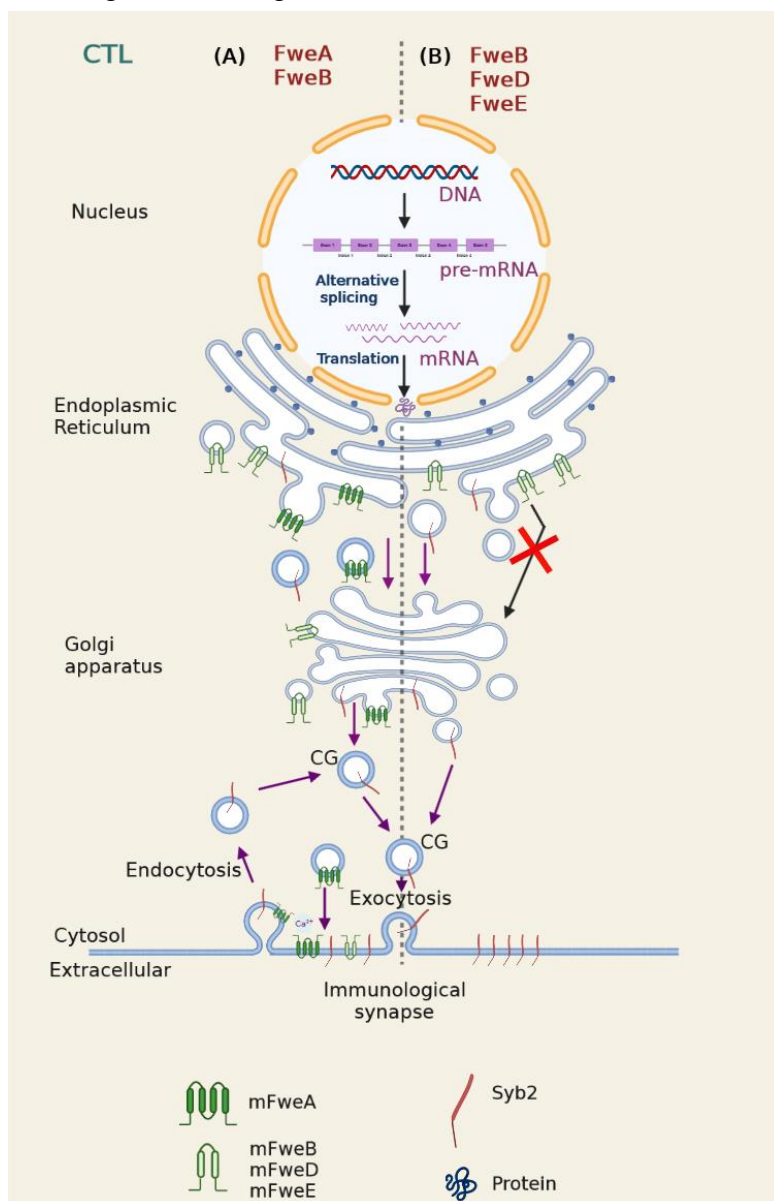
Rescuers	Partial rescuers	Non-rescuers
FweA	FweB	FweD
hFWE2	FweE	hFWE1
hFWE4	FweA (YARI to alanine) mutant	hFWE3
dfwe ubi	FweA (E74A) mutant	dfwe loseA
		dfwe loseB
		FweA (YRWL to alanine) mutant
		FweA (YRWL & YARI to alanine) mutant
		FweB (YRWL to alanine) mutant
		FweB ( $\Delta$ Exon3) mutant
		FweA (Y104A) mutant
		dfwe ubi (Y109A) mutant

**Table 13: Table summarizing Flower isoforms into rescuers and non-rescuers of CG endocytosis category based on the experimental results obtained from Fwe KO CTLs**

We think that the Flower function in endocytosis is required that it reaches the plasma membrane. Alternative splicing of Flower pre-mRNA begins at the nucleus, where the spliced mRNAs as exons are translated to protein in the cytosol and enter the endoplasmic reticulum (ER) membrane. Upon activation, cytotoxic T lymphocytes (CTLs) release Syb2 positive cytotoxic granules (CG) via exocytosis towards the immunological synapse (IS). Of the 4 mouse Fwe isoforms, FweA and B exit the ER via vesicular transport to the Golgi apparatus and are transported to the plasma membrane through secretory vesicles of unknown identity. Thus, the membrane Flower aids Syb2



endocytosis by regulating intracellular calcium (Chang et al., 2018) and is itself being endocytosed during the process (Figure 46A). In the other scenario FweB, D and E isoforms fail to exit the ER and are localized at the ER membrane and therefore do not traffic to the plasma membrane. This leads to an accumulation of Syb2 at the plasma membrane (Figure 46B). Loss of endocytosis causes less Syb2 retrieval and subsequently fewer CG are generated for the next round of the fusion process, reducing serial killing function.



**Figure 46: Localization and possible function of mouse Flower isoforms in endocytosis**

Model illustrating alternative splicing, localization and trafficking of mouse Fwe splice variants in Syb2 endocytosis of cytotoxic T lymphocytes (CTLs). Genomic DNA is transcribed to pre-mRNA containing introns (black line) and exons (purple boxes) which then generates different mRNAs after splicing. After translation in the cytosol, the different Fwe isoforms insert into the endoplasmic reticulum (ER) membrane where in (A) FweA (rescuer) and FweB (partial rescuer) are trafficked to the plasma membrane via the Golgi secretory vesicles. At the plasma membrane, Syb2 is internalized through the aid of FweA or B isoforms. In (B) FweB, D and E (non-rescuers) are localized and do not exit the ER to the plasma membrane thereby leading to accumulation of Syb2 due to the failure of the FweB, D and E isoforms in aiding endocytosis. The defect in endocytosis leads to failure in Syb2 retrieval and possible retrograde trafficking of Syb2 positive vesicles for serial killing function of CTLs.

## **6. Outlook**

A comparison of the role of Flower isoforms in regulating the molecular mechanism of endocytosis has been presented in this study. Nature has created a way to regulate different cellular pathways by producing splice variants of genes thereby controlling and balancing the complex processes occurring in the body. The presumed function of Flower isoforms in cell competition and survival is an interesting aspect, possibly presenting a chance for clinical intervention in cancer based on Flower as a target (Petrova et al., 2012; Moreno et al., 2019).

The molecular mechanism of the winner and loser Flower isoforms in cell competition is unknown. From the study presented here, we can clearly conclude that the winner isoforms were the rescuers of endocytosis and the losers were not. Studying and comparing both effects may lead to a functional link between both features. In the case of CTLs the ability to efficiently kill other cells is clearly a winning trait. How in other cell types a Flower dependent endocytosis can increase cell fitness would be an interesting topic of future research.

## 7. References

- Adler, E. M., Augustine, G. J., Duffy, S. N., and Charlton, M. P. (1991). Alien intracellular calcium chelators attenuate neurotransmitter release at the squid giant synapse. *The Journal of neuroscience: the official journal of the Society for Neuroscience*, 11(6): 1496–1507.
- Bao, L., Redondo, C., Findlay, J. B., Walker, J. H., and Ponnambalam, S. (2009). Deciphering soluble and membrane protein function using yeast systems (Review). *Molecular membrane biology*, 26(3): 127–135.
- Bárcena, J., and Blanco, E. (2013). Design of novel vaccines based on virus-like particles or chimeric virions. *Sub-cellular biochemistry*, 68: 631–665.
- Benado, A., Nasagi-Atiya, Y., and Sagi-Eisenberg, R. (2009). Protein trafficking in immune cells. *Immunobiology*, 214(7): 507–525.
- Betts, M. R., Brenchley, J. M., Price, D. A., De Rosa, S. C., Douek, D. C., Roederer, M., and Koup, R. A. (2003). Sensitive and viable identification of antigen-specific CD8<sup>+</sup> T cells by a flow cytometric assay for degranulation. *Journal of immunological methods*, 281(1-2): 65–78.
- Bonifacino, J. S., and Traub, L. M. (2003). Signals for sorting of transmembrane proteins to endosomes and lysosomes. *Annual review of biochemistry*, 72: 395–447.
- Bolte, S. and Cordelieres, F.P. (2006). A guided tour into subcellular colocalization analysis in light microscopy. *Journal of Microscopy*, 224 (3): 213-232.
- Breeden, L., and Nasmyth, K. (1985). Regulation of the yeast HO gene. *Cold Spring Harbor symposia on quantitative biology*, 50: 643–650.
- Brose, N., and Neher, E. (2009). Flowers for synaptic endocytosis. *Cell*, 138(5): 836–837.
- Burchfield, J. G., Lopez, J. A., Mele, K., Vallotton, P., and Hughes, W. E. (2010). Exocytotic vesicle behaviour assessed by total internal reflection fluorescence microscopy. *Traffic*, 11(4): 429–439.
- Catterall, W. A., and Few, A. P. (2008). Calcium channel regulation and presynaptic plasticity. *Neuron*, 59(6): 882–901.
- Capitani N., Patrussi L., D’Elios M.M., Baldari C.T. (2021). Dysfunctional Immune Synapses in T Cell Immunodeficiencies. *Cellular Primary Immunodeficiencies; Rare Diseases of the Immune System*, 43-63.
- Celniker, S. E., Wheeler, D. A., Kronmiller, B., Carlson, J. W., Halpern, A., Patel, S., Adams, M., Champe, M., Dugan, S. P., Frise, E., Hodgson, A., George, R. A., Hoskins, R. A., Lavery, T., Muzny, D. M., Nelson, C. R., Pacleb, J. M., Park, S., Pfeiffer, B. D., Richards, S., ... Rubin, G. M. (2002). Finishing a whole-genome shotgun: release 3 of the *Drosophila melanogaster* euchromatic genome sequence. *Genome biology*, 3(12): RESEARCH0079.

- Chang, H. F., Mannebach, S., Beck, A., Ravichandran, K., Krause, E., Frohnweiler, K., Fecher-Trost, C., Schirra, C., Pattu, V., Flockerzi, V., and Rettig, J. (2018). Cytotoxic granule endocytosis depends on the Flower protein. *The Journal of cell biology*, 217(2): 667–683.
- Chang, H. F., Bzeih, H., Schirra, C., Chitirala, P., Halimani, M., Cordat, E., Krause, E., Rettig, J., and Pattu, V. (2016). Endocytosis of Cytotoxic Granules Is Essential for Multiple Killing of Target Cells by T Lymphocytes. *Journal of immunology*, 197(6): 2473–2484.
- Chaplin D. D. (2010). Overview of the immune response. *The Journal of allergy and clinical immunology*, 125(2): S3–S23.
- Chattopadhyay, P. K., Betts, M. R., Price, D. A., Gostick, E., Horton, H., Roederer, M., and De Rosa, S. C. (2009). The cytolytic enzymes granzyme A, granzyme B, and perforin: expression patterns, cell distribution, and their relationship to cell maturity and bright CD57 expression. *Journal of leukocyte biology*, 85(1): 88–97.
- Chitirala, P., Ravichandran, K., Galgano, D., Sleiman, M., Krause, E., Bryceson, Y. T., and Rettig, J. (2019). Cytotoxic Granule Exocytosis from Human Cytotoxic T Lymphocytes Is Mediated by VAMP7. *Frontiers in immunology*, 10: 1855.
- Clark, D. P., Pazdernik, N. J. and McGehee, M. R. (2019). *Molecular Biology* (Third edition). Academic cell, 15: 484-520
- Coelho, D. S., Schwartz, S., Merino, M. M., Hauert, B., Topfel, B., Tiede, C., Rhiner, C., and Moreno, E. (2018). Culling Less Fit Neurons Protects against Amyloid- $\beta$ -Induced Brain Damage and Cognitive and Motor Decline. *Cell reports*, 25(13): 3661–3673.e3.
- Collawn, J. F., Kuhn, L. A., Liu, L. F., Tainer, J. A., and Trowbridge, I. S. (1991). Transplanted LDL and mannose-6-phosphate receptor internalization signals promote high-efficiency endocytosis of the transferrin receptor. *The EMBO journal*, 10(11): 3247–3253.
- Collins, B. M., McCoy, A. J., Kent, H. M., Evans, P. R., and Owen, D. J. (2002). Molecular architecture and functional model of the endocytic AP2 complex. *Cell*, 109(4): 523–535.
- Cordero, R., and Cynthia A. Szewczak. (1994). The Developmental Importance of Cell Division. *The American Biology Teacher*, 56(3): 176-179.
- Cousin M. A. (2000). Synaptic vesicle endocytosis: calcium works overtime in the nerve terminal. *Molecular neurobiology*, 22(1-3): 115–128.
- Capuano, C., Paolini, R., Molfetta, R., Frati, L., Santoni, A., Galandrini, R. (2012). PIP2-dependent regulation of Munc13-4 endocytic recycling: impact on the cytolytic secretory pathway. *Blood*, 119(10): 2252-62.
- de Saint Basile, G., Ménasché, G., and Fischer, A. (2010). Molecular mechanisms of biogenesis and exocytosis of cytotoxic granules. *Nature reviews. Immunology*, 10(8), 568–579.
- Dustin, M. L., Chakraborty, A. K., and Shaw, A. S. (2010). Understanding the structure and function of the immunological synapse. *Cold Spring Harbor perspectives in biology*, 2(10): a002311.

- Fields, S., and Song, O. (1989). A novel genetic system to detect protein-protein interactions. *Nature*, 340(6230): 245–246.
- Flicek, P., Aken, B. L., Ballester, B., Beal, K., Bragin, E., Brent, S., Chen, Y., Clapham, P., Coates, G., Fairley, S., Fitzgerald, S., Fernandez-Banet, J., Gordon, L., Gräf, S., Haider, S., Hammond, M., Howe, K., Jenkinson, A., Johnson, N., Kähäri, A., Searle, S. M. (2010). Ensembl's 10th year. *Nucleic acids research*, 38(Database issue): D557–D562.
- Fu, H., Liang, Y., Zhong, X., Pan, Z., Huang, L., Zhang, H., Xu, Y., Zhou, W., and Liu, Z. (2020). Codon optimization with deep learning to enhance protein expression. *Scientific reports*, 10(1): 17617.
- Getz, L. J., Runte, C. S., Rainey, J. K., and Thomas, N. A. (2019). Tyrosine Phosphorylation as a Widespread Regulatory Mechanism in Prokaryotes. *Journal of bacteriology*, 201(19): e00205-19.
- Gholam, C., Grigoriadou, S., Gilmour, K. C., and Gaspar, H. B. (2011). Familial haemophagocytic lymphohistiocytosis: advances in the genetic basis, diagnosis and management. *Clinical and experimental immunology*, 163(3), 271–283.
- Gil, J., and Rodriguez, T. (2016). Cancer: The Transforming Power of Cell Competition. *Current biology*, 26(4): R164–R166.
- Groscurth, P., and Filgueira, L. (1998). Killing Mechanisms of Cytotoxic T Lymphocytes. *News in physiological sciences: an international journal of physiology produced jointly by the International Union of Physiological Sciences and the American Physiological Society*, 13: 17–21.
- Gundelfinger, E. D., Kessels, M. M., and Qualmann, B. (2003). Temporal and spatial coordination of exocytosis and endocytosis. *Nature reviews. Molecular cell biology*, 4(2): 127–139.
- Heidelberger, R., Heinemann, C., Neher, E., and Matthews, G. (1994). Calcium dependence of the rate of exocytosis in a synaptic terminal. *Nature*, 371(6497): 513–515.
- Hassin, D., Garber, O. G., Meiraz, A., Schiffenbauer, Y. S., and Berke, G. (2011). Cytotoxic T lymphocyte perforin and Fas ligand working in concert even when Fas ligand lytic action is still not detectable. *Immunology*, 133(2): 190–196.
- Hochheimer, N., Sies, R., Aschenbrenner, A. C., Schneider, D., and Lang, T. (2019). Classes of non-conventional tetraspanins defined by alternative splicing. *Scientific reports*, 9(1): 14075.
- Inadome, H., Noda, Y., Kamimura, Y., Adachi, H., and Yoda, K. (2007). Tvp38, Tvp23, Tvp18 and Tvp15: novel membrane proteins in the Tlg2-containing Golgi/endosome compartments of *Saccharomyces cerevisiae*. *Experimental cell research*, 313(4): 688–697.
- Jacob, J., Duclouhier, H., and Cafiso, D. S. (1999). The role of proline and glycine in determining the backbone flexibility of a channel-forming peptide. *Biophysical journal*, 76(3): 1367–1376.

- Janeway, C.A. Jr., Travers, P., Walport, M., and Shlomchik, M. J. (2001). *Immunobiology: The Immune System in Health and Disease*. 5th edition. New York: Garland Science, Chapter 9, The Humoral Immune Response.
- Jadot, M., Canfield, W. M., Gregory, W., and Kornfeld, S. (1992). Characterization of the signal for rapid internalization of the bovine mannose 6-phosphate/insulin-like growth factor-II receptor. *The Journal of biological chemistry*, 267(16): 11069–11077.
- Kaech, S. M., Wherry, E. J., and Ahmed, R. (2002). Effector and memory T-cell differentiation: implications for vaccine development. *Nature reviews. Immunology*, 2(4), 251–262.
- Koo, S. J., Puchkov, D., and Haucke, V. (2011). AP180 and CALM: Dedicated endocytic adaptors for the retrieval of synaptobrevin 2 at synapses. *Cellular logistics*, 1(4): 168–172.
- Kirchhausen T. (1999). Adaptors for clathrin-mediated traffic. *Annual review of cell and developmental biology*, 15: 705–732.
- Kummerow, C., Schwarz, E. C., Bufe, B., Zufall, F., Hoth, M., and Qu, B. (2014). A simple, economic, time-resolved killing assay. *European journal of immunology*, 44(6): 1870–1872.
- Lancki, D. W., Weiss, A., and Fitch, F. W. (1987). Requirements for triggering of lysis by cytolytic T lymphocyte clones. *Journal of immunology*, 138(11): 3646–3653.
- Lai, M. M., Hong, J. J., Ruggiero, A. M., Burnett, P. E., Slepnev, V. I., De Camilli, P., and Snyder, S. H. (1999). The calcineurin-dynamin 1 complex as a calcium sensor for synaptic vesicle endocytosis. *The Journal of biological chemistry*, 274(37): 25963–25966.
- Leitz, J., and Kavalali, E. T. (2016). Ca<sup>2+</sup> Dependence of Synaptic Vesicle Endocytosis. *The Neuroscientist: a review journal bringing neurobiology, neurology and psychiatry*, 22(5): 464–476.
- Lemmon, M. A., and Schlessinger, J. (2010). Cell signaling by receptor tyrosine kinases. *Cell*, 141(7): 1117–1134.
- Li, T. N., Chen, Y. J., Lu, T. Y., Wang, Y. T., Lin, H. C., and Yao, C. K. (2020). A positive feedback loop between Flower and PI (4,5) P<sub>2</sub> at periaxial zones controls bulk endocytosis in *Drosophila*. *eLife*, 9: e60125.
- Lu, S., Wang, J., Chitsaz, F., Derbyshire, M. K., Geer, R. C., Gonzales, N. R., Gwadz, M., Hurwitz, D. I., Marchler, G. H., Song, J. S., Thanki, N., Yamashita, R. A., Yang, M., Zhang, D., Zheng, C., Lanczycki, C. J., and Marchler-Bauer, A. (2020). CDD/SPARCLE: the conserved domain database in 2020. *Nucleic acids research*, 48(D1), D265–D268.
- Luzio, J. P., Hackmann, Y., Dieckmann, N. M., and Griffiths, G. M. (2014). The biogenesis of lysosomes and lysosome-related organelles. *Cold Spring Harbor perspectives in biology*, 6(9): a016840.
- Magupalli, V. G., Schwarz, K., Alpadi, K., Natarajan, S., Seigel, G. M., and Schmitz, F. (2008). Multiple RIBEYE-RIBEYE interactions create a dynamic scaffold for the formation of synaptic ribbons. *The Journal of neuroscience: the official journal of the Society for Neuroscience*, 28(32): 7954–7967.

- Marks, M. S., Ohno, H., Kirchnausen, T., and Bonracino, J. S. (1997). Protein sorting by tyrosine-based signals: adapting to the Ys and wherefores. *Trends in cell biology*, 7(3): 124–128.
- Marks, M. S., Roche, P. A., van Donselaar, E., Woodruff, L., Peters, P. J., and Bonifacino, J. S. (1995). A lysosomal targeting signal in the cytoplasmic tail of the beta chain directs HLA-DM to MHC class II compartments. *The Journal of cell biology*, 131(2): 351–369.
- Marks, B., and McMahon, H. T. (1998). Calcium triggers calcineurin-dependent synaptic vesicle recycling in mammalian nerve terminals. *Current biology: CB*, 8(13): 740–749.
- Marshall, J. S., Warrington, R., Watson, W., and Kim, H. L. (2018). An introduction to immunology and immunopathology. *Allergy, asthma, and clinical immunology: official journal of the Canadian Society of Allergy and Clinical Immunology*, 14(2): 49.
- Marshall, M. R., Pattu, V., Halimani, M., Maier-Peuschel, M., Müller, M. L., Becherer, U., Hong, W., Hoth, M., Tschernig, T., Bryceson, Y. T., and Rettig, J. (2015). VAMP8-dependent fusion of recycling endosomes with the plasma membrane facilitates T lymphocyte cytotoxicity. *The Journal of cell biology*, 210(1): 135–151.
- Mayle, K. M., Le, A. M., and Kamei, D. T. (2012). The intracellular trafficking pathway of transferrin. *Biochimica et biophysica acta*, 1820(3): 264–281.
- Matti, U., Pattu, V., Halimani, M., Schirra, C., Krause, E., Liu, Y., Weins, L., Chang, H. F., Guzman, R., Olausson, J., Freichel, M., Schmitz, F., Pasche, M., Becherer, U., Bruns, D., and Rettig, J. (2013). Synaptobrevin2 is the v-SNARE required for cytotoxic T-lymphocyte lytic granule fusion. *Nature communications*, 4: 1439.
- Maritzen, T., and Haucke, V. (2018). Coupling of exocytosis and endocytosis at the presynaptic active zone. *Neuroscience research*, 127: 45–52.
- Merino, M. M., Levayer, R., and Moreno, E. (2016). Survival of the Fittest: Essential Roles of Cell Competition in Development, Aging, and Cancer. *Trends in cell biology*, 26(10): 776–788.
- McCance, K.L. and Huether, S.E. (2014). *Pathophysiology: The Biologic Basis for Disease in Adults and Children*. Brashers VL and Rote NS: 7th edition.
- Merino, M. M., Rhiner, C., Portela, M., and Moreno, E. (2013). "Fitness fingerprints" mediate physiological culling of unwanted neurons in *Drosophila*. *Current biology*, 23(14): 1300–1309.
- Mitxitorena, I., Saavedra, E., and Barcia, C. (2015). Kupfer-type immunological synapses in vivo: Raison D'être of SMAC. *Immunology and cell biology*, 93(1): 51–56.
- Monks, C. R., Freiberg, B. A., Kupfer, H., Sciaky, N., and Kupfer, A. (1998). Three-dimensional segregation of supramolecular activation clusters in T cells. *Nature*, 395(6697): 82–86.
- Morata, G., and Ripoll, P. (1975). Minutes: mutants of *drosophila* autonomously affecting cell division rate. *Developmental biology*, 42(2): 211–221.

- Moreno, E., Basler, K., and Morata, G. (2002). Cells compete for decapentaplegic survival factor to prevent apoptosis in *Drosophila* wing development. *Nature*, 416: 755–759.
- Murphy, K. and Weaver, C. (2017). *Janeway's Immunobiology*, 9th edition
- Murphy, J.W. (1996). Cell-Mediated Immunity. In: Howard D.H., Miller J.D. (eds) *Human and Animal Relationships. The Mycota (A Comprehensive Treatise on Fungi as Experimental Systems for Basic and Applied Research)*, vol 6. Springer, Berlin, Heidelberg.
- Nandi, D., Pathak, S., Verma, T., Singh, M., Chattopadhyay, A., Thakur, S., Raghavan, A., Gokhroo, A., and Vijayamahantesh (2020). T cell costimulation, checkpoint inhibitors and anti-tumor therapy. *Journal of biosciences*, 45: 50.
- Nucifora, P. G., and Fox, A. P. (1999). Tyrosine phosphorylation regulates rapid endocytosis in adrenal chromaffin cells. *The Journal of neuroscience: the official journal of the Society for Neuroscience*, 19(22): 9739–9746.
- Onnis, A., and Baldari, C. T. (2019). Orchestration of Immunological Synapse Assembly by Vesicular Trafficking. *Frontiers in cell and developmental biology*, 7: 110.
- Ohno, H., Aguilar, R. C., Yeh, D., Taura, D., Saito, T., and Bonifacino, J. S. (1998). The medium subunits of adaptor complexes recognize distinct but overlapping sets of tyrosine-based sorting signals. *The Journal of biological chemistry*, 273(40): 25915–25921.
- Owen, D.J., and Evans, P.R. (1998). A structural explanation for the recognition of tyrosine-based endocytotic signals. *Science*, 282: 1327–1332.
- Paing, M. M., Johnston, C. A., Siderovski, D. P., and Trejo, J. (2006). Clathrin adaptor AP2 regulates thrombin receptor constitutive internalization and endothelial cell resensitization. *Molecular and cellular biology*, 26(8): 3231–3242.
- Pandey K. N. (2009). Functional roles of short sequence motifs in the endocytosis of membrane receptors. *Frontiers in bioscience*, 14: 5339–5360.
- Pandey K. N. (2010). Small peptide recognition sequence for intracellular sorting. *Current opinion in biotechnology*, 21(5): 611–620.
- Pennock, N. D., White, J. T., Cross, E. W., Cheney, E. E., Tamburini, B. A., and Kedl, R. M. (2013). T cell responses: naive to memory and everything in between. *Advances in physiology education*, 37(4): 273–283.
- Petrova, E., López-Gay, J. M., Rhiner, C., and Moreno, E. (2012). Flower-deficient mice have reduced susceptibility to skin papilloma formation. *Disease models and mechanisms*, 5(4): 553–561.
- Prajapati, R. S., Das, M., Sreeramulu, S., Sirajuddin, M., Srinivasan, S., Krishnamurthy, V., Ranjani, R., Ramakrishnan, C., and Varadarajan, R. (2007). Thermodynamic effects of proline introduction on protein stability. *Proteins*, 66(2): 480–491.
- Rettig, J. and Stevens, D. (2017). Synaptic Transmission in the Immune System. *e-Neuroforum*, 23(4): A167-A174.



- Rhiner, C., López-Gay, J. M., Soldini, D., Casas-Tinto, S., Martín, F. A., Lombardía, L., and Moreno, E. (2010). Flower forms an extracellular code that reveals the fitness of a cell to its neighbors in *Drosophila*. *Developmental cell*, 18(6): 985–998.
- Richman, D.D., Whitley, R.J. and Hayden, F.G. (2017). *Clinical Virology* (4<sup>th</sup> edition), p321.
- Shivhare, D., Musialak-Lange, M., Julca, I., Gluza, P., and Mutwil, M. (2021). Removing auto-activators from yeast-two-hybrid assays by conditional negative selection. *Scientific reports*, 11(1): 5477.
- Saheki, Y., and De Camilli, P. (2012). Synaptic vesicle endocytosis. *Cold Spring Harbor perspectives in biology*, 4(9): a005645.
- Sankaranarayanan, S., and Ryan, T. A. (2001). Calcium accelerates endocytosis of vSNAREs at hippocampal synapses. *Nature neuroscience*, 4(2): 129–136.
- Schlessinger J. (2000). Cell signalling by receptor tyrosine kinases. *Cell*, 103(2): 211–225.
- Schneider, C. A., Rasband, W. S., and Eliceiri, K. W. (2012). NIH Image to ImageJ: 25 years of image analysis. *Nature methods*, 9(7): 671–675.
- Sharp, P.A. (2005). The discovery of split genes and RNA splicing. *Trends in biochemical sciences*, 30: 279–81.
- Sorek, R., and Amitai, M. (2001). Piecing together the significance of splicing. *Nature biotechnology*, 19(3): 196.
- Stolt, P. C., and Bock, H. H. (2006). Modulation of lipoprotein receptor functions by intracellular adaptor proteins. *Cellular signalling*, 18(10): 1560–1571.
- Stamm, S., Ben-Ari, S., Rafalska, I., Tang, Y., Zhang, Z., Toiber, D., Thanaraj, T. A., and Soreq, H. (2005). Function of alternative splicing. *Gene*, 344: 1–20.
- Takaba, H., and Takayanagi, H. (2017). The Mechanisms of T Cell Selection in the Thymus. *Trends in immunology*, 38(11): 805–816.
- Takata, H., and Takiguchi, M. (2006). Three memory subsets of human CD8<sup>+</sup> T cells differently expressing three cytolytic effector molecules. *Journal of immunology*, 177(7): 4330–4340.
- Takahama, Y. (2006). Journey through the thymus: stromal guides for T-cell development and selection. *Nature reviews. Immunology*, 6(2): 127–135.
- Tai, A. W., Chuang, J. Z., Bode, C., Wolfrum, U., and Sung, C. H. (1999). Rhodopsin's carboxy-terminal cytoplasmic tail acts as a membrane receptor for cytoplasmic dynein by binding to the dynein light chain Tctex-1. *Cell*, 97(7): 877–887.
- Thiele, D., Gruta, N. L., Nguyen, A., and Hussain, T. (2020). Hiding in Plain Sight: Virtually Unrecognizable Memory Phenotype CD8<sup>+</sup> T cells. *International journal of molecular sciences*, 21(22): 8626.
- Traub, L. M., and Bonifacino, J. S. (2013). Cargo recognition in clathrin-mediated endocytosis. *Cold Spring Harbor perspectives in biology*, 5(11): a016790.

- Trowbridge, I. S., Collawn, J. F., and Hopkins, C. R. (1993). Signal-dependent membrane protein trafficking in the endocytic pathway. *Annual review of cell biology*, 9: 129–161.
- Trapani, J. A. (2012). Granzymes, cytotoxic granules and cell death: the early work of Dr. Jurg Tschopp. *Cell death and differentiation*, 19(1): 21–27.
- Tweedie, S., Ashburner, M., Falls, K., Leyland, P., McQuilton, P., Marygold, S., Millburn, G., Osumi-Sutherland, D., Schroeder, A., Seal, R., Zhang, H., and FlyBase Consortium (2009). FlyBase: enhancing *Drosophila* Gene Ontology annotations. *Nucleic acids research*, 37(Database issue): D555–D559.
- van der Sluijs, P., Zibouche, M., and van Kerkhof, P. (2013). Late steps in secretory lysosome exocytosis in cytotoxic lymphocytes. *Frontiers in immunology*, 4: 359.
- Weinreich, M. A., and Hogquist, K. A. (2008). Thymic emigration: when and how T cells leave home. *Journal of immunology*, 181(4): 2265–2270.
- Yao, C. K., Lin, Y. Q., Ly, C. V., Ohyama, T., Haueter, C. M., Moiseenkova-Bell, V. Y., Wensel, T. G., and Bellen, H. J. (2009). A synaptic vesicle-associated  $\text{Ca}^{2+}$  channel promotes endocytosis and couples exocytosis to endocytosis. *Cell*, 138(5): 947–960.
- Yao, C. K., Liu, Y. T., Lee, I. C., Wang, Y. T., and Wu, P. Y. (2017). A  $\text{Ca}^{2+}$  channel differentially regulates Clathrin-mediated and activity-dependent bulk endocytosis. *PLoS biology*, 15(4): e2000931.
- Yu, C. S., Chen, Y. C., Lu, C. H., and Hwang, J. K. (2006). Prediction of protein subcellular localization. *Proteins*, 64(3): 643–651.

## 8. Publications

1. Chitirala, P., Chang, H. F., Martzloff, P., Harenberg, C., **Ravichandran, K.**, Abdulreda, M. H., Berggren, P. O., Krause, E., Schirra, C., Leinders-Zufall, T., Bensele, F., Brose, N., and Rettig, J. (2020). Studying the biology of cytotoxic T lymphocytes in vivo with a fluorescent granzyme B-mTFP knock-in mouse. *eLife*, 9: e58065.
2. Chitirala, P., **Ravichandran, K.**, Schirra, C., Chang, H. F., Krause, E., Kazmaier, U., Lauterbach, M. A., and Rettig, J. (2020). Role of V-ATPase  $\alpha 3$ -Subunit in Mouse CTL Function. *Journal of immunology*, 204(10): 2818–2828.
3. Chitirala, P., **Ravichandran, K.**, Galgano, D., Sleiman, M., Krause, E., Bryceson, Y. T., and Rettig, J. (2019). Cytotoxic Granule Exocytosis from Human Cytotoxic T Lymphocytes Is Mediated by VAMP7. *Frontiers in immunology*, 10: 1855.
4. Ratai, O., Hermainski, J., **Ravichandran, K.**, and Pongs, O. (2019). NCS-1 Deficiency Is Associated with Obesity and Diabetes Type 2 in Mice. *Frontiers in molecular neuroscience*, 12: 78.
5. Chang, H. F., Mannebach, S., Beck, A., **Ravichandran, K.**, Krause, E., Frohnweiler, K., Fecher-Trost, C., Schirra, C., Pattu, V., Flockerzi, V., and Rettig, J. (2018). Cytotoxic granule endocytosis depends on the Flower protein. *The Journal of cell biology*, 217(2): 667–683.
6. Chang, H. F.\*, Bzeih, H.\*, Chitirala, P., **Ravichandran, K.**, Sleiman, M., Krause, E., Hahn, U., Pattu, V., and Rettig, J. (2017). Preparing the lethal hit: interplay between exo- and endocytic pathways in cytotoxic T lymphocytes. *Cellular and molecular life sciences*, 74(3): 399–408.

## In Progress

1. Hsin-Fang Chang, Claudia Schirra, Momchil Ninov, Ulrike Hahn, **Keerthana Ravichandran**, Elmar Krause, Ute Becherer, Henning Urlaub, Salvatore Valitutti, Cosima T. Baldari, Michael L. Dustin, Reinhard Jahn and Jens Rettig (2021). Identification of a novel class of cytotoxic granules as origin of supramolecular attack particles in T lymphocytes (Nature Communication)
2. Dorina Zöphel, Adrian Angenendt, Lea Kaschek, **Keerthana Ravichandran**, Chantal Hof, Sandra Janku, Markus Hoth and Annette Lis (2021). Better cytotoxicity against cancer at older age: increased perforin and granzyme levels in cytotoxic T cells boost cancer cell elimination.

## Awards

1. Best mini-proposal award of 1866 € was given by SFB 894 for proposal writing entitled 'Localization and validation of Flower protein in exo-endocytic pathways' - October 2018
2. 3rd prize for the best poster presentation entitled "Effect of Flower isoforms in cytotoxic granule endocytosis of cytotoxic T lymphocytes" during the 6th colloquium conducted by IRTG 1830 - March 2020

## 9. Disclosure

This work was funded by:

### **The Sonderforschungsbereich 894 (SFB894):**

Calcium Signals: Molecular Mechanisms and Integrative Functions

and

### **IRTG 1830 (German/Canadian Research Training Group)**

Complex Membrane Proteins in Cellular Development and Disease

From November 1st, 2018- August 31st, 2021.

All Experiments were performed in the department of Cellular Neurophysiology, Prof. Dr. Jens Rettig Laboratory, CIPMM-University of Saarland, 66421, Homburg (Saar), Germany.



The curriculum vitae was removed from the electronic version of the doctoral thesis for reasons of data protection!